

---

**Geomorphology, sedimentary processes and development of  
deep-sea channels at the convergent margin off Japan as  
revealed by bathymetric, submersible and seismic data**

**Dissertation**

**zur Erlangung des Doktorgrades der Naturwissenschaften  
im Fachbereich Geowissenschaften  
der Universität Hamburg**

Vorgelegt von

Shiguo WU

aus dem Institute of Oceanology, Chinese Academy of Sciences

7 Nanhai Road, Qingdao 266071, P. R. China

Hamburg

June, 2003

---

Als Dissertation angenommen vom Fachbereich Geowissenschaften der  
Universität Hamburg

auf Grund der Gutachten von Prof. Dr. How Kin Wong  
und Dr. Thomas Lüdmann

Hamburg, den 28. November 2001

Prof. Dr. H. Schleicher  
Dekan  
des Fachbereiches Geowissenschaften

**Contents**

<b>1. Introduction .....</b>	<b>6</b>
1.1 Geological background .....	6
1.2 Objectives of this study .....	9
1.3 Methods and material .....	10
<b>2. Geomorphology of the Nankai and the Zenisu deep-sea channels .....</b>	<b>14</b>
2.1 Definition of deep-sea channel .....	14
2.2 Nankai deep-sea channel .....	14
2.3 Zenisu Ridge .....	16
2.4 Zenisu deep-sea channel .....	17
<b>3. Bottom sediments of the Nankai and Zenisu troughs from     sidescan imaging and submersible observation .....</b>	<b>25</b>
3.1 Deep sea channel revealed by using sidescan imagery .....	39
3.2 Debris flow on the western slope of the Nankai Trough .....	40
3.3 Deposits in the central Nankai Trough .....	44
3.4 Sedimentary processes on the northern slope of the Zenisu Ridge ...	46
3.5 Sedimentary processes on the southern slope of the Zenisu Ridge and the floor of the Zenisu Trough .....	46
3.5.1 Turbidites of different ages on the southern slope of the Zenusu Ridge .....	47
3.5.2 Debris avalanche at the base of the Zenisu Ridge .....	49
3.5.3 Seep communities at the base of the slope of the Zenisu Ridge .....	52
3.5.4 Turbidites in the trough axis channel .....	52
3.6 Element geochemistry of the sediments in the Zenisu deep sea channel .....	60

3.6.1 Samples and analyses .....	60
3.6.2 Depth distribution of the elements .....	64
3.6.3 Correlation analysis of the elemental concentrations .....	64
3.6.4 The source of sedimentary material .....	65
3.6.5 Conclusions from the elemental geochemistry of sediments .....	66
3.7 Seep communities and sedimentary facies .....	66
3.8 Comparison of sedimentary processes between the Nankai Trough and the Zenisu Trough .....	67
<b>4. Seismic units and facies .....</b>	<b>68</b>
4.1 Seismic sequences and stratigraphic units in the Nankai Trough .....	69
4.2 Seismic sequences and stratigraphic units in the Zenisu Trough .....	78
4.3 Seismic sequence units of the Zenisu Ridge .....	82
4.4 Correlation and chronology of the seismic units .....	82
<b>5. Structure of the eastern Nankai Trough .....</b>	<b>86</b>
5.1 Structural elements of the Nankai Trough .....	87
5.1.1 Forearc basin and accretionary wedges .....	90
5.1.2 Deformation of the trough axis and the decollement .....	91
5.1.3 Structure of the Zenisu Ridge from seismic and geochemical data .....	92
5.2 Thrust faults on the southern slope of the Zenisu Ridge .....	93
5.2.1 Thrust faults revealed by seismic data .....	93
5.2.2 Deformations observed from a submersible .....	95
5.3 Neotectonics and the regional stress field of the Nankai Trough .....	96

---

5.4 Evolution of the accretionary prism .....	100
5.5 Neotectonics and sedimentation .....	101
5.5.1 Active faults and nascent subduction zone .....	101
5.5.2 Characteristics of the sedimentary units and their implications for the formation of the Zenisu Ridge .....	101
5.5.3 Ridge subduction: the Zenisu and paleo-Zenisu ridges .....	102
<b>6. Tectonic development and evolution of the deep-sea channels .....</b>	<b>104</b>
6.1 Tectonics and evolution of the Nankai deep-sea channel .....	104
6.2 Tectonics and development of the Zenisu deep-sea channel .....	108
<b>7. Conclusions .....</b>	<b>112</b>
<b>8. Summary .....</b>	<b>113</b>
<b>Acknowledgement .....</b>	<b>115</b>
<b>References .....</b>	<b>116</b>

## 1. Introduction

### 1.1 Geological background

The Nankai Trough off central Japan is the surface expression of a subduction zone between Southwest Japan and the Philippine Sea plate which has been active since 15-12 Ma (Kobayashi, 1995; Okuda and Honda, 1988, Fig. 1.1). Accretion along the present Nankai Trough has developed mainly since the latest Pliocene or the early Pleistocene. Present convergence rates along this trough are 2-4 cm/yr in a NNW direction (Kobayashi, 1995; Okuda and Honda, 1988). In the northern part of the Philippine Sea plate is the Shikoku Basin, which has an age of 24-15 Ma (from magnetic lineations) and a typical oceanic crustal structure (Kinoshita and Yamano, 1995; Kobayashi et al., 1995; Le Pichon et al., 1987; Pickering et al., 1993).

The Nankai Trough can be divided morphologically and tectonically into an eastern and a western segment. The structural style and possible fluid migration of the western segment has been studied by multichannel seismic reflection profiling (Aoki et al., 1982; Ashi and Taira, 1992; Kinoshita and Yamano, 1995; Moore et al., 1990; Moore and Shipley, 1993; Park et al., 2000). Stoffa et al. (1992) conducted a high-resolution study of the shallow structures using expanding spread (ESP) and split spread (SSP) seismic profiles, and determined that the decollement is developed within a low velocity zone. DSDP and ODP drill holes penetrated the trough-fill strata, permitting sedimentation and dewatering processes in the western Nankai Trough and the adjacent Shikoku Basin to be investigated (Pickering et al., 1993; Taira et al., 1993; also see Fig. 1.1).

In contrast to the western Nankai Trough, the tectonics and morphology of the eastern Nankai Trough is more complex. Previous studies show that: (1) the eastern Nankai Trough is involved in the collision between the Izu-Ogasawara and Honshu island arcs, resulting in a complex structural development (Le Pichon et al., 1992; Tokuyama et al., 1998). Generally, the distribution of thrust faults and uplift of the Zenisu Ridge suggest a compressive stress field in the eastern Nankai Trough (Aoki, 1982; Kato et al., 1983; Le Pichon et al., 1992; Tokuyama et al., 1998; Wu et al., 1999). Similarly, widespread erosion and the occurrence of backthrusts in the eastern Nankai accretionary wedge indicate the dominance of compression; (2) seismic activity of the Nankai Trough is relatively low compared to the neighboring subduction zones in which large earthquakes repeatedly rupture segments of this boundary in cycles of 100 years.

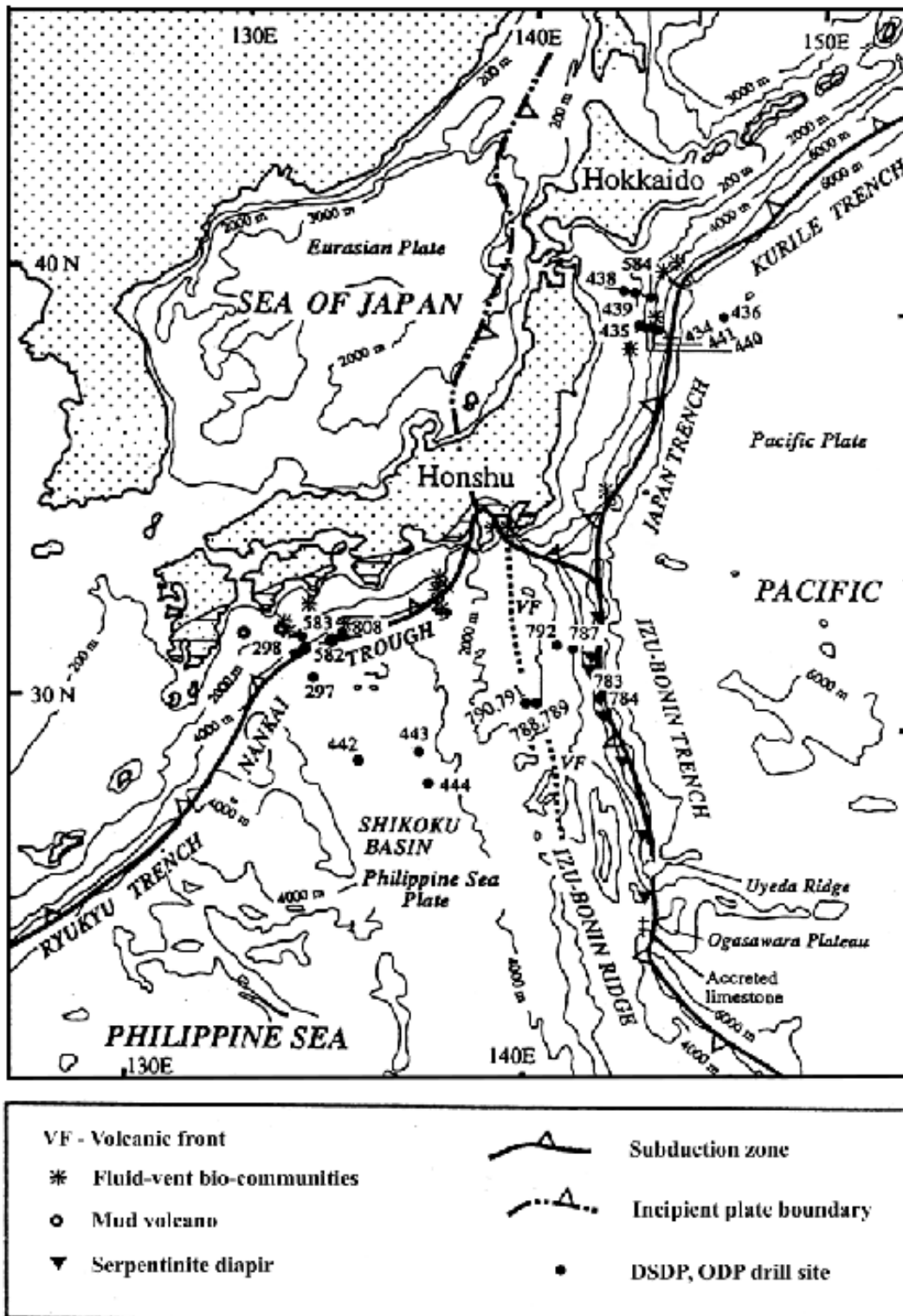


Fig. 1.1 Map of Nankai Trough and vicinity showing major tectonic features and locations of DSDP and ODP drill sites (after Pickering et al., 1993).

However, rupturing of the last large earthquake of 1944 did not extend east of 138° E (Le Pichon et al., 1996). Current predictions foresee the occurrence of a magnitude 8 earthquake (to be called the Tokai earthquake) that would rupture the easternmost portion of the eastern Nankai Trough early this century (Le Pichon et al., 1996); (3) numerous seep communities and gas hydrate occurrences have been reported from the eastern Nankai Trough (Ashi, 1997; Ashi and Taira, 1993; Matsumoto et al., 1998; Tsuji et al., 1998). The accompanying dewatering processes are controlled by active faults as well as by the sedimentary facies (Ashi et al., 1998; Tokuyama et al., 1998); and (4) both our seismic data and observations from a submersible show that the Zenisu Ridge exterior to the accretionary prism is characterized by compressive structures in its upper layers which may be interpreted as the result of intra-oceanic subduction along its southern margin (Lallemand et al., 1992; Le Pichon et al., 1987, 1989; Tokuyama et al., 1998).

Bathymetrically, the eastern Nankai Trough situated northwest of the Zenisu Ridge is characterized by channel development which shows a fluvial morphology at the seafloor (Fig. 1.2). The Nankai Trough is a southwestward extension of the Fuji River, to which it joins off the Kii Peninsula (Shimamura, 1988; Taira and Niitsuma, 1985). We suggest that it is an important pathway along which terrigenous material is transported to the deep sea by turbidity currents. Thus, it is a key area for a better understanding of deep sea sedimentary processes at this convergent continental margin. The Zenisu deep-sea channel extends from the Izu-Ogasawara Arc and vanishes within the Zenisu Trough. Headstream of it is a volcanically active area, so that sediments of the Zenisu Trough are rich in volcanoclastic detritus (Sakamoto et al., 2000; Wu et al., 2000).

A number of MCS surveys have been carried out in the eastern Nankai Trough prior to our studies (Aoki, et al., 1982; Kato et al., 1983; Okimura et al., 1999; Okuda and Honda, 1988; Tokuyama et al., 1998; Wu et al., 1999). Aoki et al. (1982) focused on a tectonic comparison between the eastern and western Nankai Trough. They were the first to point out that compressive structures occur in the upper sedimentary section of the Zenisu Ridge and to doubt that the Zenisu Ridge is part of the Izu-Ogasawara Islands Arc. Okuda and Honda (1988) discussed the slope sequences as well as the origin of the forearc basin and the accretionary wedge. Recently, the western Nankai Trough was drilled within the framework of ODP and DSDP. The tectonics of subduction on this active margin has been studied in the past two decades in the *Kaiko Tokai* project (Kagami et al., 1985; Kaiko I Research Group, 1996; Le Pichon et al., 1987, 1989, 1992; Moore et al., 1993; Okuda and Honza, 1988; Tokuyama et al., 1998). During the past few years, numerous surveys have been carried out using the submersibles *Shinkai 2000*, *Shinkai 6500* and *ROV* to study deep-sea seep communities and gas hydrates in this area (Ashi, 1997; Ashi et al., 1996; Sakamoto et al., 2000).

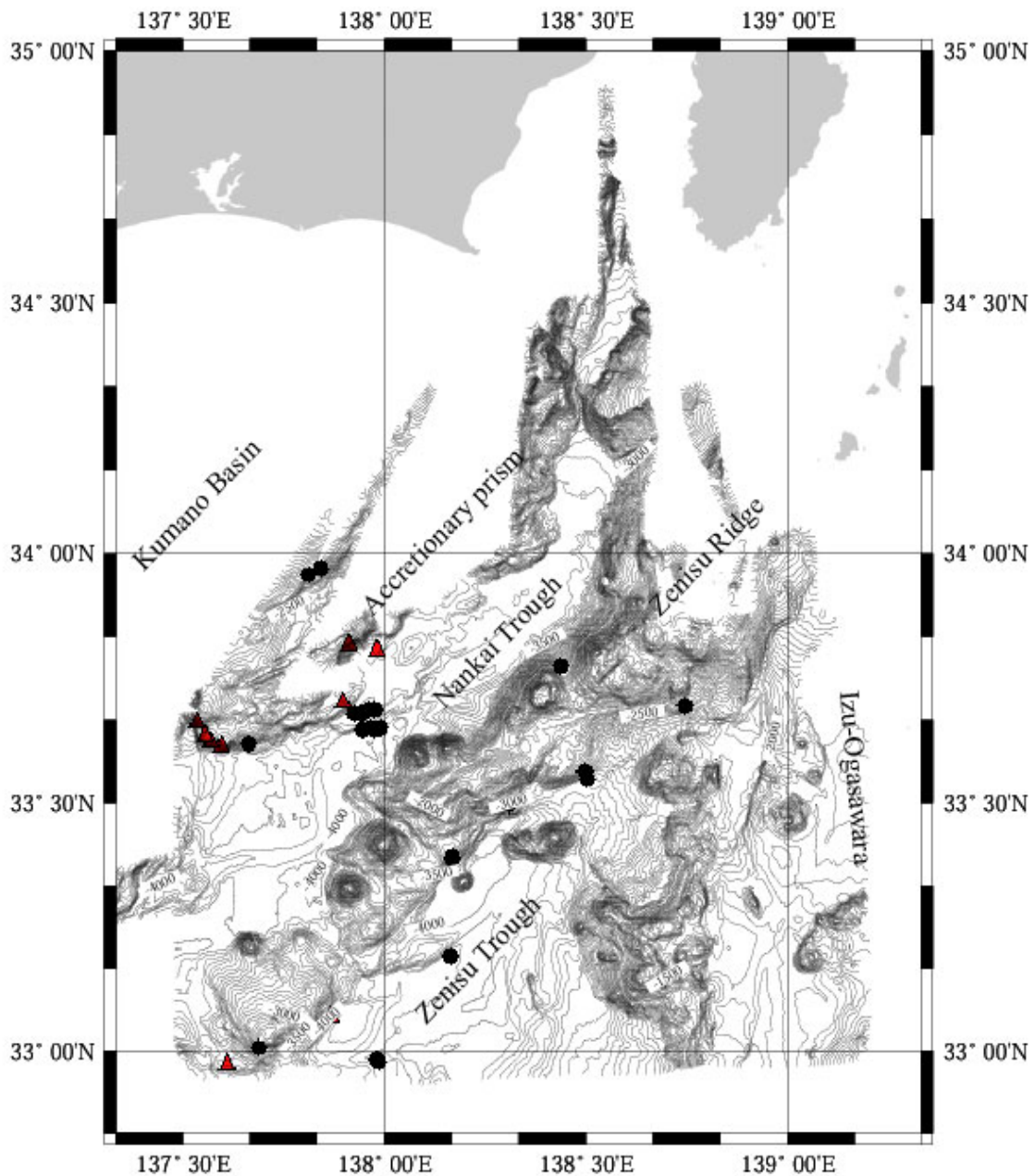


Fig. 1.2 Submersible dive sites in the eastern Nankai Trough where dives have been executed. Dots: dive sites of *Shinkai 6500*; Triangles: dive sites of the *Nautilie*.

## 1.2 Objectives of this study

Deep-sea channels occur in the eastern Nankai Trough and the Zenisu Trough. Since deep-sea channels are still poorly known, their topography, sedimentary

processes and tectonics are investigated in detail in this study by using SeaBeam bathymetry, submersible data, as well as sidescan sonar and seismic data.

A second objective is the compaction-driven dewatering of seafloor sediments as they are accreted to the overriding plate along the deep-sea channels. Numerous fluid seeps associated with chemosynthetic biological communities have been discovered on the seafloor of the Nankai Trough where submersible exploration has been carried out (Le Pichon et al., 1987; 1989). Whether cold seepage communities also exist in the Zenisu Trough and if so in what geological setting form another complex of open questions in this study. The last scientific objective is to reconstruct the development of the deep-sea channels, and to clarify the relationship between the regional tectonic evolution and the development of these deep-sea channels.

### 1.3 Methods and material

The manned submersible *Shinkai 6500* with a dive capability of 6500 m is playing an evermore important role in deep sea research and resource development. It represents state-of-the-art technology in material research, ship-building, mechanical engineering and electronics. The complete system consists of the manned submersible, its support vessel R/V *Yokosuka* and a dive support system for navigation and telecommunication using acoustics and electronics (Fig. 1.3). Although submersible imaging data on seafloor structure and sedimentation in the eastern Nankai Trough are plentiful, the Zenisu deep-sea channel is still not well studied from this point of view. For this reason, I executed dives 523 and 556 with the submersible *Shinkai 6500* to study the sedimentation and active tectonics on the southern slope of the Zenisu Ridge and in the Zenisu Trough. I also studied the video tapes of dives 521 and 523 of cruise YK99-09 Leg 2 of the R/V *Yokosuka*, dives 555-557 of cruise YK00-06 Leg 1 of the R/V *Yokosuka*, and dives 322, 323, 371, and 399-401 of the *Kaiko Tokai* cruise with the R/V *Yokosuka*. Photographs taken during dives of the *Kaiko Tokai* project were also examined. The dive sites are shown in Fig. 1.2.

The laboratory work include grain-size, microfossil, major element and trace element analyses. The grain-size analyses were carried out at the sedimentary laboratory of the Institute of Oceanology, Chinese Academy of Sciences by using the Cilas 940L laser grain-size analyser of Cilas Co. Ltd. Nannofossil identification was done at the Nippon Geological Co. Ltd. and major elements were measured with the RIX3000 XRF of Rigaku Electronics Co. Ltd. at JAMSTEC.

A total of 454 km G-gun and 682 km air gun seismic data were acquired in order to study the seismic sequences and their facies during cruise KH96-02 of the R/V *Hakuho-mura* (Fig. 1.4). The box survey consists of 8 parallel lines, each approxi-

mately 55 km in length and spaced 1600 m apart. Each of the four G-gun arrays has a volume of 150 cubic inches and were operated at a pressure of 200 bars. The shot interval and receiver group interval were both 25 m, the CMP stacking is therefore 60 fold. In another configuration, the shot and receiver intervals were 50 and 25 m respectively, and stacking was 30 fold. Processing of the MCS lines and the G-gun data were carried out at the Japan Geoscience Institute with the Software iXL of the company *MIT* installed on a *Sun 2/4* workstation. Single channel seismic data (KAIKI Rsearch Group I, 1986) were also used in the discussions.

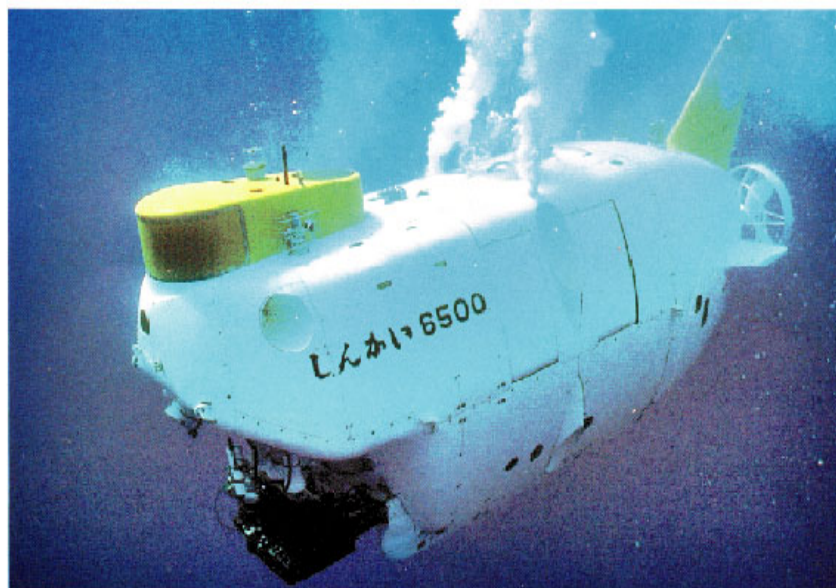


Fig. 1.3 (Upper) Photograph of the manned submersible Shinkai 6500. (Lower) Author leaving the submersible at the end of dive 556.

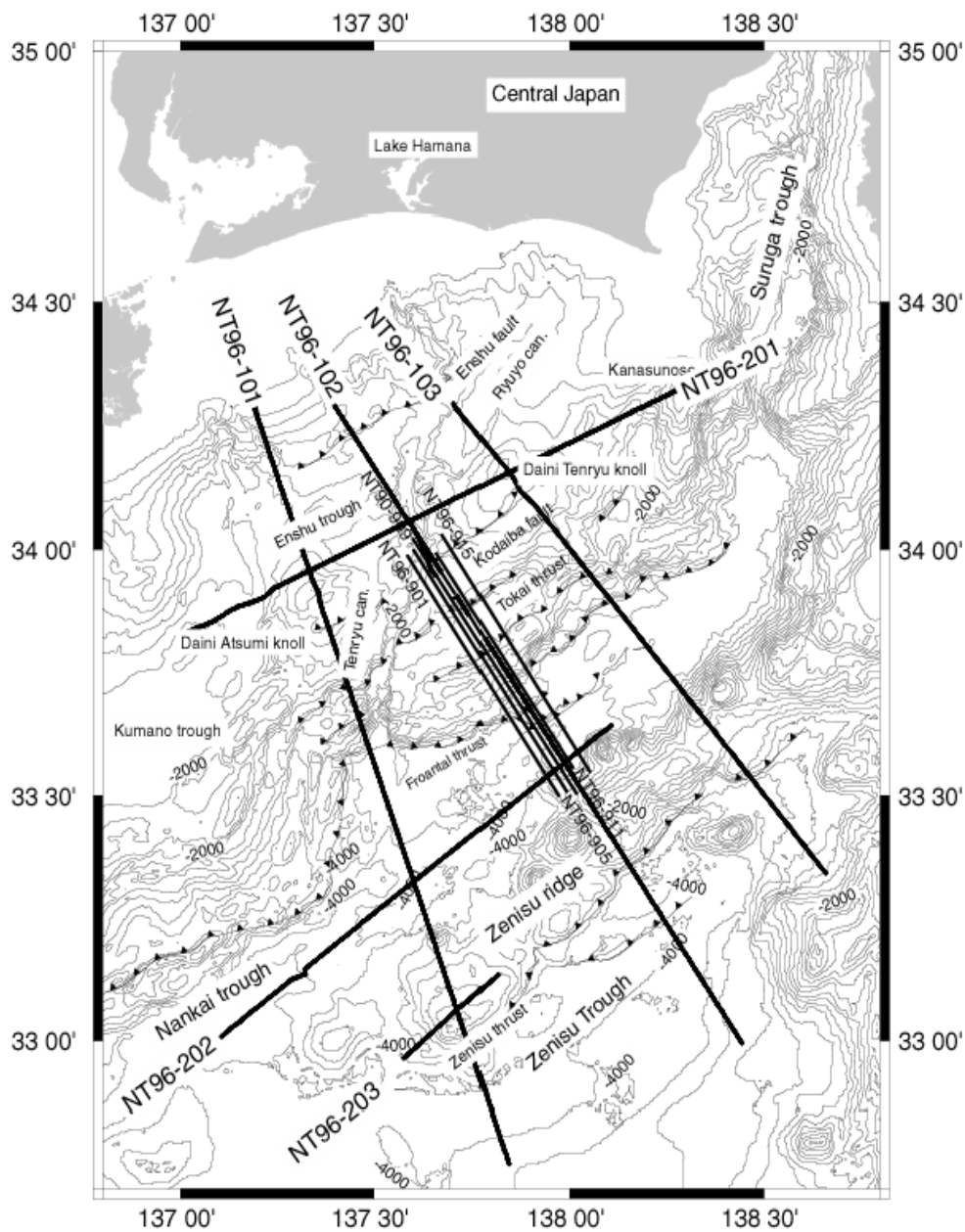


Fig. 1.4 Bathymetric map with location of seismic profiles. Thick straight lines give the airgun seismic tracks from cruise KH96-02 of the R/V *Hakuho-maru*. Thinner straight lines show the G-gun seismic profiles used in this study. Fine lines with triangles show the major thrusts mapped by seismic survey and submersible observation. The isobaths are at a depth interval of 200 m.

Swath bathymetric data were collected during cruise YK99-09 Leg 2 and cruise YK00-06 Leg 1 of the R/V *Yokosuka* by means of a SeaBeam 2100 system. Sidescan images were derived from these data, as well as from those of the *Kaiko Tokai* Project (Tokuyama et al., 1998). Data processing and image plotting were carried out with the SeaBeam software. A similar data set collected during cruise KR97-05 of the R/V *Kaiyo* was also used in this dissertation.

The sidescan sonar data set used was collected during cruises 99-09 Leg 2 and 00-06 Leg 1 of the R/V *Yokosuka*. The center part of these sidescan data derived from SeaBeam data was omitted due to amplitudes that are too high. This is done by deleting the central 200 pixels (100 pixels for each side) of a 2000 pixel sweep. Data that are obviously too high and/or too low are removed by filtering. The average sidescan amplitude at a given angle of incidence for the entire data set was then estimated. Using this average, the recorded sidescan amplitudes are normalized so that their average is the same regardless of the angle of incidence or receiver channel. Lastly, the data are gridded using 10 m spline interpolation with weighted mean.

## **2. Geomorphology of the Nankai and Zenisu deep-sea channels**

### **2.1 Definition of deep-sea channels**

Deep-sea channels are long conduits which traverse the deep seafloor and feed into the abyssal transport system. Such channels in the deep-sea can be divided into five types: canyons, fan channels, oceanic channels, trench-axis channels and boundary channels (Carter, 1988). Shepard and Dill (1966) introduced a classification scheme for channels on the deep seafloor and fan valleys. Those on the deep seafloor strike parallel to the continental margin in or along trenches and can be easily distinguished from those on deep-sea fans. The Nankai and Zenisu deep-sea channels are situated along the Nankai Trough and Zenisu Trough respectively, and are almost parallel to the landward slope of Honshu Island. Therefore, the depressions in the Nankai and Zenisu troughs which show river-like sectional and plan views and have erosional features on bathymetric and seismic sections (Fig. 2.1) are called deep-sea channels in this dissertation.

Much of our knowledge on seafloor morphology has come from conventional echo-sounding. The lowest recognizable limit of channel relief of 2-4 m is approximately reached in our high-resolution bathymetry and 3.5 kHz echograms. Our data include swath bathymetric data collected by a SeaBeam 2100 system during cruise 97-05 of the R/V Kairei, and cruises 99-09 Leg 2 and 00-06 Leg 1 of the R/V Yokosuka. Fig. 2.2 shows the track lines of the latter two cruises that have good data quality. The geomorphology of the study area is characterized by deep-sea channels developed on both sides of the Zenisu Ridge (Fig. 2.1), namely by the Nankai deep-sea channel northwest of the ridge, and by the Zenisu deep-sea channel southeast of it.

### **2.2 Nankai deep-sea channel**

The Nankai deep-sea channel is situated in the eastern Nankai Trough and strikes nearly parallel to the landward slope of the trough. Bathymetric studies show that the eastern Nankai Trough has an average water depth of 4000 m and runs parallel to the Zenisu Ridge in its southern part (Figs. 1.2 and 2.1). Its spatial extent has been defined by high-resolution SeaBeam swath bathymetric surveys conducted during cruise KR97-05 of the R/V Kairei, cruise YK99-09 Leg 2 of the R/V Yokosuka, and cruise YK00-06 Leg 1 of the R/V Yokosuka (Fig. 2.2) as well as during the earlier Kaiko Tokai project (Tokuyama et al., 1998).

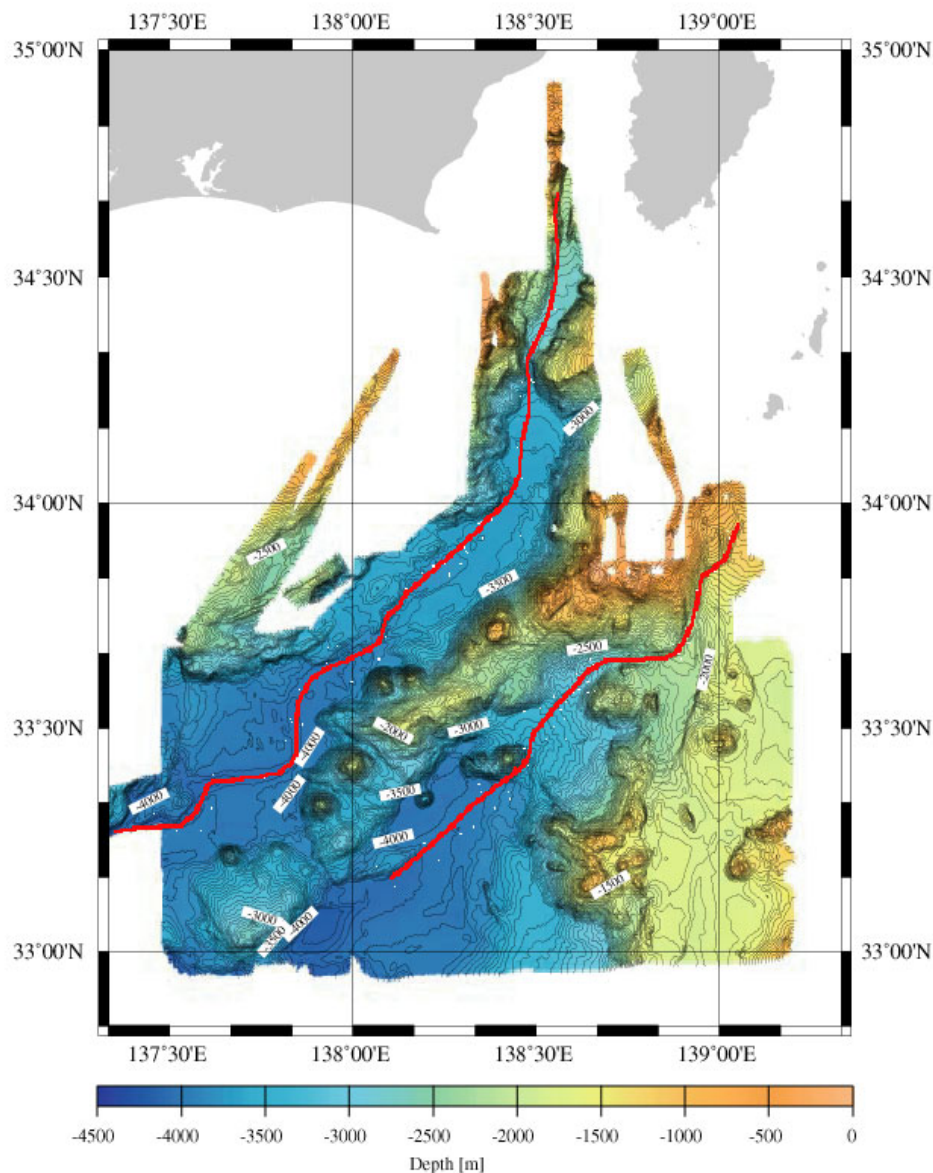


Fig. 2.1 SeaBeam bathymetric map of the study area surveyed during cruises YK99-09 Leg 2 and YK00-06 Leg 1 of the R/V *Yokosuka*, showing the Nankai deep-sea channel in the northwest and Zenisu deep-sea channel in the southeast. The contour interval is 50 m. A 250 m grid was used. Mercator projection.

The Nankai Trough is recognized as a remarkably continuous deep-sea channel which originates from the submarine canyon of the Fuji River in the Suruga Trough (Soh et al., 1995) and extends for about 400 km toward the west, gradually becoming less distinct until it disappears south of Kii peninsula (Shimamura, 1988). The most striking feature of the channel is its straight course as recognized in the high-resolution bathymetry map (Fig. 2.1).

The channel relief of the Nankai Trough in the survey area ranges generally between 50-150 m (Fig. 2.3). The incised parts where the channel relief reaches locally a maximum of 250 m is of tectonic origin and marks a frontal thrust of the subduction system (Fig. 1.3). Minor topographies of the channel are either depositional or they are represented by erosional levees, mid-channel bars and thalweg meanders. The channel width varies from a few hundred meters to one kilometer (Fig. 2.1). The channel course shows a zigzag pattern with N-S and N 70°-90° E segments subparalleling the subduction front (Figs. 2.1 and 2.3). We suggest that the Nankai Trough is controlled by two former structural lines striking N-S and E-W respectively. It is a product of the subduction process.

### **2.3 Zenisu Ridge**

The Zenisu Ridge is located at the southeastern part of the Nankai Trough and strikes NE-SW from the Izu-Ogasawara Arc to the Shikoku Basin. It is approximately 200 km long and <40 km wide. The water depth over the ridge increases southwestward, the maximum being about 4000 m at its southwesternmost part. The ridge can be divided into three segments according to its morphology (Fig. 2.4):

The northern segment lies north of 33° 40' N and is a typical segment of the Izu-Ogasawara Arc. Acidic volcanoes (such as those on the Kozushima and Nijima islands) are common. The topography and composition of volcanoes are the same as that of the Izu-Ogasawara Island Arc (Ikeda and Yuasa, 1989; Sakamoto et al., 2000).

The middle segment (between 33° 20' N and 33° 40' N) is characterized by steep knolls (Figs. 2.4 and 2.5). Steep slopes are developed on the northern flank of this ridge segment, while terraces and gentle slopes are found on the southern flank (Figs. 2.5 and 2.6a, b). The bathymetry suggests that fractures exist on the southeastern flank of the Zenisu Ridge and this is confirmed by submersible observations (Le Pichon et al., 1987; Lallemand et al., 1989; Wu et al., 2000). The ridge, being formed in different stages, consists of rocks ranging from basalt to andesite (Sakamoto et al., 2000).

The southern segment of Zenisu Ridge lies between 33° 20' N and 33° 00' N. This segment has a relatively gentle morphology (Fig. 2.6c) and consists of oceanic basalt. Only one seamount has been discovered so far (at 33° 12' N and 137° 40' E). Here, the western ridge flank is gentle and folds are absent. On the eastern margin of this ridge segment, however, steep scarps of two thrust faults occur as confirmed by submersible observations (Le Pichon et al., 1989).

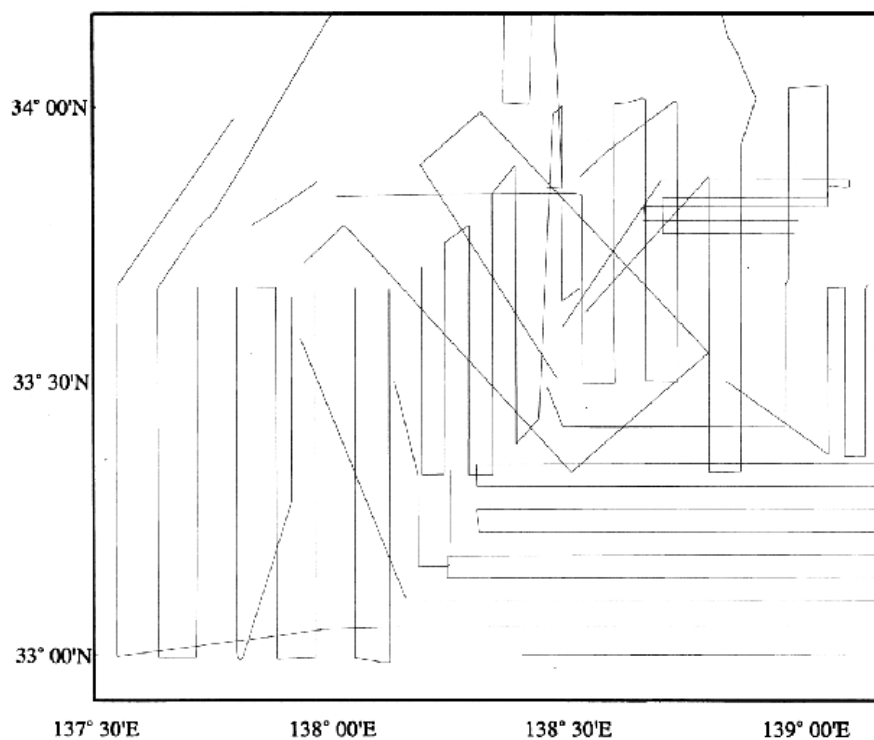


Fig.2.2 Seabeam survey track lines of cruises YK99-09 Leg 2 and YK00-06 Leg 1 of the R/V *Yokosuka*.

## 2.4 Zenisu deep-sea channel

The Zenisu deep-sea channel starts from the Izu-Ogasawara Arc and can be divided into three segments based on SeaBeam swath bathymetric data (Figs. 2.7 and 2.8). The upper segment (the Zenisu Canyon) lies north of 33° 40' N and has a N-S to N 70° E trend. The uppermost part of the canyon is narrow and is ca. 1-2 km wide, 150-750 m deep (Fig. 2.9a, b). The gradient down-channel along this segment is more than 2°. The middle segment trends nearly E-W at 33° 40' N but transits to N 43° E south of 33° 40' N. Its slope along the channel is about 1.2°. The lower part of the Zenisu deep-sea channel (the Trough-Axis Channel) merges with the Zenisu Trough which strikes N 43° E. This channel has a thalweg 40-50 m deep and 500-1000 m wide. On the seismic profiles, the channel-levee and upper fan system is characterized by a

stack of several lenticular acoustic units (Nakimura et al., 1987). Each is about 100 m thick and 7 km wide, and consists of a central chaotic facies grading laterally into a convergent bedded or transparent facies. The latter are interpreted as a channel-levee complex deposited during a sea-level lowstand (Figs. 2.9c, d).

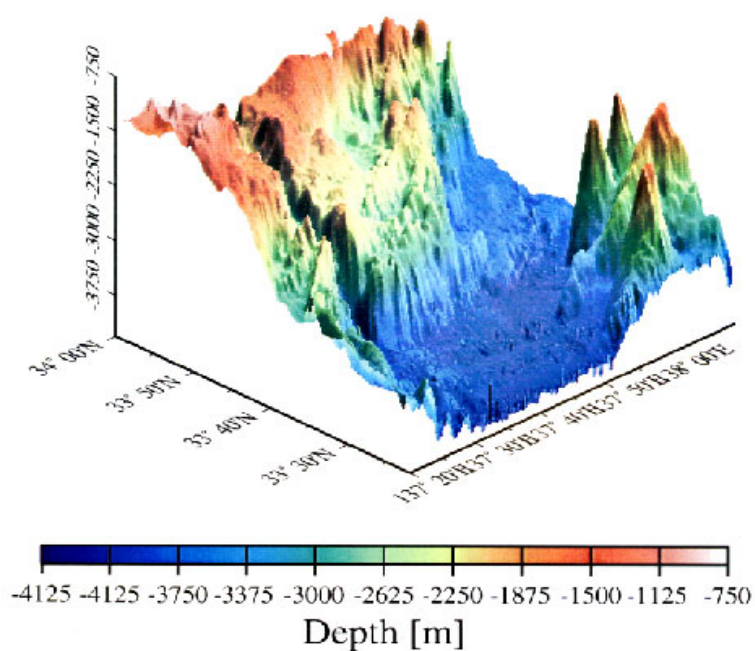


Fig. 2.3 Three dimensional bathymetric block diagram showing the morphological features of the Nankai deep-sea channel.

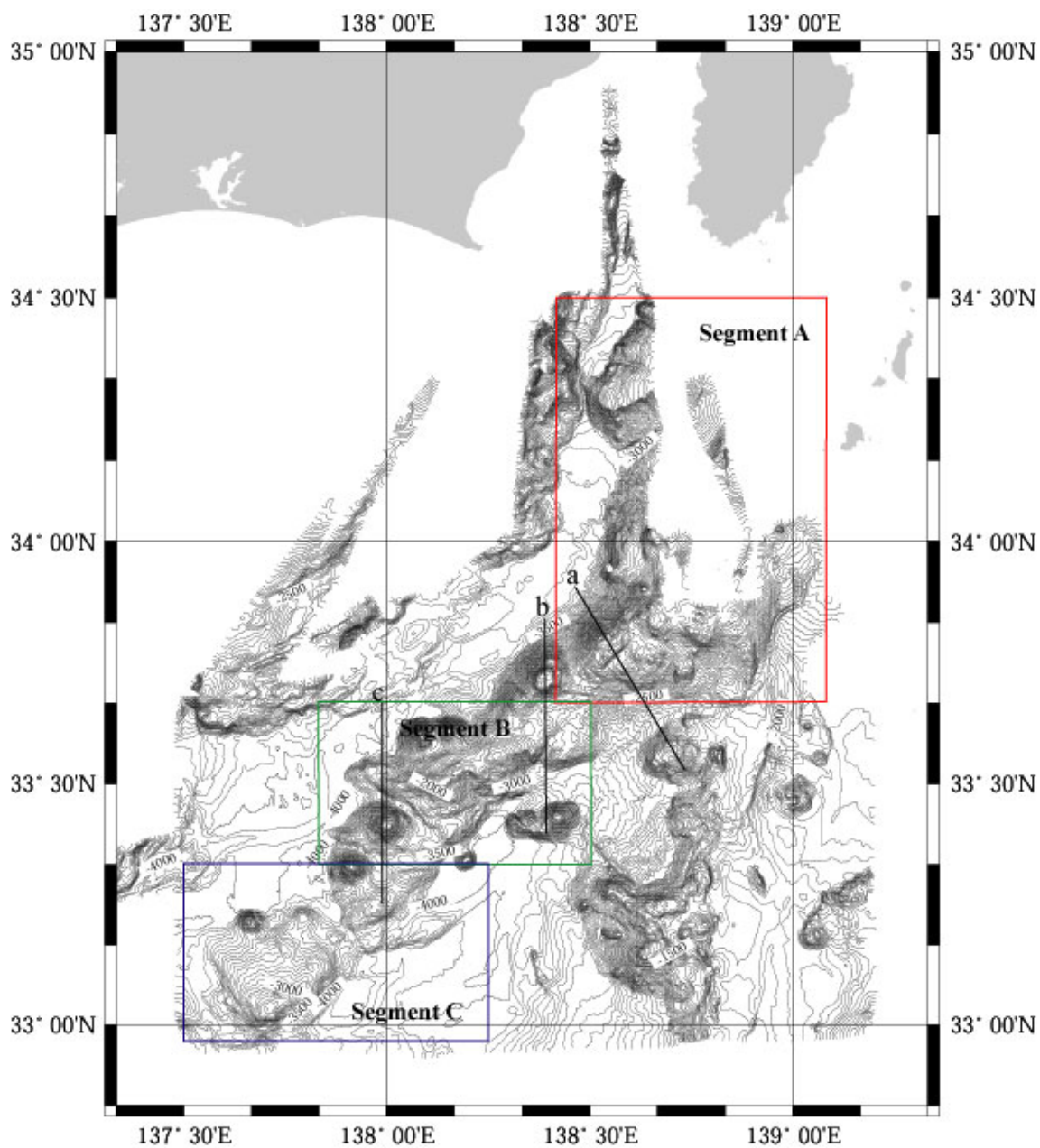


Fig. 2.4 SeaBeam bathymetric map of the Zenisu Ridge showing division into three segments in accordance with the bathymetric features. Contour interval is 50 m. Black thick lines show the location of bathymetric cross-section in Fig. 2.6.

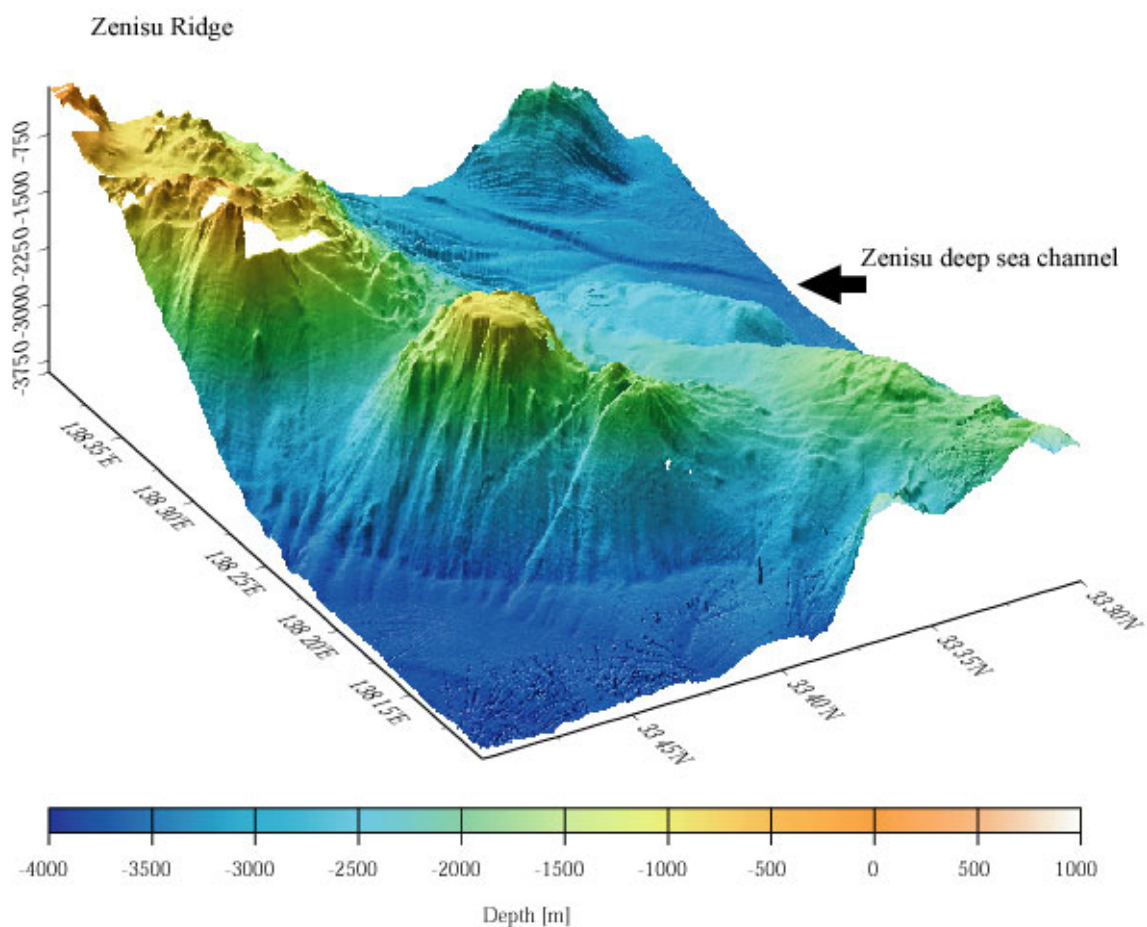


Fig. 2.5 Three dimensional bathymetric block diagram showing the morphological features of the Zenisu Ridge. Seamounts represent Quaternary volcanos.

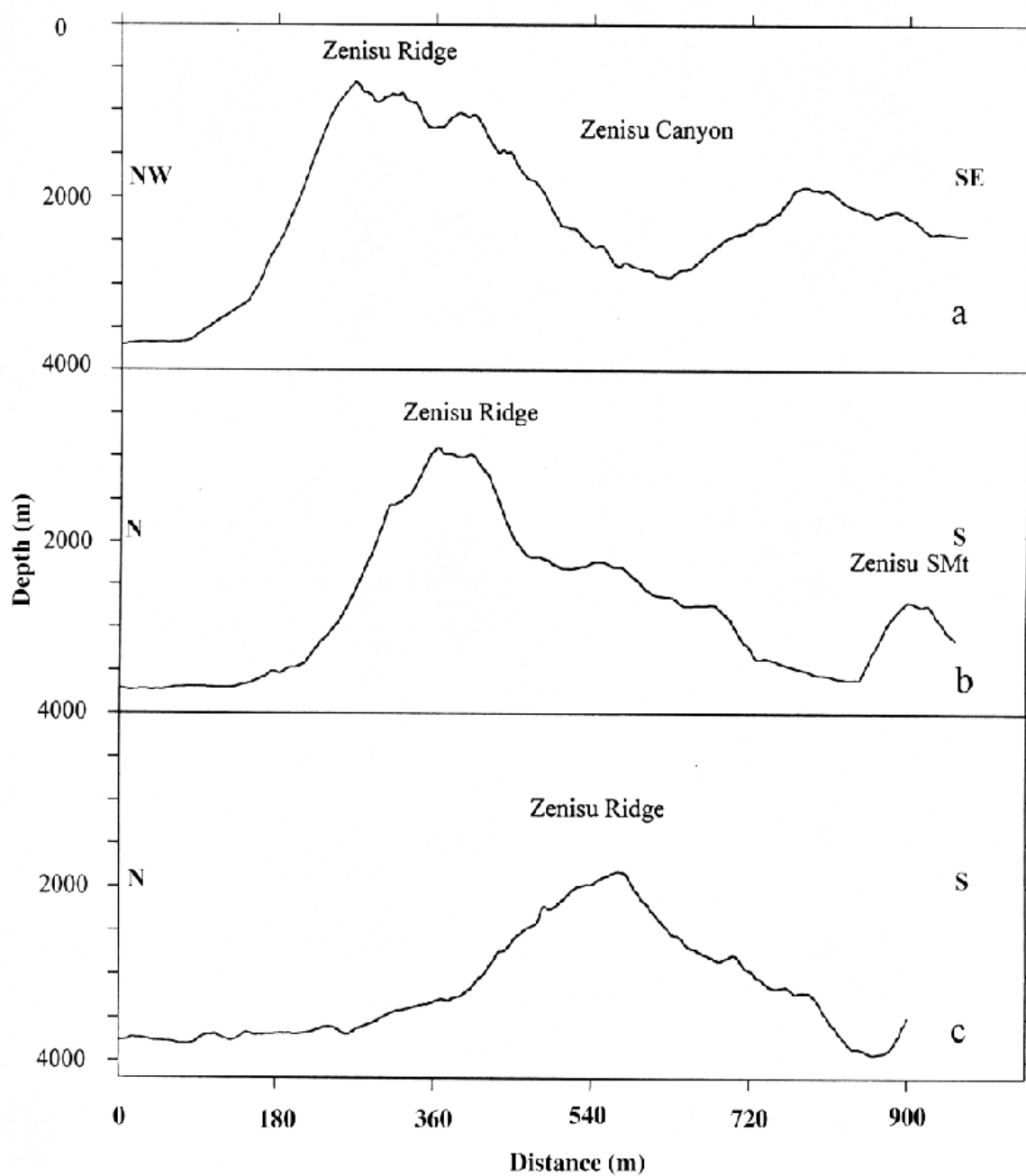


Fig. 2.6 Bathymetric cross-sections of the Zenisu Ridge surveyed by R/V *Yokosuka* in 1999 and 2000. Sections a, b and c are from north to south. For locations of cross-sections see Fig. 2.4.

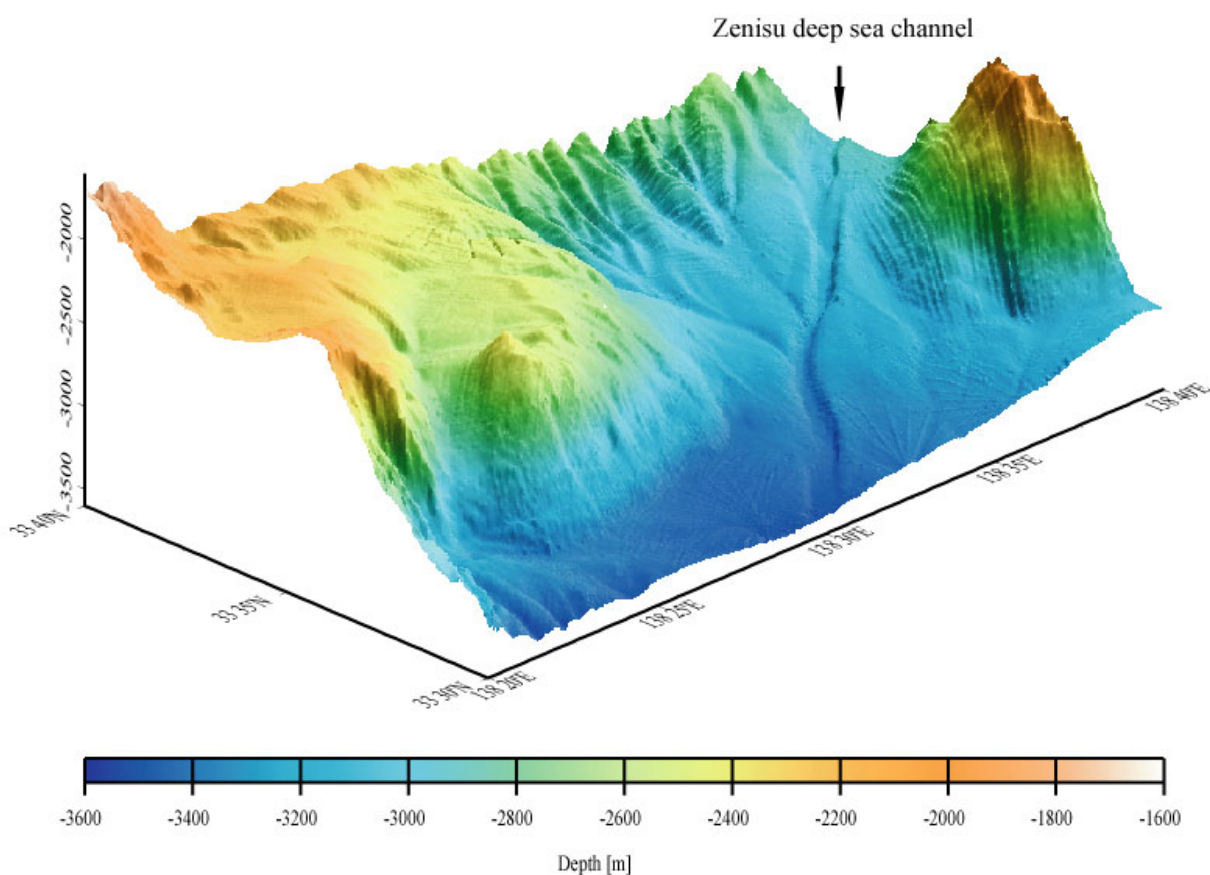


Fig. 2.7 Three dimensional bathymetric block diagram showing the morphological features of the Zenisu deep sea channel. Channel morphology is clearly recognizable in the east.

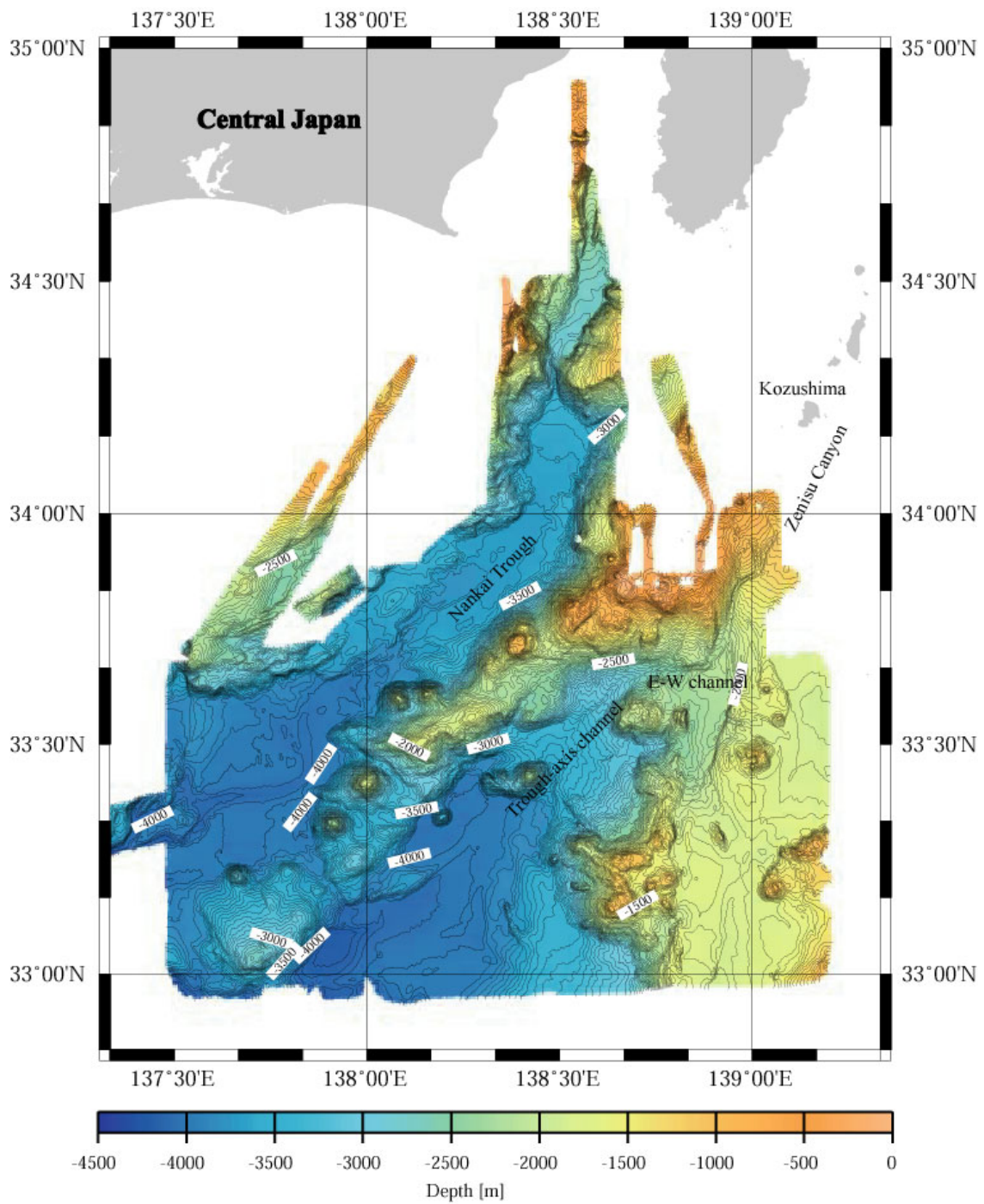


Fig. 2.8 SeaBeam bathymetry of the Zenisu deep-sea channel showing division into the Zenisu Canyon, east-west channel and the trough-axis channel. Contour interval is 50 m.

Turbidite deposits usually occur in a lowstand systems tract. We suggest that channel turbidity activity in this convergent margin is still very strong during the Holocene sea-level rise. Since the channel topography is distinct today, it must be an active conduit for sediments supplied to the Zenisu Trough despite the Holocene sea-level high. The sediment supply is sufficient to mask the modification of the channel morphology caused by tectonically-driven subsidence. Large amounts of detritus are provided by volcanoes of the Izu-Ogasawara Ridge. As the new channel formed, the amount of sediment fed to it gradually decreased due to tectonic subsidence.

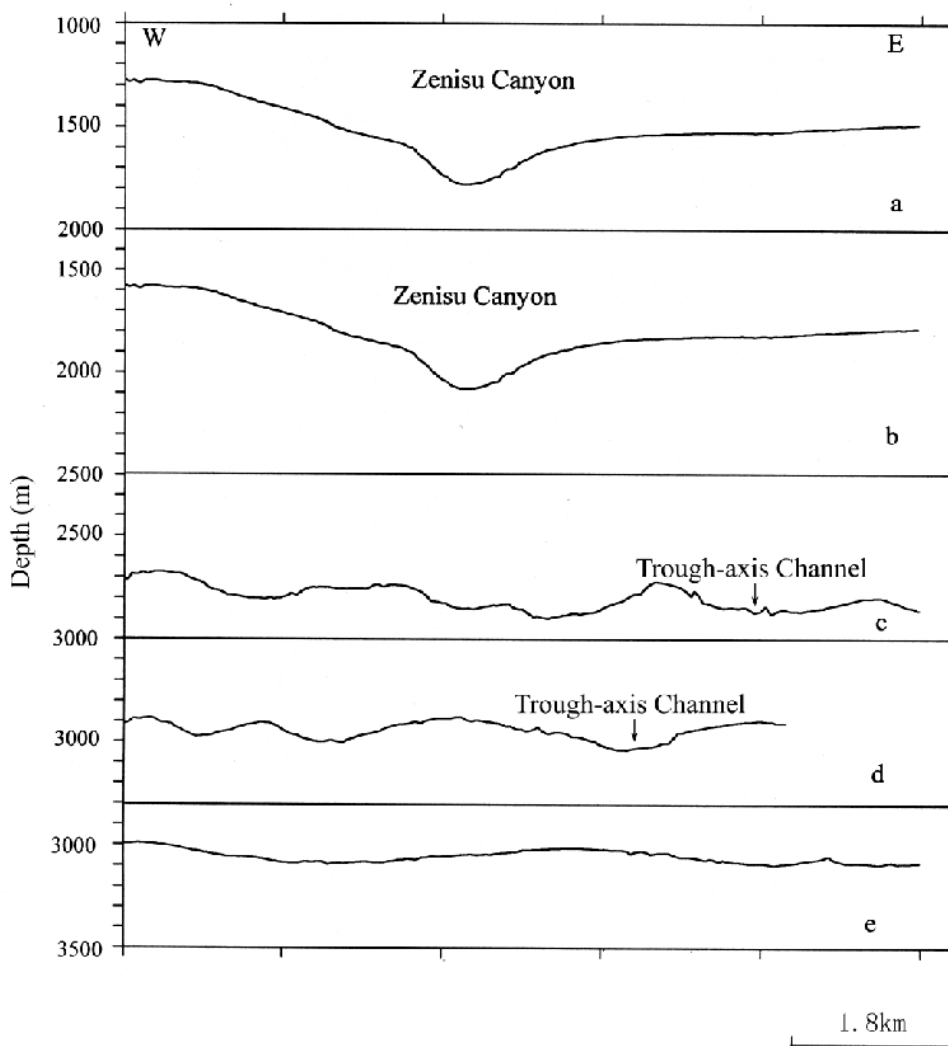


Fig. 2.9 Bathymetric sections across the Zenisu deep-sea channel surveyed during cruises YK99-09 Leg 2 and YK00-06 Leg 1 of the R/V *Yokosuka*. Sections a and b show the morphology of the Zenisu Canyon, c, d and e that of the trough-axis channel and the distal part of the Zenisu deep-sea channel.

### **3. Bottom sediments of the Nankai and Zenisu troughs (sidescan imaging and observations from a submersible)**

The erosion, transport and deposition of sediments in deep-sea channels are controlled largely by sediment gravity flow processes: flows in which sediment-fluid mixtures move under the influence of gravity (Middleton and Hampton, 1973, 1976; Lowe, 1979, 1982; Middleton and Southard, 1984; Reading, 1996; Damuth et al., 1995). Sediment gravity flows are formed by a broad group of genetically related processes ranging from slumping, debris flow to turbidity current activity.

Ultimately, deep-sea channel sedimentation is controlled by plate tectonic configuration, climate and eustatic sea-level change (Reading, 1996; Nichols, 1999). However, more directly, sediment supply is probably the single most important factor in shaping the depositional style. This includes the grain size and composition of the sediment, the volume, rate and frequency at which it is made available for deposition, and the number and position of input points. In convergent margins, the tectonic factor dominates sedimentation. It includes: (1) the regional stress regime, which can affect the relative rates of uplift and subsidence in the source area and the basin; and (2) rates of uplift and morphology of the trough. Subduction along the Nankai Trough and possible nascent subduction along the southern margin of the Zenisu Ridge controlled accommodation for sediments and submarine canyon extension. The magnitude and frequency of seismicity may also be important. Ikehara et al. (1999) demonstrated a close relationship between turbidity current activity and earthquakes in the eastern Nankai Trough. Therefore, tectonics must be the dominating factor that controls deposition in this area, while climate and sea level play less important roles because of the lack of a wide shelf for the adjustment of sediment accommodation.

Modern turbidity currents have been repeatedly observed during submersible dives (Fig. 3.1). In this dissertation, I shall use a more general classification for the gravitational sedimentary processes based on the typical range of flow characteristics found in nature, rather than restricting the classes to strictly-defined end numbers (Middleton and Hampton, 1973). For example, natural debris flows are characterized by a complex interaction of particle support mechanics, and we mapped two important gravity flow deposits. The most important bathymetric characteristics are dominated by turbidite deposition which resulted in channel-levee systems in the Zenisu Trough.

Debris flow which can be mapped by sidescan sonar imaging, high-resolution bathymetry and submersible observations are also important (Fig. 3.2, 3.3, 3.4, 3.5, 3.6, 3.7, 3.8, 3.9, 3.10). The main region of debris flow is found at the slope base. In addition, modern hemipelagic sediments cover part of the Zenisu Ridge. Seep communities also occur at the slope base (Figs. 3.7II and 3.10III) and fine sediments cover the accretionary wedge and the ridge slope (Kobayashi et al., 1992; Le Pichon et al., 1989).

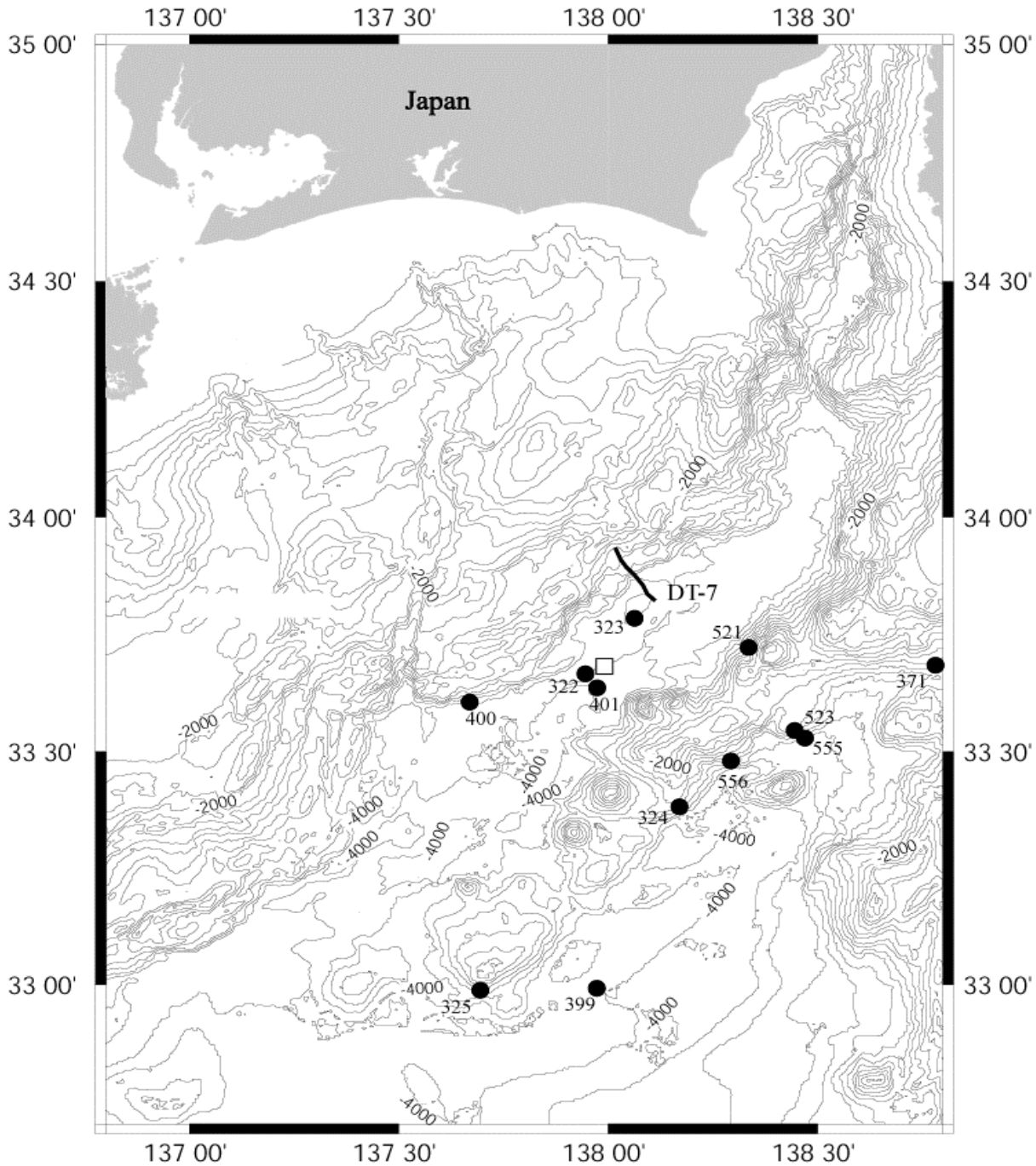


Fig. 3.1 Location of submersible dives reported in this dissertation. Solid circles show the locations of dives executed by the *Shinkai 6500*. Square is the ROV dive site. Bathymetric contour interval is 200 m.

Erosion occurred on most of the lower slope of the Nankai accretionary prism, uplifting the Zenisu Ridge and the adjacent Izu-Ogasawara Arc, even though there is a thin cover of hemipelagic sediments locally on the accretionary slope and the Zenisu Ridge (Fig. 3.3). Rock outcrops on the accretionary slope and the ridge are revealed by

sidescan sonar imagery (Fig. 3.2, 3.11, 3.12) and during several manned submersible dives. Rock outcrops on the Zenisu Ridge were observed during dive 521. Local erosion and rock outcrops also occur on the trough floor (Figs. 3.4 to 3.8).

Deep-sea biological and chemical processes have unique characteristics in the deep-sea channels of convergent margins. We observed these processes from a submersible and mapped them using sidescan sonar data. The statistics of submersible dives, the results of which have been used in this study, are shown in Table 3.1; dive locations are given in Fig. 3.1. The sediment distribution derived from the submersible observation and sidescan sonar data are summarized in Fig. 3.3.

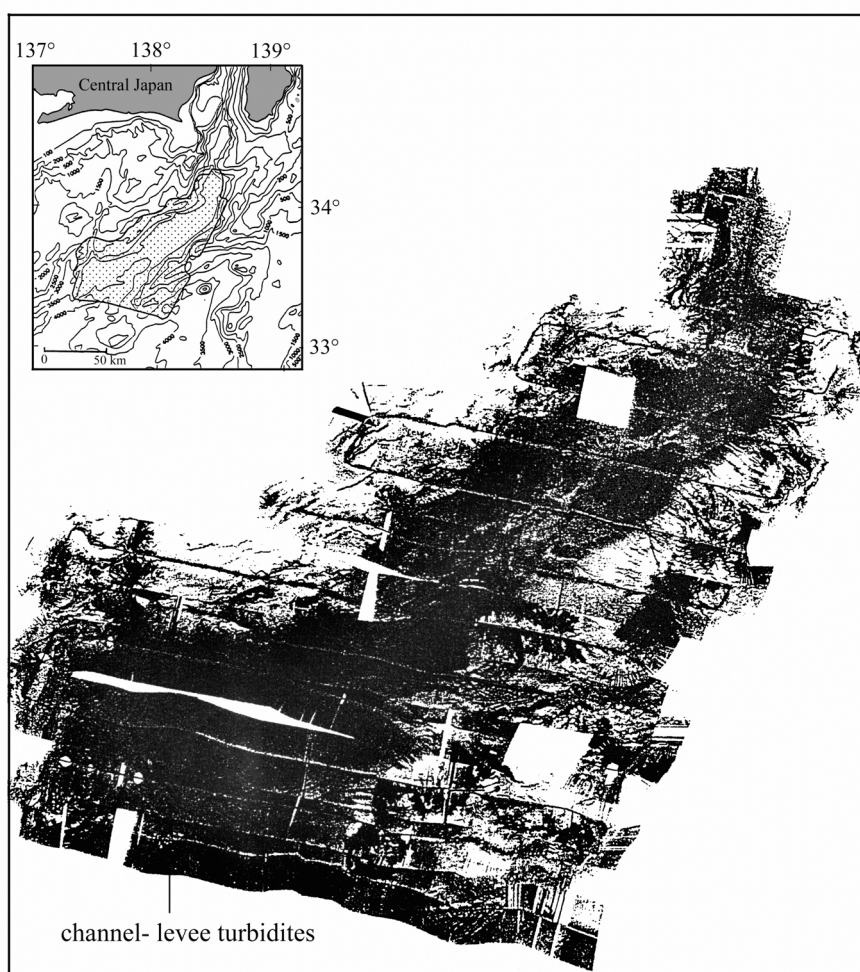


Fig. 3.2 Sidescan image of the eastern Nankai Trough and Zenisu Ridge. Inset shows the location of the sidescan image. The dark regions comprise turbiditic sands and silts in the Nankai Trough, as well as volcanoes and rock outcrops on the Zenisu Ridge (after Tokuyama, 1998).

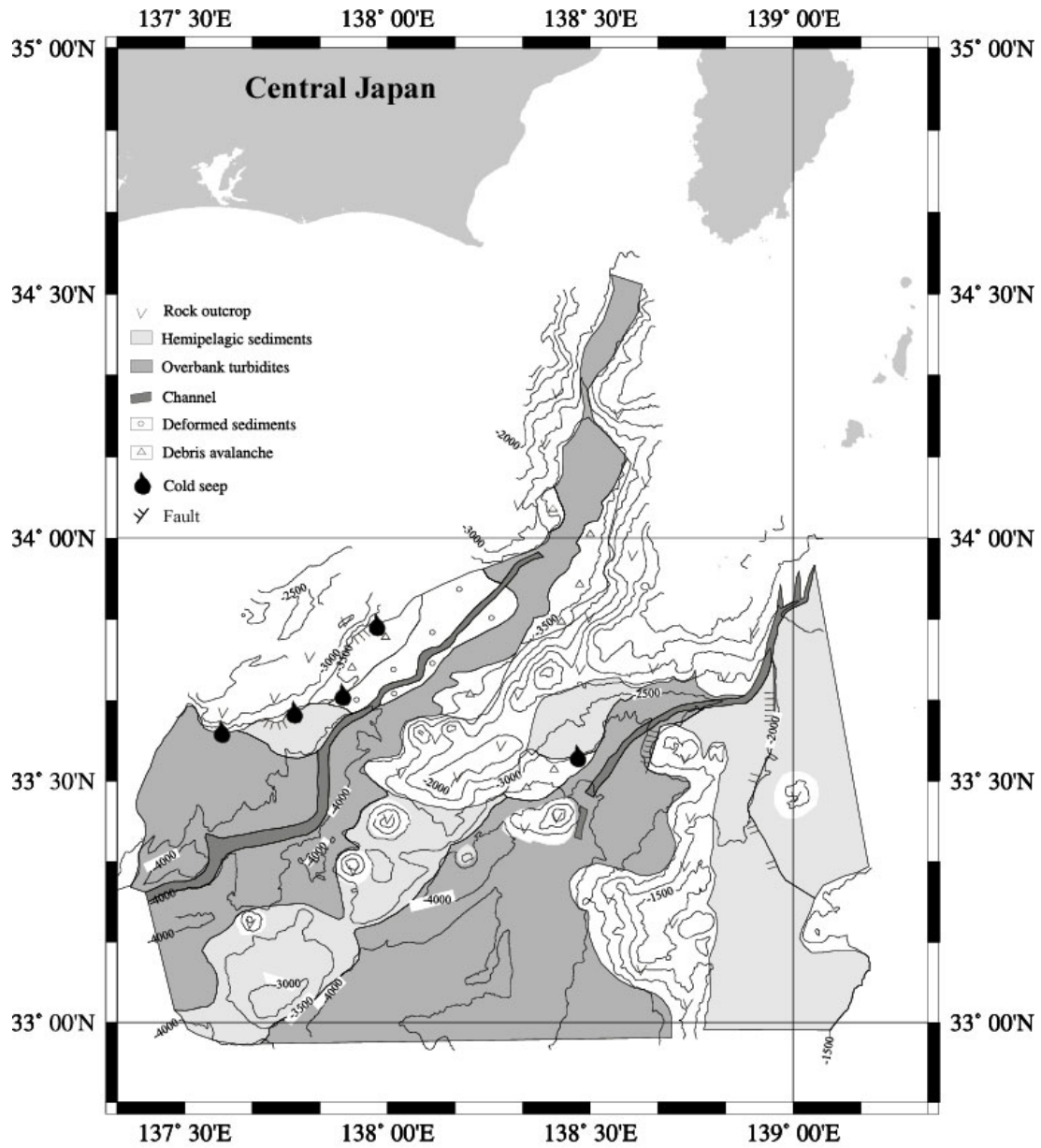


Fig. 3.3 Distribution of bottom sediment types in the Nankai Trough observed from submersibles and deduced from seismic data.

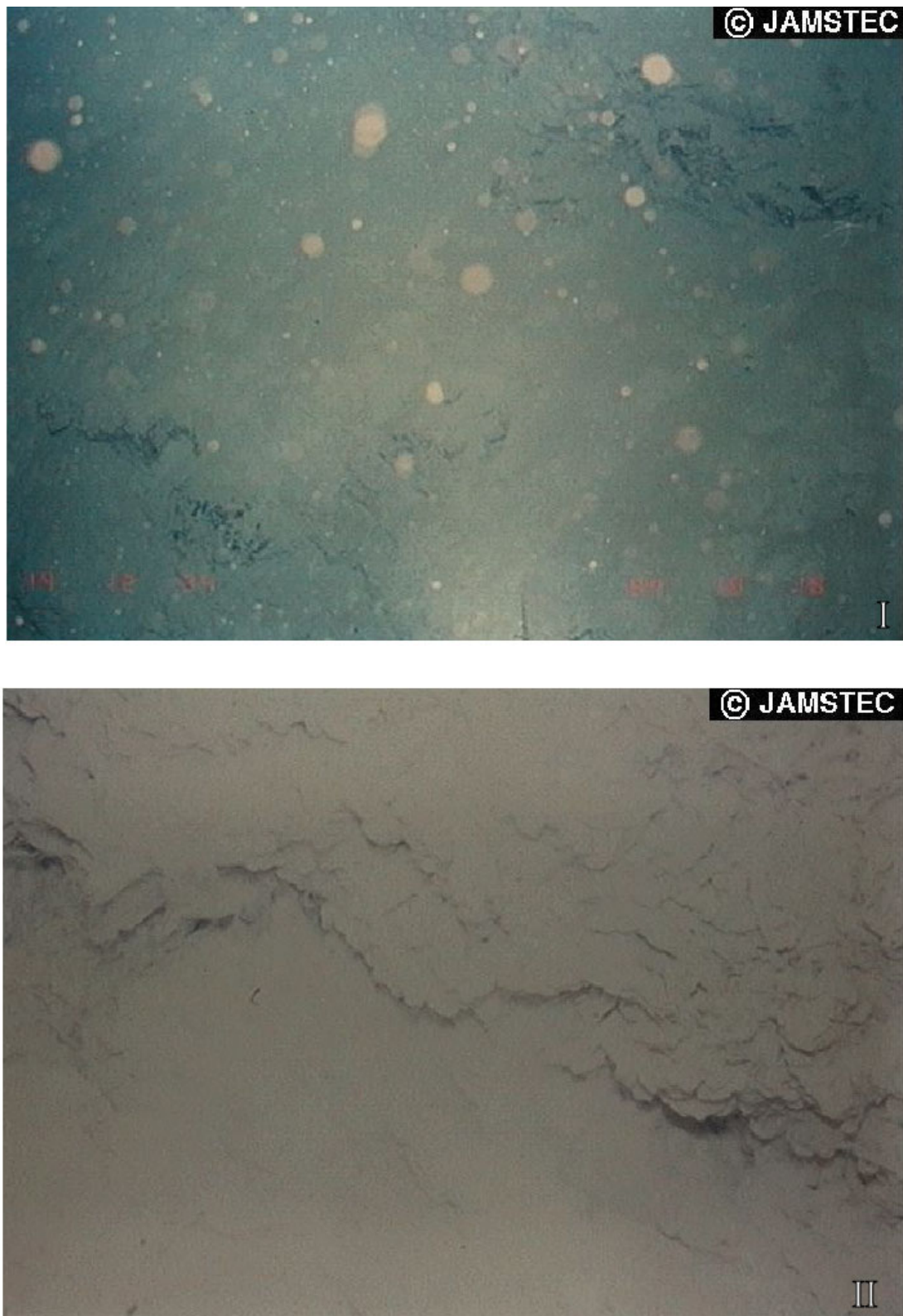


Fig. 3.4a Outcrop of mudstones and debris flow deposits (the dominating lithologic unit) observed during dive 400 on the northern slope of the Nankai deep-sea channel. Photo I, debrites and mudstones; Photo II: fine mud turbidites on the lower slope of the Nankai Trough.

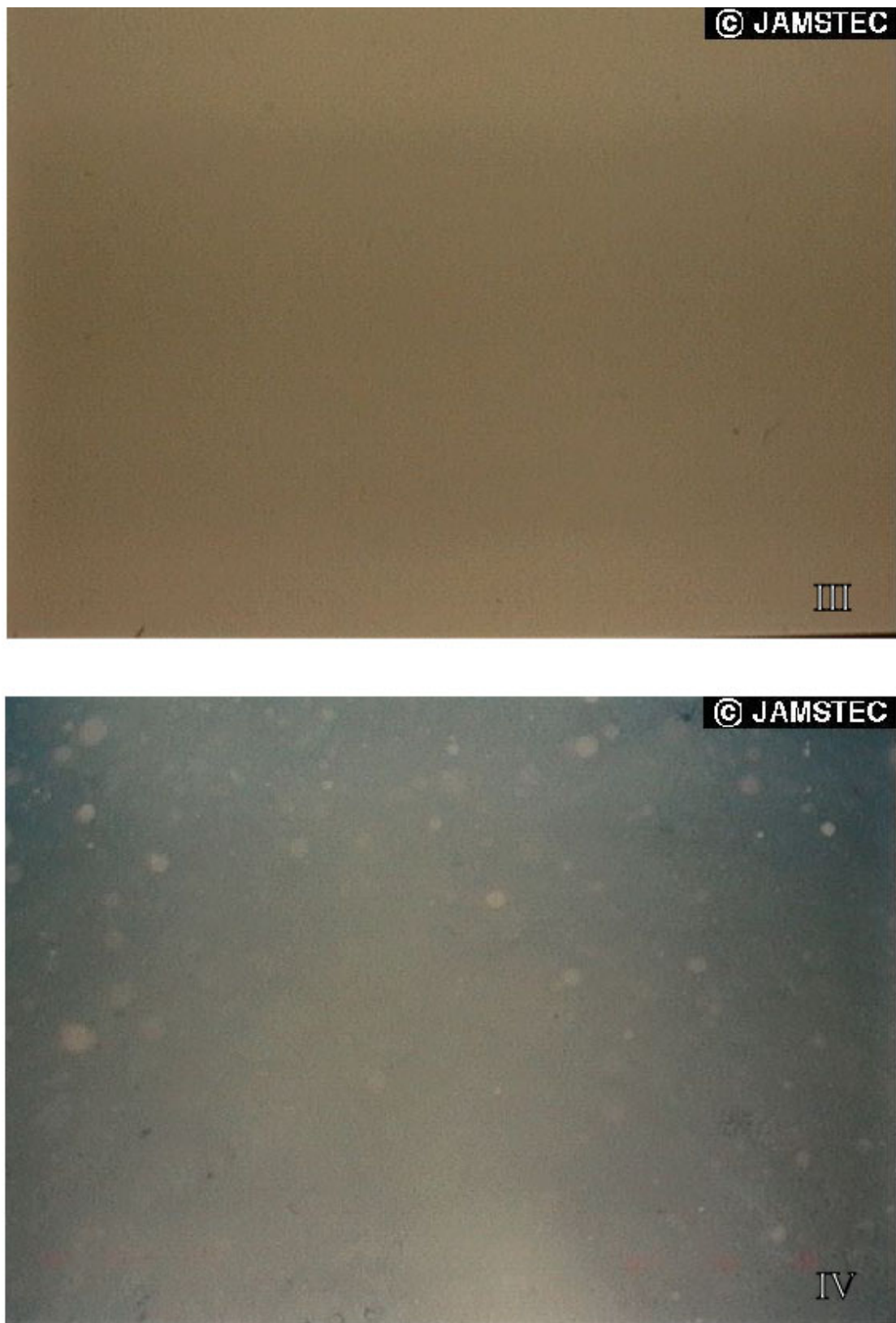


Fig. 3.4b Mud seafloor (Photo III) and turbidity flow (Photo IV) observed during dive 400 on the northern slope of the Nankai Trough.

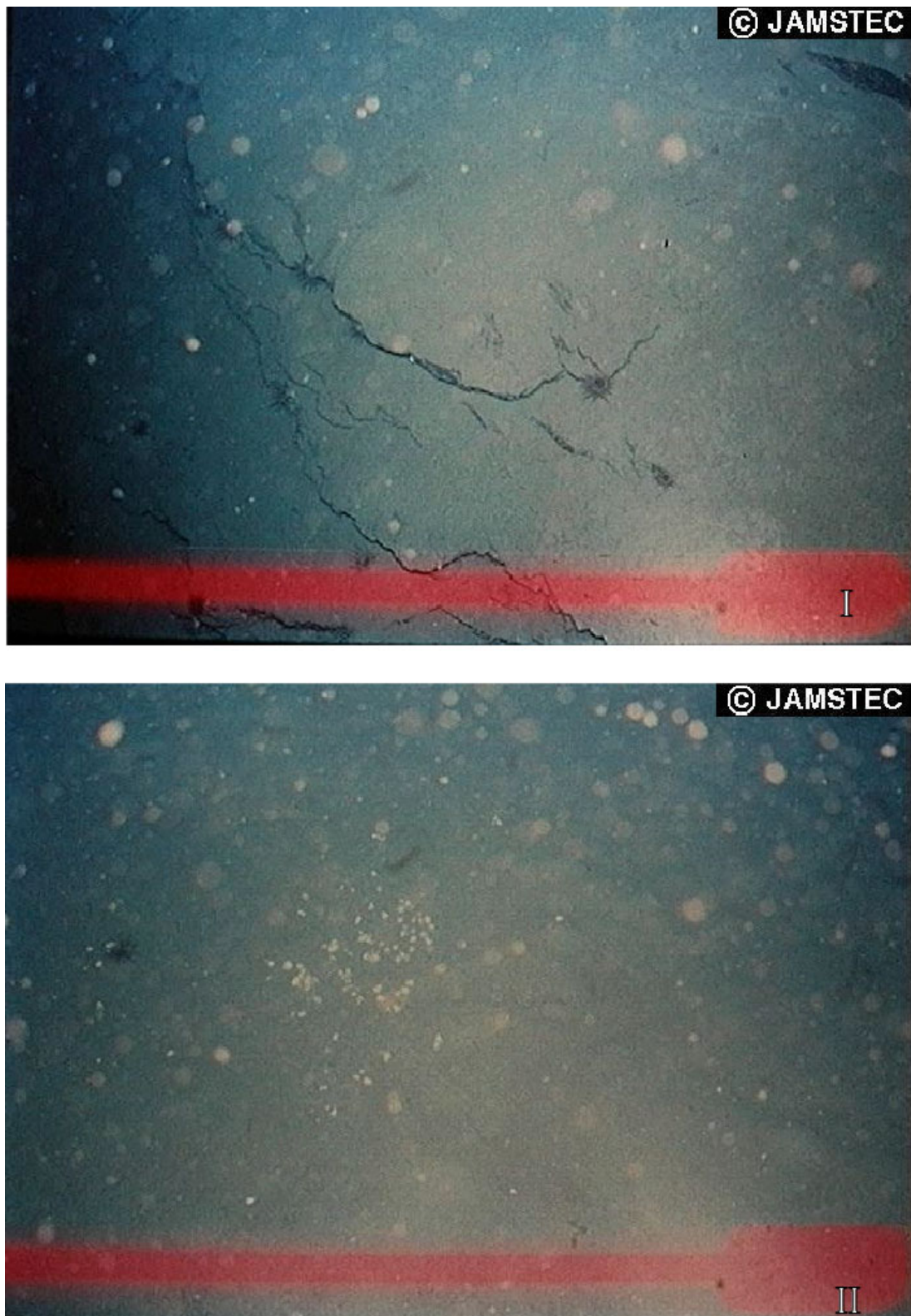


Fig. 3.5 Thin coarse sediments and carbonate limestones at the frontal thrust fault of the central floor of the Nankai deep-sea channel observed during dive 322. Photos I, II: Outcrop of mudstones which is the dominating lithological unit. Note the two fracture systems oriented perpendicular to each other.



Fig. 3.6a Coarse sediment with outcrop of mudstones observed during dive 323 in the Nankai deep-sea channel. Photos I, II: finely laminated mudstones and debris at the a cliff.



Fig. 3.6b Photos III, IV: fine turbidite sediment observed during dive 323 in the Nankai deep-sea channel.



Fig. 3.7 Photo I: coarse calcareous turbiditic deposits observed during dive 401 at the central part of the Nankai deep-sea channel. Photo II: seep communities at the central part of the channel.

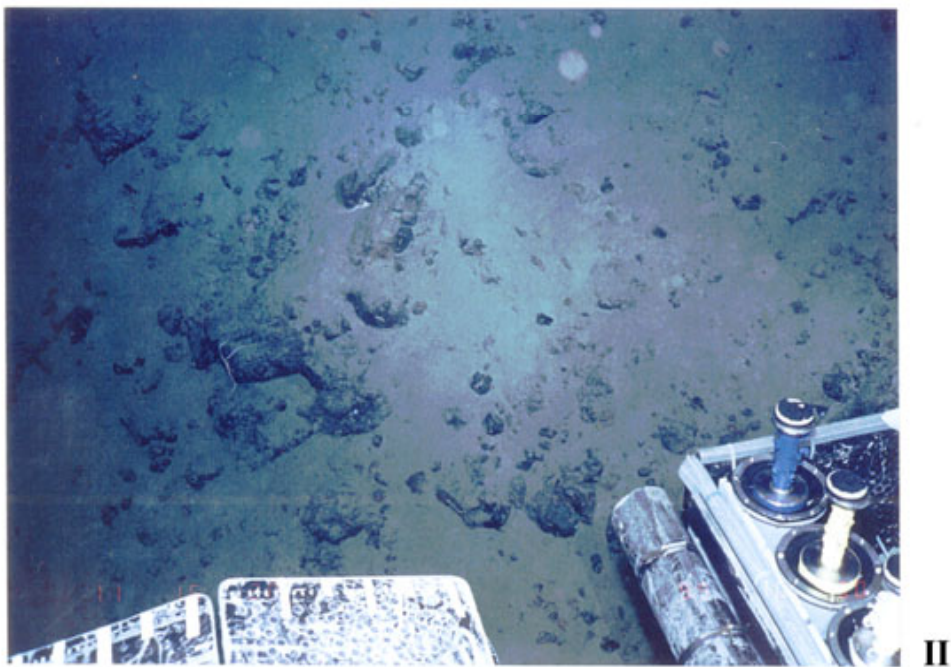
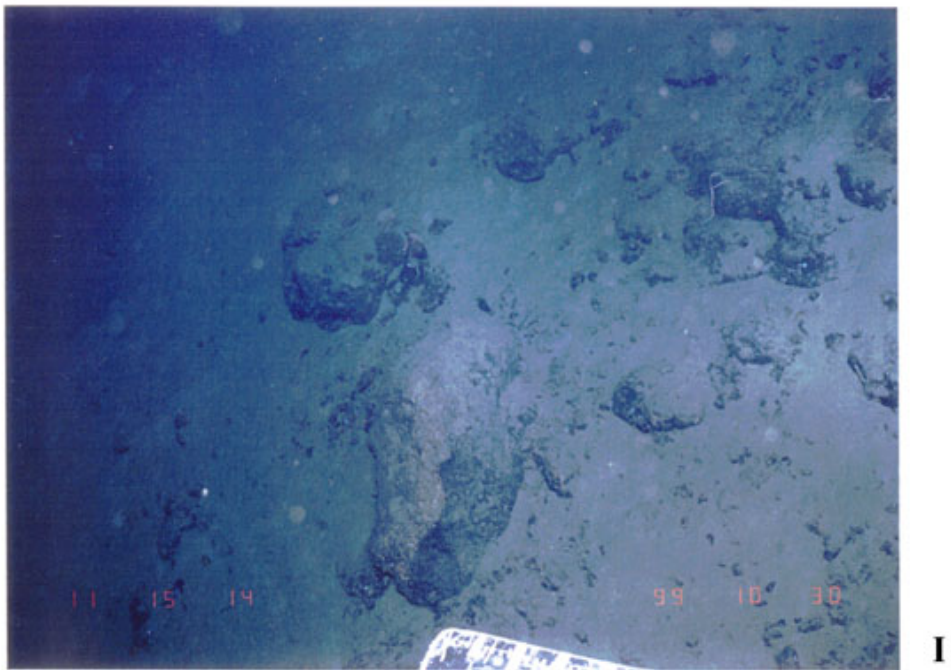


Fig. 3.8a Photos I, II: volcaniclastic breccia on the southern slope of the Nankai Trough.



Fig. 3.8b Photo III: outcrop of basaltic (basaltic andesite) volcanic breccia at the northern cliff of the Zenisu Ridge (sampled by submersible). Photo IV: fresh andesite, hydrothermal Mn-oxide and altered andesite (crust). Photo V: angular volcanic rocks and altered aphyric basalt.

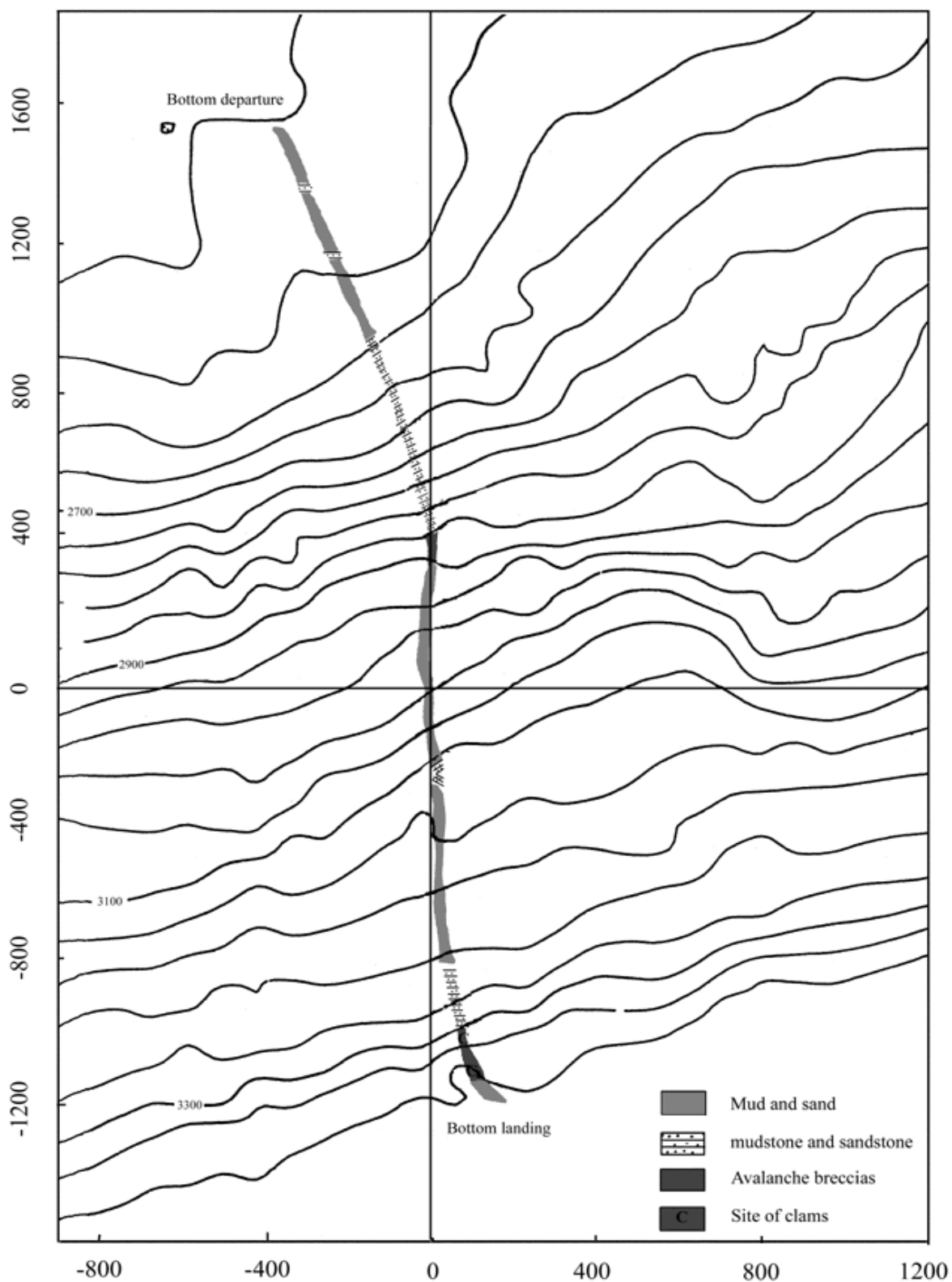


Fig. 3.9 Bathymetry and track line of dive 523. See Fig. 3.1 for location of dive site.

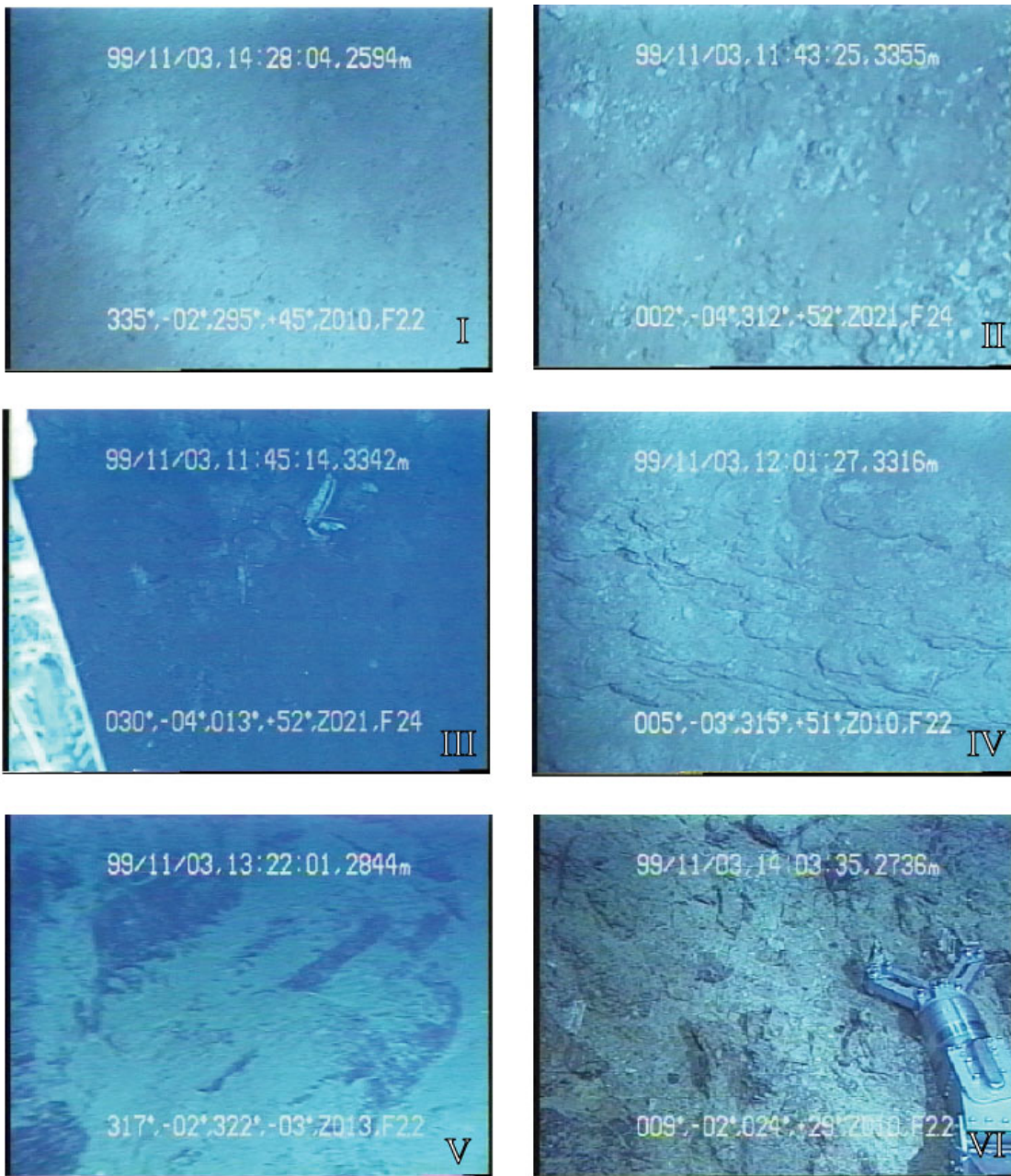


Fig. 3.10 Observations during submersible dive 523 on the southern slope of the Zenisu Ridge. Photos I, erosional seafloor. Photo II: Debris flow sediments on the seafloor of Zenisu Trough. Photo III: deep sea community and debris. Photo IV: Outcrop of lithologically dominant mudstones at lower scarp of the slope. Photo V: Outcrop of mud stones with two well-developed fracture systems striking 290° and 358° respectively. The fracture planes are steep. Photos VI: Sampling (semiconsolidated mudstone) by using the submersible *Shinkai 6500*.

### 3.1 Deep sea channel revealed by using sidescan imagery

Sonar system can be divided into three categories: echo-sounders, sidescan sonars, and multibeam sonars. Echo-sounders transmit one single beam. Oriented vertically. Sidescan sonars generally transmit two beams, one on each side. And multibeam sonars transmit several tens of on each side. These systems may acquire bathymetry, or acoustic imagery or both. The most recent generation of multibeam systems is hull-mounted shallow-towed, deep-towed, or is autonomous.

Early sidescan imagery of the ocean floor were made with a deep-tow transducer operating at 120 kHz or 240 kHz towed a few meters above the sea bottom by several thousand meters of conductor cable (Spiess and Mudie, 1970). Large drag forces made low towing speeds necessary ( $<1.0$  m/s-1). The next major technical advance was made with the construction of a dual-scan, long-range towed sonar known as GLORIA (Blondel and Murton, 1997). A new method of producing contoured bathymetric plots using echoes from the off-track region was developed for the United States Navy during the 1960s. The configuration of the transducers allows a large number of sideways reflected signals to be received. Several multibeam systems are now commercially available for deep-sea surveys. These include the Seabeam 2100.

The multibeam echo-sounding system consists of 12 kHz projectors. The swath width varies from  $120^\circ$  for the SeaBeam system at intermediate water depths to  $90^\circ$  in deeper waters. The total swath width for the sidescan image is about  $160^\circ$  and a 2000 pixel image for 1 ping is obtained. The system includes a 4 kHz subbottom profiler subsystem. The data obtained include bathymetric data, sidescan records (binary sidescan image), nautical information, and correction parameters such as the water velocity structure. An important parameter which controls the accuracy of depth and position is the vertical sound velocity profile.

The eastern Nankai Trough is a subduction zone where oceanic crust is destroyed. The deep seafloor is characterized by extreme topographic relief, and the trenches are dominated by tectonic and sedimentary processes. Investigation of the deep ocean trenches poses serious technological problems primarily because of their large depths and their extreme bathymetric variation and, to a lesser extent, their narrowness. Surface-towed sonar devices require high power to produce echoes with acceptable signal-to-noise ratios from a vertical two-way travel path that can be as much as 20 km. For sidescan sonars, the large depths result in a wide nadir zone from which little usable data are returned. This is complicated by the narrowness of the deep-ocean trenches.

Before attempting any interpretation of the sidescan sonar imagery (Fig. 3.11), it is important to know a number of details about the acquisition system. For many who are experienced in the field of sidescan sonar interpretation, these parameters are

automatically taken into consideration. However, for the less experienced, a check-list of parameter that needed to be considered is compiled. During interpretation, this check-list is referred to repeatedly.

Our SeaBeam 2100 sidescan sonar data cover the entire Zenisu deep sea channel (Fig. 3.11) and provide images of large scale features including the channel extension, seamounts and sediment (Fig. 3.12). The most striking feature of this image is the large area of smooth, low backscatter. This suggests an area of thick, soft sedimentary fill in the Zenisu trough. Brighter areas are regions of coarser sediment and rougher morphology. The dark tree-like structures on the sidescan image are the channels. The main channel extends N55° E.

On both sides of the map, high backscatter patches indicate outcrops of volcanic rock and seamount (Fig. 3.12). The axis of the deep sea channel near the slope also has a high backscatter. The high backscattering strengths of these features probably reflects a coarse sediments supply or erosion along the deep sea channel (Fig. 3.13).

Our sidescan sonar images, swath bathymetric data and submersible observation show that the three observed types of sonar imagery correspond to three different sediment types in the study area. The first with light backscatter indicates turbidites of different ages which are distributed on the bottom and flank of the trough floor. The second corresponds to debris avalanche deposits along the foot of the slope, which is part of the filled channel-levee and fan system (Wu et al., 2000). These sediments were transported from the Izu-Ogasawara Arc via the Zenisu Canyon. The seafloor itself is subjected to erosion during the sea-level highstand of the Holocene. Rock outcrops, boulders and gravel have been observed only in the west, in particular along tracks of the Nautila and the Shinkai 6500. The third sonar image type is interpreted as hemipelagic mud on the slope, including biogenic deposits.

Slumps and slides: extensive, often lobate downslope deposits with contrasting backscatter, rough surface textures, blockiness, and acoustic shadows at the headwalls.  
Debris flows: uniform, generally with medium backscatter, sometimes with lineations;  
Turbidity currents: low backscatter is confined to the channel as the acoustic signal is attenuated.

### **3.2 Debris flow on the western slope of the Nankai Trough**

On the western slope of the Nankai Trough, many dives (Table 3.1) have been carried out to study the deformation and sedimentation of the accretionary wedge as well as the dewatering processes and seep communities. Mudstone and sandstone occur on the steep scarps of the accretionary prism. Fig. 3.4, photos I and II show rock

outcrops covered by very thin fine-grained sediments. Fig. 3.4, photos III and IV show several clams and pebbles scattered on muddy sediments on the lower slope. Debrites with seep communities were frequently observed on the slope from the submersibles Nautila and Shinkai 6500 (Le Pichon et al., 1987; 1992).

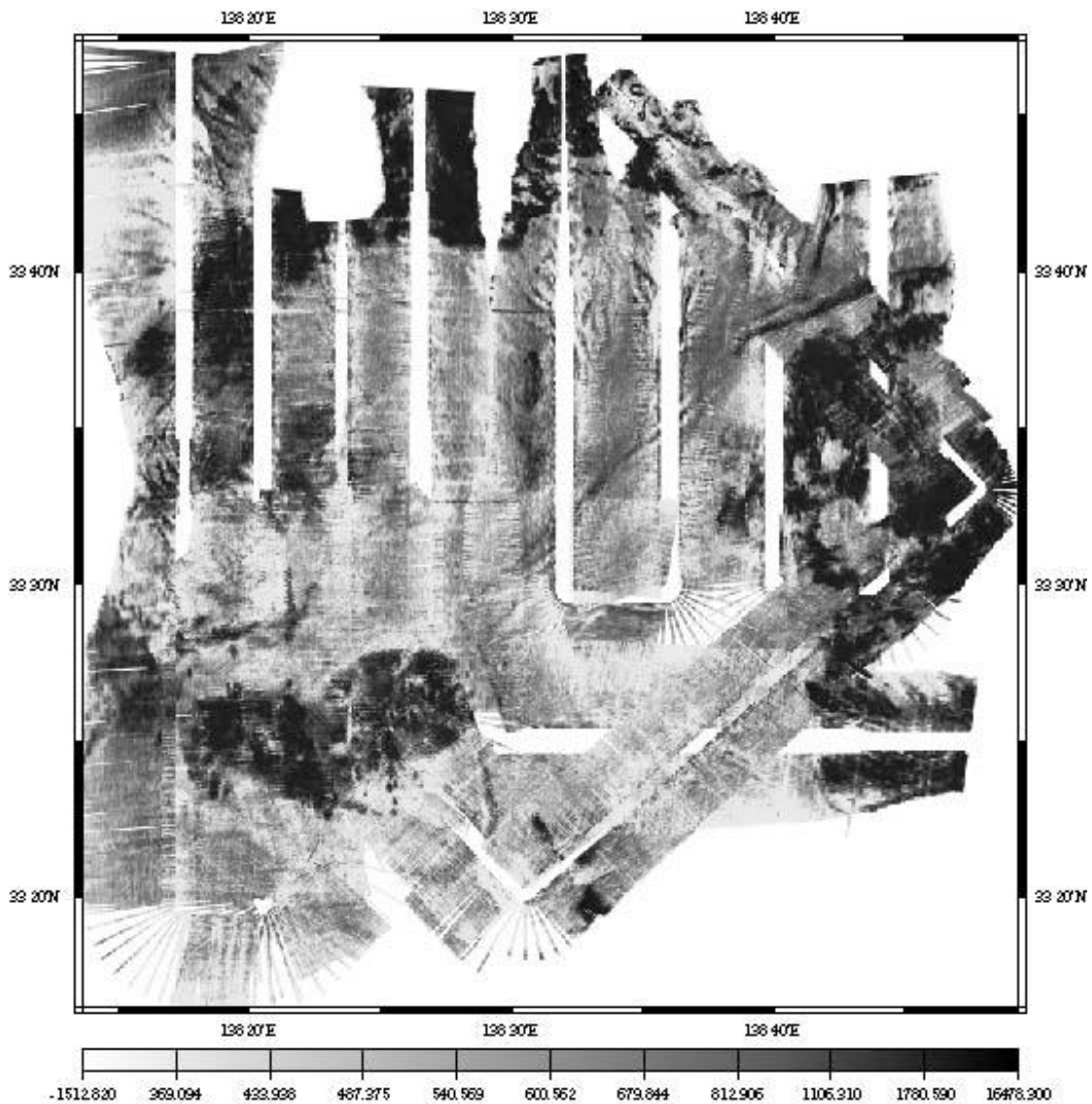


Fig. 3.11 Multibeam sonar image of the Zenisu deep sea channel collected during cruises YK99-09 Leg 2 & YK00-06 Leg 1 of the R/V Yokosuka. SeaBeam 2100 edited data, angle correction and low-pass smoothing filter were applied. Mercator projection was used in the mapping.

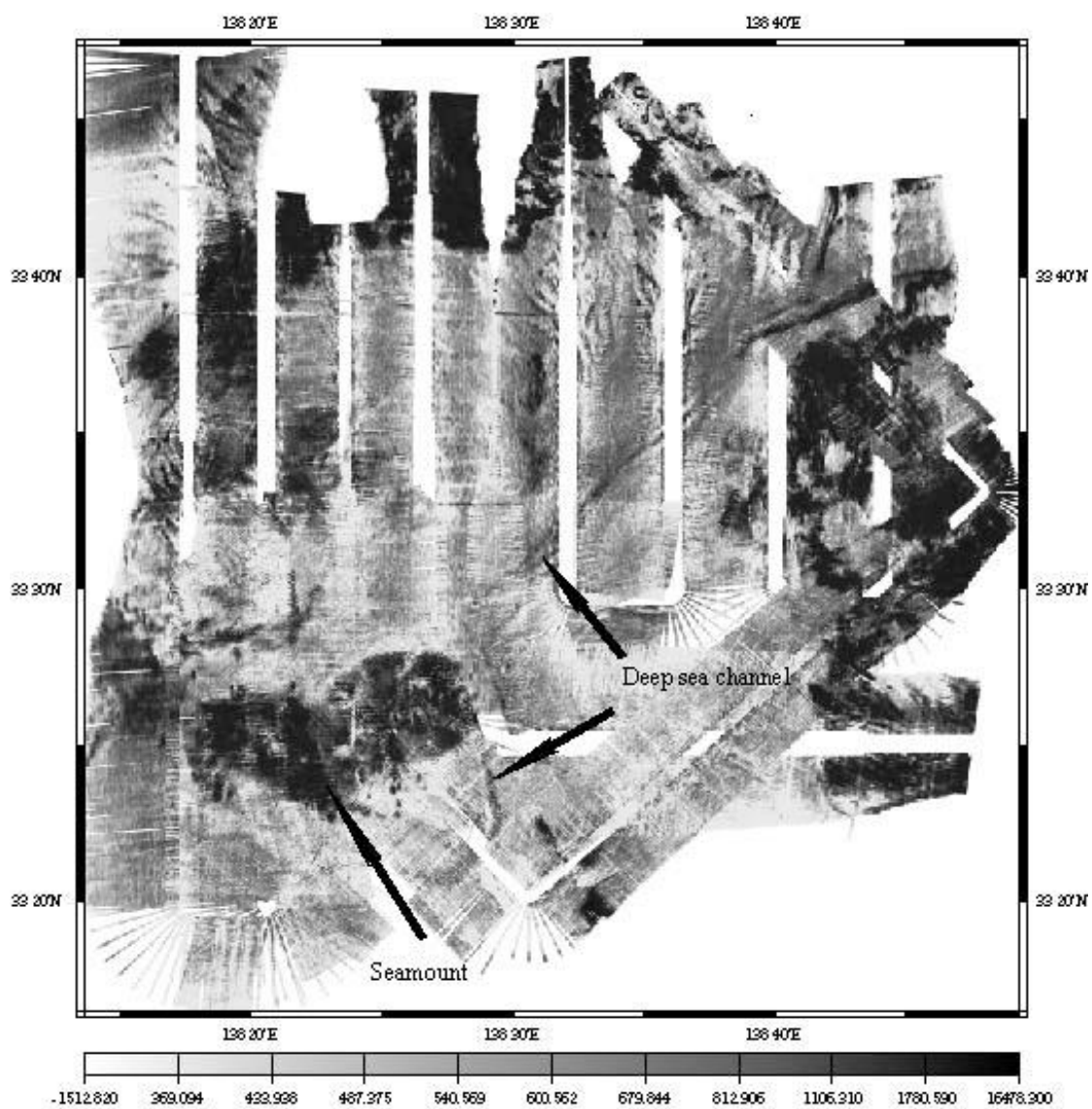


Fig. 3.12 Multibeam sonar image. Dark color indicates seamount or outcrops of volcanic rocks. Lineament in gray is the Zenisu deep sea channel.

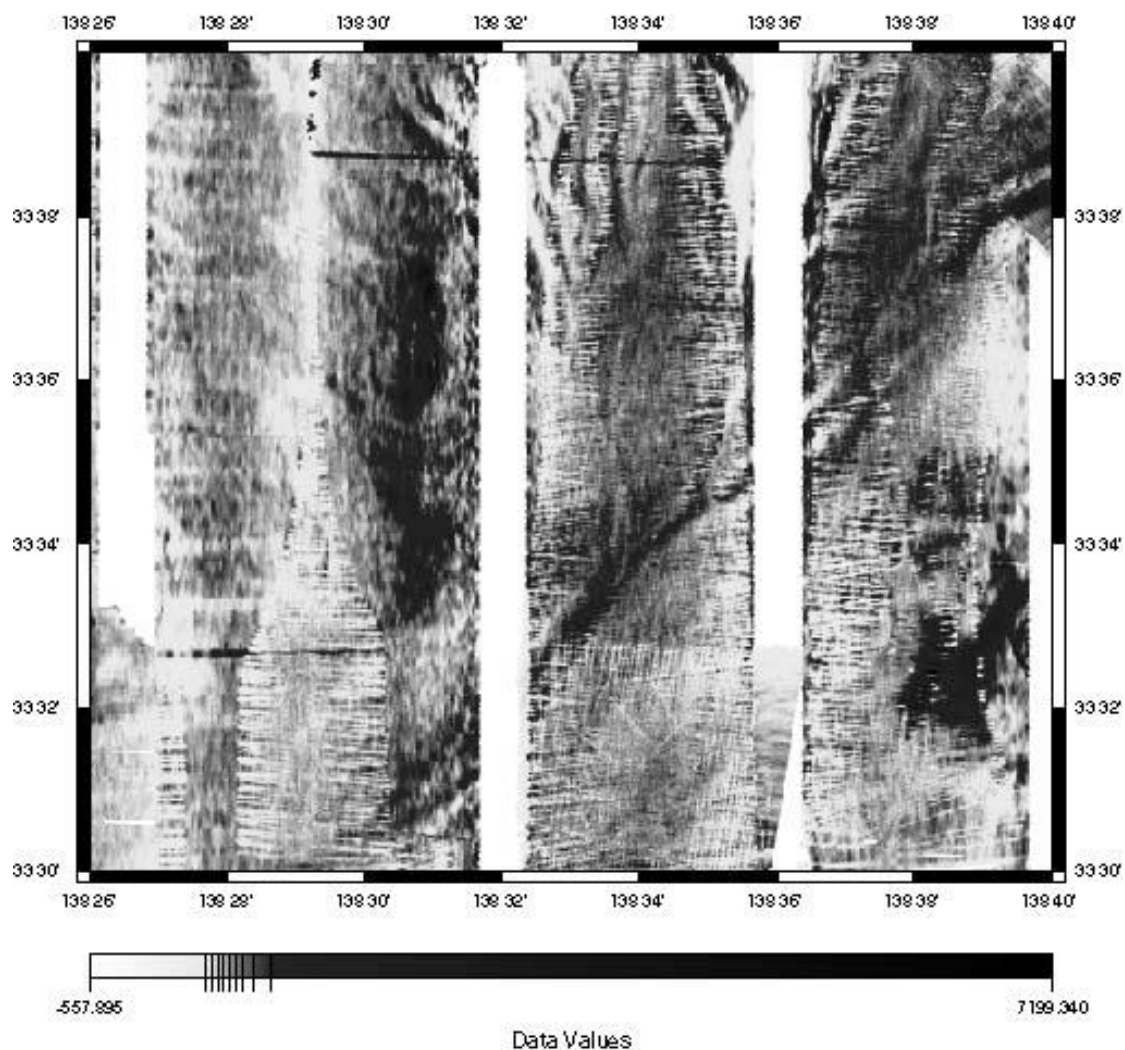


Fig. 3.13 Multibeam sonar image. The dark color show the deep sea channel.

A large range of debris flow deposits were mapped by using the 4000 m class Deep Tow System and the ROV Kaiko (Fig. 3.3). According to results from the Deep Tow System of the Japan Marine Science and Technology Center (JAMSTEC) which is equipped with color and monochromatic TV, debris sediments are widely distributed on the lower accretionary slope and the adjacent seafloor. Rock outcrops, boulders and gravel have been observed only along the tracks DT-7C and DT-10C on the western slope of the Nankai Trough during cruise KH8-1 of the R/V Hakuho-mura (Kobayashi et al., 1992; see Fig. 3.1 for dive location). These boulder and gravel deposits are distributed discontinuously in a preferred direction. They probably represent breccias related to the accretionary prism of the Yuki Ridge. Boulders, gravel and fine-grained sediments are typical debris deposits. They dominate along the entire track with only two exceptions: rock outcrops along a steep scarp at dive time 15:52:46 h, and

bioclastic sediments at dive time 16:19:00 h succeeded by mud. Current-induced bedforms are absent. From 16:14 to 16:18 h, shell beds are encountered. The shells are broken implying that they have experienced reworking (Kobayashi et al., 1992).

Dive site 5 of Le Pichon et al. (1987) on the lower accretionary wedge is located on rugged terrain with numerous scarps, some of those near the center of the track are over 50 m in height. With only a few exceptions, talus and rock outcrops occur over the entire track. The talus material is poorly sorted and angular. Gravel, sand and silt deposits are observed within a small canyon. Other features recorded include debris apron and numerous living as well as dead clams.

### 3.3 Deposits in the central Nankai Trough

During our survey cruises (YK99-09 Leg 2 and YK00-06 Leg 1 of the R/V Yokosuka) two dives (dives 557 and 558) were carried out in the central Nankai Trough for the detailed observation of seep communities in addition to previous submersible dives and deep tow surveys to study the sedimentary processes and fluid activity (Kobayashi et al., 1992; Le Pichon et al., 1989; 1992; see Fig. 1.3). Other dives (68-70, 401-404, 113-115, 322, 323, 401-404) concentrated on sedimentation processes at the central part of the trough (Henry et al., 1989; Kobayashi et al., 1989; Le Pichon et al., 1987; 1989).

In the central part of the channel, turbidity currents are common (Figs. 3.4 photo II and 3.5 photo II, dives 400 and 322). Coarse turbidites have been recovered by dredging and coring from the central channel where the bottom sediments consist mostly of sand, but bedforms indicative of bottom currents are absent. Deposits on the flat seafloor on both sides of the channel are fine-grained (Fig. 3.7).

On the flat seafloor of the trough, several sediment samples were collected from a submersible. At a site at 3761 m water depth, a 12 cm long core (ROV dive, Fig. 3.1) collected during cruise 97-05 of the R/V Kairei shows that the upper 3 cm is composed of olive-brown mud, which grades to 6 cm of grayish-olive sandy mud, which is in turn underlain sharply by olive-gray mud laid down under reducing conditions. Laminations have not been seen. Two other cores of dark mud were also collected, one of which consists of 9 cm of laminated mud of various colors. Several clams of the *Calyptogena* spp. were observed along the frontal thrust fault during this dive, while Henry et al. (1992) found cold seep communities away from the frontal thrust fault on a shallow detachment fault.

Table 3.1 Observations using the submersible *Shinkai 6500*

Dive	Date	Observer	Location	Depth (m)
68	07.22.1991	X. Le Pichon	central NT	4015
69	07.23.1991	S. Earlt	central NT	4018
70	07.24.1991	P. Henry	central NT	3830
113	05.24.1992	T. Gamo	central NT	3751
114	05.25.1992	J. Segawa	central NT	3750
115	05.26.1992	N. Yoshida	central NT	3760
322	07.27.1996	K. Kobayashi	central NT	4036
323	07.28.1996	A. Takeuchi	central NT	3793
324	07.30.1996	P. Henry	south ZR slope	3806
325	07.31.1996	S. Mazzotti	south ZR slope	3275
326	08.01.1996	M. Hattori	central NT	3844
327	08.03.1996	H. Tokuyama	seafloor of ZT	4145
371	07.22.1997	J. Segawa	Zenisu Canyon	2686
399	10.16.1997	H. Tokuyama	central NT	4123
400	10.18.1997	Y. Kono	central NT	3969
401	10.20.1997	K. Nakayama	central NT	3784
402	10.21.1997	P. Henry	central NT	4033
403	10.23.1997	S. Lallemand	central NT	3722
404	10.25.1997	K. Tachibana	central NT	3848
521	10.31.1999	I. Sakamoto	ZR north slope	2374
523	11.03.1999	S. Wu	ZR south slope	3390
555	07.10.2000	S. Ohta	ZR south slope	3390
556	07.11.2000	S. Wu	ZR south slope	4000
557	07.12.2000	S. Ohta	NT west slope	3980

Carbonate deposits were observed only at the steep scarps of the frontal thrust fault (Fig. 1.4) in the central Nankai Trough (Fig. 3.5 photo I; dive 322). During dive 323, subhorizontal massive mudstones were reported (Figs. 3.6I, II). The dominating rock formation is a poorly- consolidated, layered mudstone of late Quaternary age (nannozone NN21, younger than 0.23 Ma) that is generally affected by two perpendicular Y joints (Le Pichon, 1992). Fine sediments are widespread on the flat part of the trough (Figs. 3.6; 3.7a). Seep communities were encountered during dives 401-404, 557 and 558. Fig. 3.7 photo II shows the distribution of clams at the central part of the channel.

### **3.4 Sedimentary processes on the northwestern slope of the Zenisu Ridge**

The manned submersible dive 521 during cruise YK99-09 Leg 2 of the R/V Yokosuka (Fig. 3.1) was conducted on the northwestern slope of the Zenisu Ridge. It started from a water depth of 2600 m and ended at 1000 m to study the volcanic sedimentation and tectonics of the Zenisu Ridge. The most common deposits are debris flow sediments which were also sampled during the dive (Fig. 3.8). The debrites include volcanoclastic grains (Fig. 3.8a) and terrigenous material. There are no dive data on the lowest part of the slope. Seismic data collected within the Kaiko Tokai Project show that debris flow sediments also dominate on the lower slope (Kimura et al., 1987). These debris flow deposits are very widespread on the slope of the northern Zenisu Ridge (Okimura et al., 1999). They consist of volcanic detritus with the same composition as the source rocks. Fig. 3.8 photo III shows an outcrop of volcanic rocks which vary from basalts to andesites. Fig. 3.8 photos IV and V show these basaltic and andestic rocks respectively.

### **3.5 Sedimentary processes on the southeastern slope of the Zenisu Ridge and the floor of the Zenisu Trough**

Several dives (dives 324, 325, 371, 399, 523, 555 and 556) were executed on the southeastern slope of the Zenisu Ridge and in the adjacent Zenisu Trough (Fig. 3.1), of which two (dives 523 and 556) were executed and one (dive 555) co-opted by me. Three types of sediment facies were distinguished during dive 523 on the southern Zenisu slope (Fig. 3.9). These are: turbidites of different ages on the southern slope of the Zenisu Ridge and the floor of the Zenisu Trough, debris avalanche deposits along the base of the Zenisu Ridge, and hemipelagic muds including biogenic deposits on the slope (Fig. 3.3).

### 3.5.1 Turbidites of different ages on the southeastern slope of the Zenisu Ridge

Dive 523 was conducted on the southeastern Zenisu Ridge at 33° 34.00' N, 138° 26.3719' E (Fig. 3.9). The survey track is directed up a low hill with a flat top which rises from a flat surrounding seafloor. The average slope angle is 16°, with maximum values on the upper and lower sections reaching 30° and 35° respectively. The water depth along the track decreases from 3389 to 2559 m. Five samples (mudstones and fine sandstones) were collected at 4 sites along the survey track. Rocks outcrop along the entire track except at the flat top of the hill and the gentle section on mid-slope (Fig. 3.10).

Evidence for an active fault observed during this dive includes: (1) inclined mudstone beds at the steep slope of the section; (2) widespread occurrence of avalanche breccias and sediment slides suggesting uplift and faulting; and (3) small fault planes or joints developed in the sedimentary layers. Most of the slope is covered by mudstone and siltstone with rock outcrops. Video camera imagery shows that these outcrops are uniform in color and structure. Avalanche breccias, small slides and a few shells (less than 10 individuals at each site) were observed at the base of the slope. The breccias vary in size but are angular. A thin mud veneer covers the gentle section in mid-profile (12:30-12:40). Thin- and medium-bedded mudstones with joint fractures occur at the middle of the track line (Fig. 3.10 photo IV). Mudstones or sandstones are widespread along the track except at the top, channel floor and gentle mid-section of the swell. Inclined strata were observed at the base of the southern Zenisu Ridge.

Two types of turbidites occur on the slope of the Zenisu Ridge (Figs. 3.9 and 3.10). The first, younger turbidites (Unit A, see Fig. 4.11) forms a channel or trough-filled channel- levee and fan system. They are restricted to the trough axis channel, and consist of late Pleistocene fine sand and mud transported from the Izu-Ogasawara Arc via the Zenisu Canyon, which was cut retrogressively during the Holocene sea-level rise. These turbidites make up a typical channel-levee system for the most part, but grades into a trough-fill turbidite system southward. Tokuyama et al. (1998) suggested that these sediments are less than 1 Ma in age, while our biostratigraphy of dive 523 shows that they consist mostly of Pleistocene sediments. The older turbidites (Unit B) are exposed along the dive track on the southern flank of the Zenisu Ridge. Rock samples SP1 and SP2 (Fig. 3.14) show graded bedding, cross-stratifications and erosional surfaces typical of a turbidity flow.

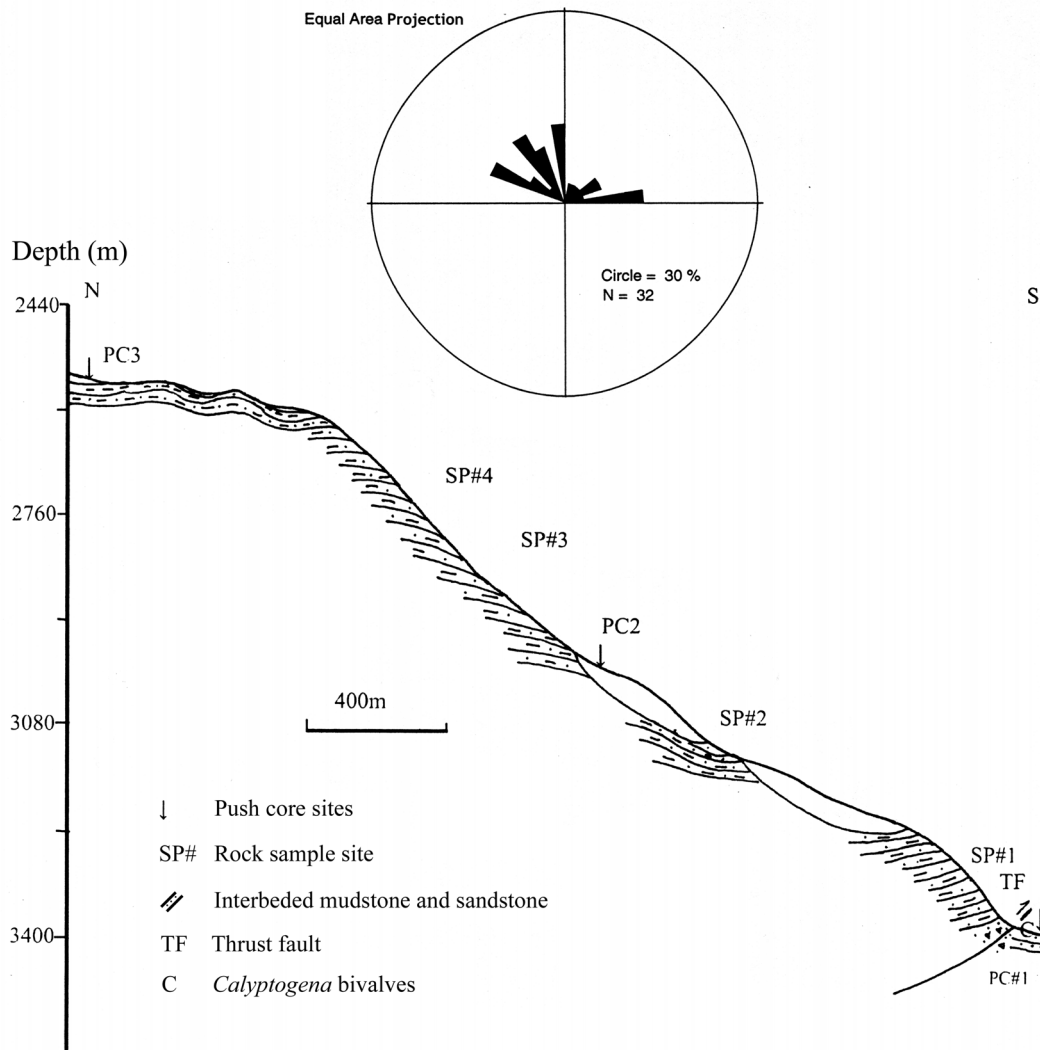


Fig. 3.14. Schematic geological profile along the track of dive 523. Insert is a joint rose diagram.

The grain size distribution of push cores PC11, PC13, PC15 and PC17 collected from dive 523 are shown in Tables 3.2 to 3.5. Grain size parameters of sediments sampled during dives 523 and 556 are shown in Table 3.6. The bottom sediments range from clayey silt to silty clay. Sorting of the sediments range from 1.522 to 1.933 (poorly-sorted). The skewness varies from positive to negative. Positive skewness suggests sandy silt because of sand enrichment in some deposits. Table 3.4 gives the

grain size distribution of sediments from sample PC15 of dive 523. The cumulative grain size curves (Fig. 3.16) are not typical of turbidity current deposits, but rather suggest an admixture of hemipelagic sediments and volcanoclastic turbidites.

Nannofossils from four rock samples collected during dive 523 were analyzed. The calcareous nannofossils from sample 6K523R3 include: *Discoaster asymmetricus*, *Discoaster brouweri*, *Discoaster pentaradiatus*, *Discoaster surculus*, *Discoaster tamalis*, *Pseudoemiliana lacunose* and *Reticulofenestra pseudumbilica*. At ODP site 808C, the last occurrence of *Discoaster tamalis* lies within the upper part of nannofossil zone NN16, and the top of zone 15 (3.65 Ma) is marked by the last occurrence of *Reticulofenestra pseudumbilica*. The first occurrence of *Discoaster asymmetricus* represents nannozone NN13 which is about 4.1 Ma in age (Olafsson, 1993). Since this zone is comparable to the subzone CN11b12a of Okuda and Bukry (1980), it is Pliocene in age (4.16-2.65 Ma).

What led to the debris flow sedimentation? For the Amazon fan, results of Ocean Drilling Project Leg 155 show that large-scale mass transport deposits make up a significant component of the fan sediments. Each mass-failure event was the result of a catastrophic failure of the continental slope and has been dated and corrected for climate-induced sea-level changes. Two different mechanisms could have triggered these catastrophic slumps: (1) rapid drops in sea level which destabilized the continental slope gas hydrate reservoirs, causing slope failure and giving rise to mass transport deposits during glacial times, and (2) deglaciation of the Andes and the consequent flushing of the Amazon River sediments (Flood and Damuth, 1987; Maslin et al., 1998). On a convergent margin, tectonics and earthquakes may trigger debris flow activity in the channels (Ishi et al., 1999; Ito et al., 1999; Mchugh and Ryan, 2000).

### **3.5.2 Debris avalanche at the base of the Zenisu Ridge**

Internally fractured debris avalanche sediments are distributed along the base of the Zenisu Ridge. These deposits have been observed over a small area during dive 523 and 556. Southwest of the dive area is a large submarine landslide readily distinguishable on the SeaBeam bathymetry (Fig. 3.15). It is marked by a normal fault scarp on the upper slope and ca. 5×5 km<sup>2</sup> of debris on the lower slope. The abundance of submarine landslides demonstrates the importance of mass-wasting processes during the evolution of this ridge.

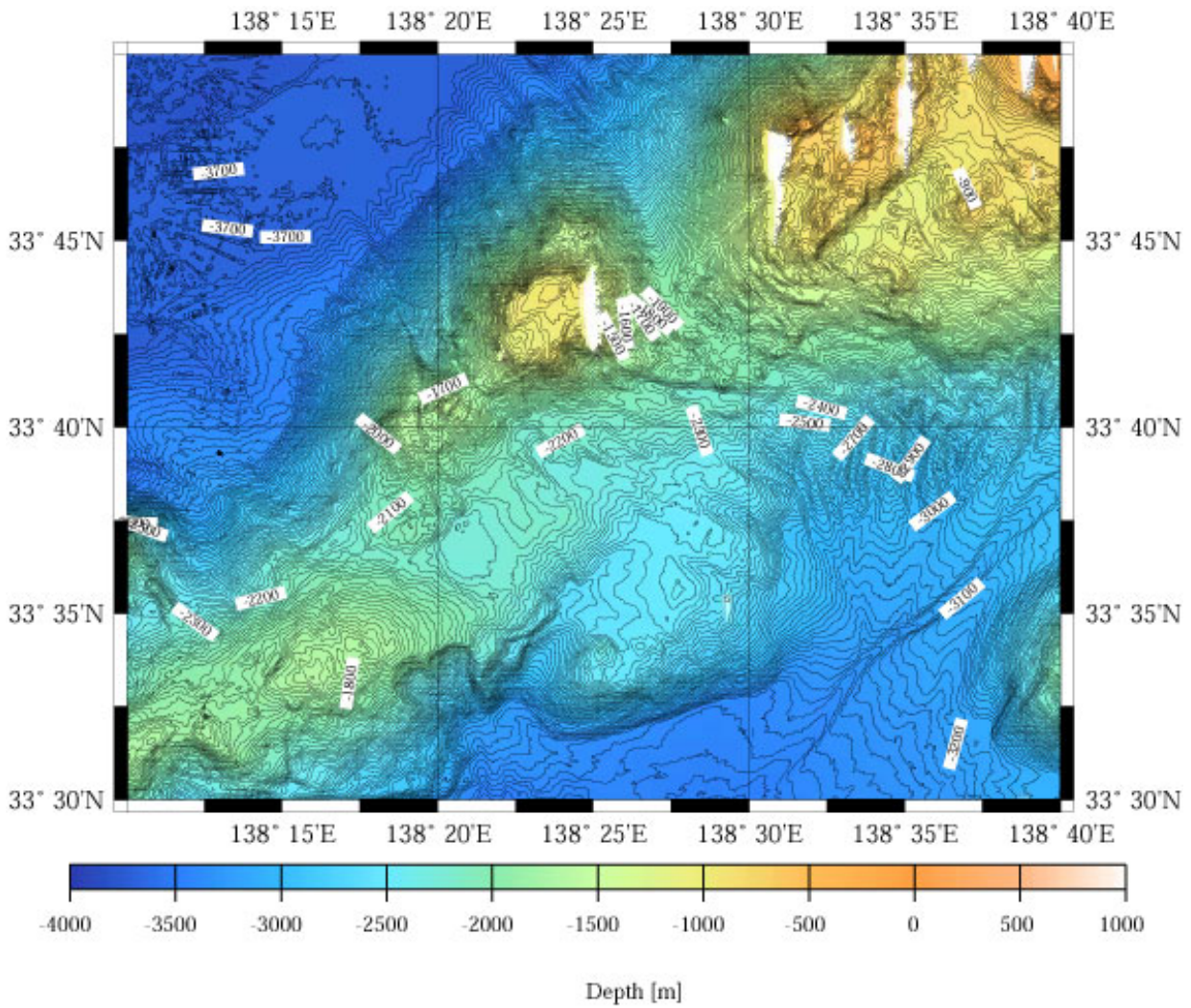


Fig. 3.15 Swath bathymetric map of debris flow sediments on the base of the slope of the Zenisu Ridge.

### 3.5.3 Seep communities at the base of the slope of the Zenisu Ridge

On accretionary margins, seep communities are frequently related to outcrops of recently active thrust faults (Davis et al., 1990; Le Pichon et al., 1987; Moore et al., 1990; Minshull and White, 1989; Suess et al., 1998).

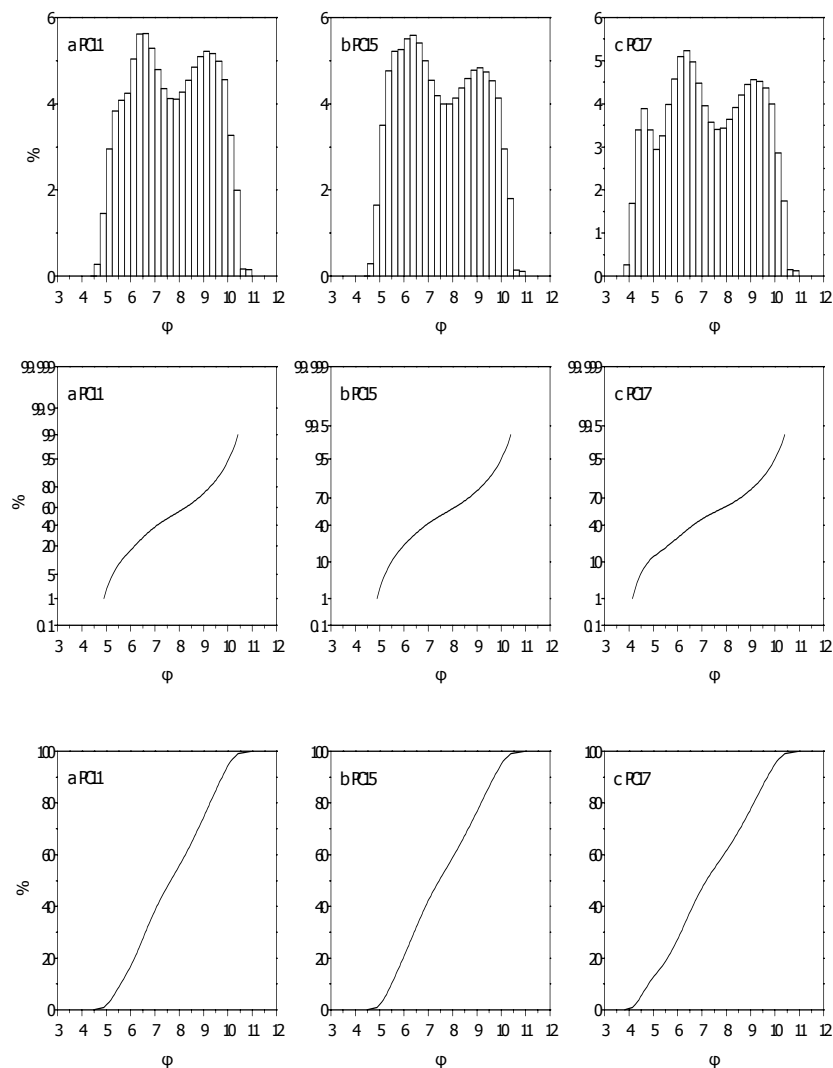


Fig. 3.16 Results of grain size analyses of three sediment samples PC11, PC15 and PC17 from dives 523 and 556 showing an admixture of turbidite and hemipelagic sediments. Upper and middle curves: Cumulative frequency; lower curve: Frequency.

Such cold seep communities have been repeatedly reported from the eastern Nankai Trough (Le Pichon et al., 1987; 1989; Kobayashi et al., 1992; Kobayashi, 2000, Ohta et al., 1987; Fujioka and Taira, 1989; Henry et al., 1992; Ogawa et al., 1996), and have been interpreted to reflect active faulting and fluid flow (Fujioka et al., 1989; Kobayashi et al., 1992, Le Pichon et al., 1987; 1992; Henry et al., 1992). In the Zenisu Trough, Wu et al. (1999) discovered the first seep communities during cruise KY99-09 Leg 2 of the R/V Yokosuka. The vesicomyid white clams observed during dive 523 of 1999 were successfully sampled during dive 555 in 2000. Two sampled species are: the new, large *Calyptogena* sp. and a species common to the recently described *Calyptogena* (*Archivesica*) *tsubasa* collected from the Tenryu Canyon area (Fig. 3.17; Gamo et al., 1992).

The occurrence of dense beds of *Calyptogena* bivalves, buccinid snails and white galatheid *Munidopsis* sp. provides unequivocal supporting evidence for nascent subduction and concomitant seepage at the base of the southeastern flank of the Zenisu Ridge (dives 523, 555). The dark sediments collected together with the bivalves smelled of hydrogen sulfide on board, and the thickness of the gills of each *Calyptogena* specimen suggests their nutritional dependency on chemosynthetic symbionts.

#### **3.5.4 Turbidites in the Zenisu trough axis channel**

Video tape imagery was carried out during dive 371 at E-W channel in the central channel of the Zenisu Trough. This dive executed by Segawa in 1997 started from the base of the channel and ended on the middle slope of the Zenisu Ridge. The sedimentary structures observed include ripple marks and migrating sediment waves on the flat seafloor. The ripple marks were found at 11:59:37, 12:05:47 (CAM2) during dive 371 (Fig. 3.18). They suggest coarse sands and strong bottom currents, the latter being confirmed by submersible observations which yielded >1 knot flow speed on the channel slope. A thin sediment blanket, occasional outcrops of basement mudstones, occurrence of suspension feeders such as sea whips, together with a high concentration of marine snow during the dive suggest intense turbidity current activity and an erosive sedimentological environment during dive 399 (Fig. 3.19), as well as dives 371 and 556. The turbiditic activity in the trough axis channel occurred during the Holocene.

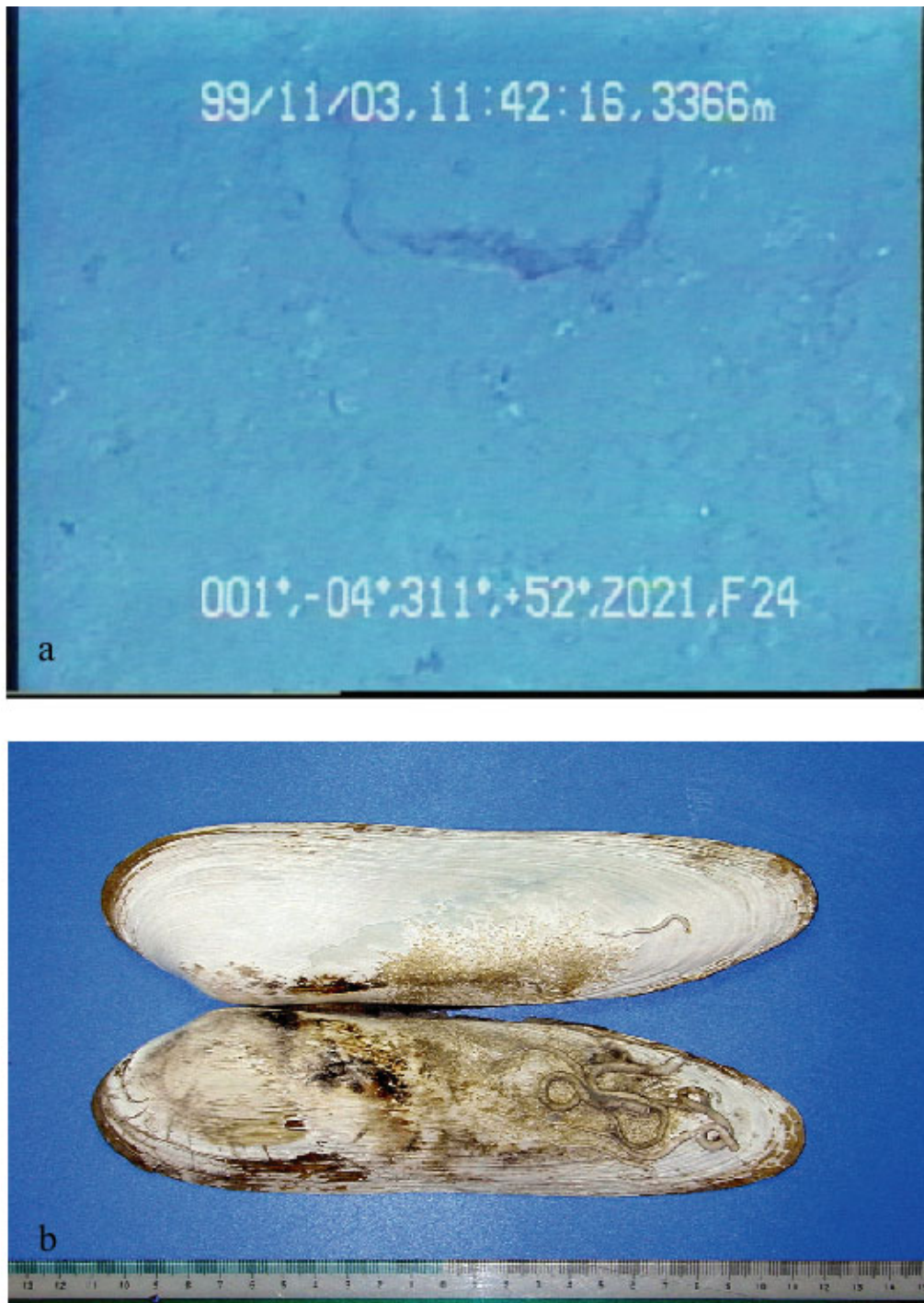


Fig. 3.17 Deep-sea cold seep community at the base of the Zenisu Ridge. a: photo at the location where a deep-sea community of *Calyptogena* spp. is discovered; and b: *Calyptogena tsubasa* sampled during dive 555.





Table 3.6 Grain size parameters of sediments sampled during dives 523 and 556.

SAMPLE	MEDIAN	MEAN	SORT	SKEW	KURT	SD (%)	ST(%)	CLAY%	STC_TYPE
PC11	7.649	7.68	1.537	-0.251	1.791	0	55.75	44.25	C-St
PC11A	7.612	7.643	1.577	-0.576	1.851	0	56.22	43.78	C-St
PC12	7.69	7.678	1.585	-0.499	1.831	0	54.68	45.32	C-St
PC12A	7.689	7.7	1.534	-0.382	1.785	0	55.11	44.89	C-St
PC13	7.687	7.697	1.522	-0.4	1.777	0	55.36	44.64	C-St
PC14	7.597	7.619	1.611	-0.594	1.88	0	56.1	43.9	C-St
PC15	7.443	7.541	1.558	0.701	1.807	0	58.92	41.08	C-St
PC16	7.421	7.525	1.551	0.721	1.804	0	59.5	40.5	C-St
PC17	7.179	7.283	1.766	-0.313	2.062	0.26	61.22	38.51	C-St
PC18	6.532	6.716	1.933	1.433	2.398	4.68	67.93	27.4	C-St
PC21	7.688	7.697	1.583	-0.535	1.834	0	54.61	45.39	C-St
PC21A	7.693	7.694	1.583	-0.577	1.837	0	54.64	45.36	C-St
PC22	7.743	7.757	1.402	0.372	1.654	0	55.35	44.65	C-St
PC23	7.714	7.688	1.579	-0.739	1.857	0	54.67	45.33	C-St
PC31	7.223	7.25	1.858	-0.88	2.175	2.49	57.93	39.58	C-St
PC32	7.199	7.221	1.848	-0.838	2.165	2.44	58.93	38.64	C-St
PC33	7.335	7.363	1.769	-0.734	2.063	0.21	59.14	40.64	C-St
PC34	7.24	7.303	1.8	-0.671	2.097	0.64	59.61	39.75	C-St
PC35	7.371	7.394	1.753	-0.72	2.043	0.14	58.62	41.24	C-St
PC36	7.019	7.111	1.886	-0.436	2.19	2.87	60.04	37.09	C-St
PC37	6.417	6.69	1.899	1.5	2.368	2.51	70.9	26.59	C-St
PC38	6.966	7.14	1.709	0.699	2.047	1.09	65.81	33.1	C-St

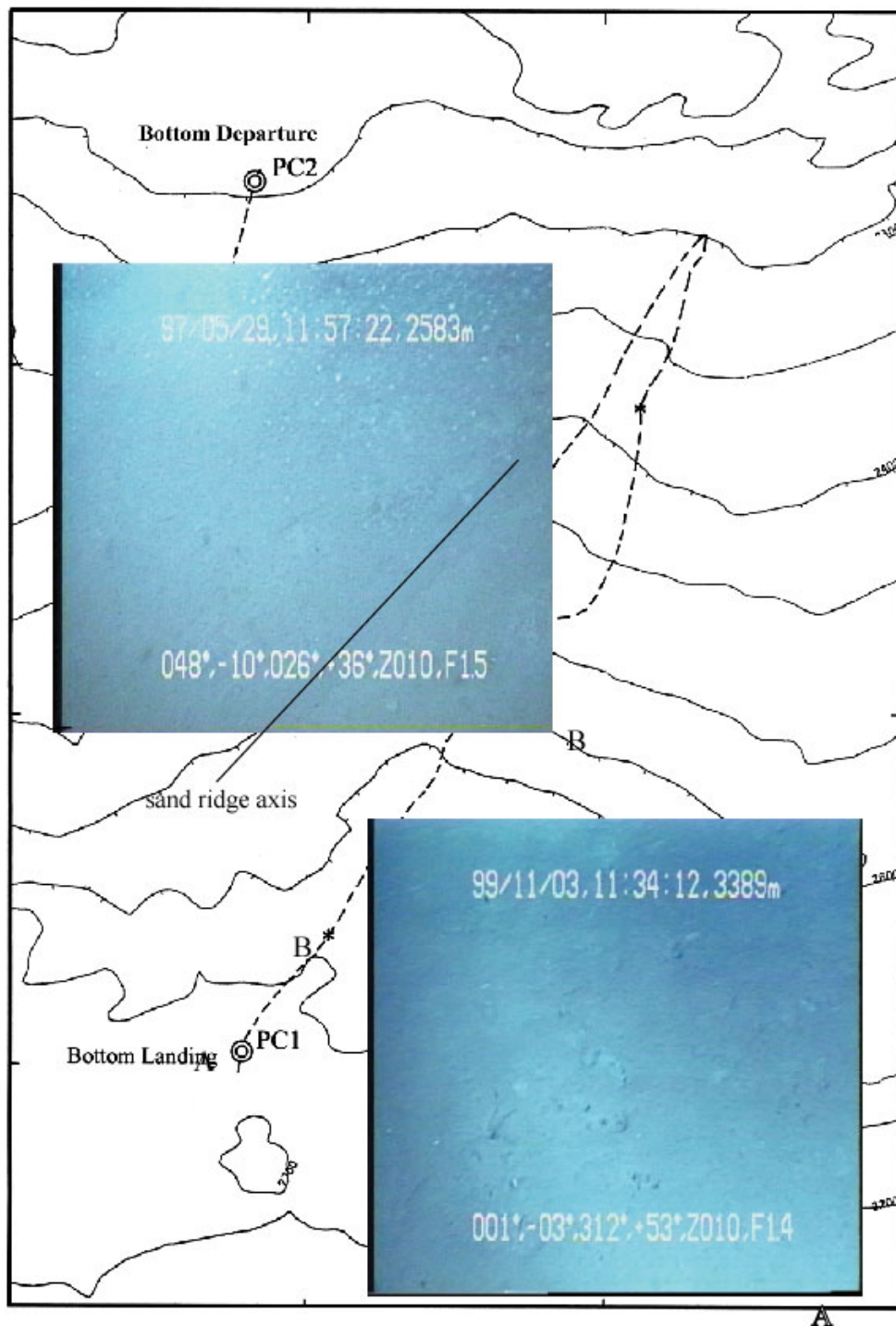


Fig. 3.18 Track line of Shinkai dive 371. Erosional seafloor occurs near the axis of the Zenisu deep-sea channel (Photo A), and sand waves occur along track B (Photo B). See Fig. 3.1 for location of dive site.



Fig. 3.19 Fine turbidites on the surface of the trough axis channel within the central Zenisu Trough from dive 399.

### 3.6 Elemental geochemistry of sediments in the Zenisu deep sea channel

#### 3.6.1 Samples and analyses

Two push cores PC1 and PC3 were collected during cruise YK99-09 of the R/V Yokosuka in 1999; their positions are shown in Fig. 3.14. The cores were sampled every 3 cm. The samples were dried at 60-70°C and sieved to obtain the size fraction of <0.125 mm. The dried sediment samples, each weighing about 0.1 g at 110 °C, were put into cyclo-tetra-fluorinethane with HF and HNO<sub>3</sub>, and then analyzed using ICP- AES (mean error <10%). The analysis results are shown in Table 3.7.

Table 3.7 Elemental composition of sediments of the push cores.

Sample	Ca	Fe	Al	Ti	Mg	Na	K	Cu	Ni	V	Co	Sr	Li	Rb
PC1-1	4.72	3.68	6.62	0.3	1.28	2.63	1.92	142	29.8	96.1	18.3	276	40.4	78.5
PC1-2	4.91	3.64	6.56	0.3	1.31	2.67	1.91	147	35.1	101	24.2	283	41.1	75
PC1-3	5.3	3.45	6.67	0.31	1.28	2.6	1.93	168	34.5	100	21.8	300	40.8	73.4
PC 1-4	5.68	3.35	6.51	0.28	1.24	2.59	1.93	140	24.3	98.4	19.1	305	39.6	69.8
PC 1-5	5.86	3.29	6.46	0.29	1.21	2.65	1.89	136	35.1	94.5	12.3	299	38.4	67.9
PC 1-6	5.86	3.34	6.56	0.29	1.25	2.71	1.88	167	26.8	93.7	17.3	300	37.1	66.1
PC 1-7	5.8	3.21	6.51	0.28	1.17	2.76	1.9	165	34.2	88.2	13.3	306	34.1	71.6
PC 1-8	6.11	3.06	6.52	0.27	1.09	2.59	1.83	143	19	84.6	15.4	306	30.9	66
PC 1-9	6.81	3.62	6.51	0.31	1.27	2.47	1.7	153	35.1	103	18	340	36.3	73.5
PC3-1	7.1	3.62	6.56	0.29	1.19	2.28	1.7	143	29.8	99.7	12.2	329	31	65.8
PC 3-2	7.13	3.56	6.3	0.28	1.21	2.46	1.69	118	20.5	94.3	10.5	327	30.4	64.6
PC 3-3	7.58	3.39	6.31	0.28	1.18	2.42	1.69	144	22.3	96.5	14.9	333	30.9	63
PC 3-4	7.58	3.39	6.19	0.28	1.19	2.33	1.66	160	26.6	104	12.4	320	30	58.7
PC 3-5	9.08	3.57	6.25	0.3	1.24	2.26	1.46	183	21.3	130	17	385	28.6	52.7
PC 3-6	9.22	3.38	6.14	0.28	1.18	2.31	1.54	157	25.7	111	22.3	398	30.3	56.4
PC 3-7	8.65	3.36	6.25	0.28	1.16	2.52	1.74	167	20.7	103	12.8	387	34.3	65.5
PC 3-8	9.43	3.69	6.4	0.29	1.21	2.48	1.75	215	23.3	109	12.9	399	35.6	67.1

Ca-K (%); Cu-Rb (ppm)

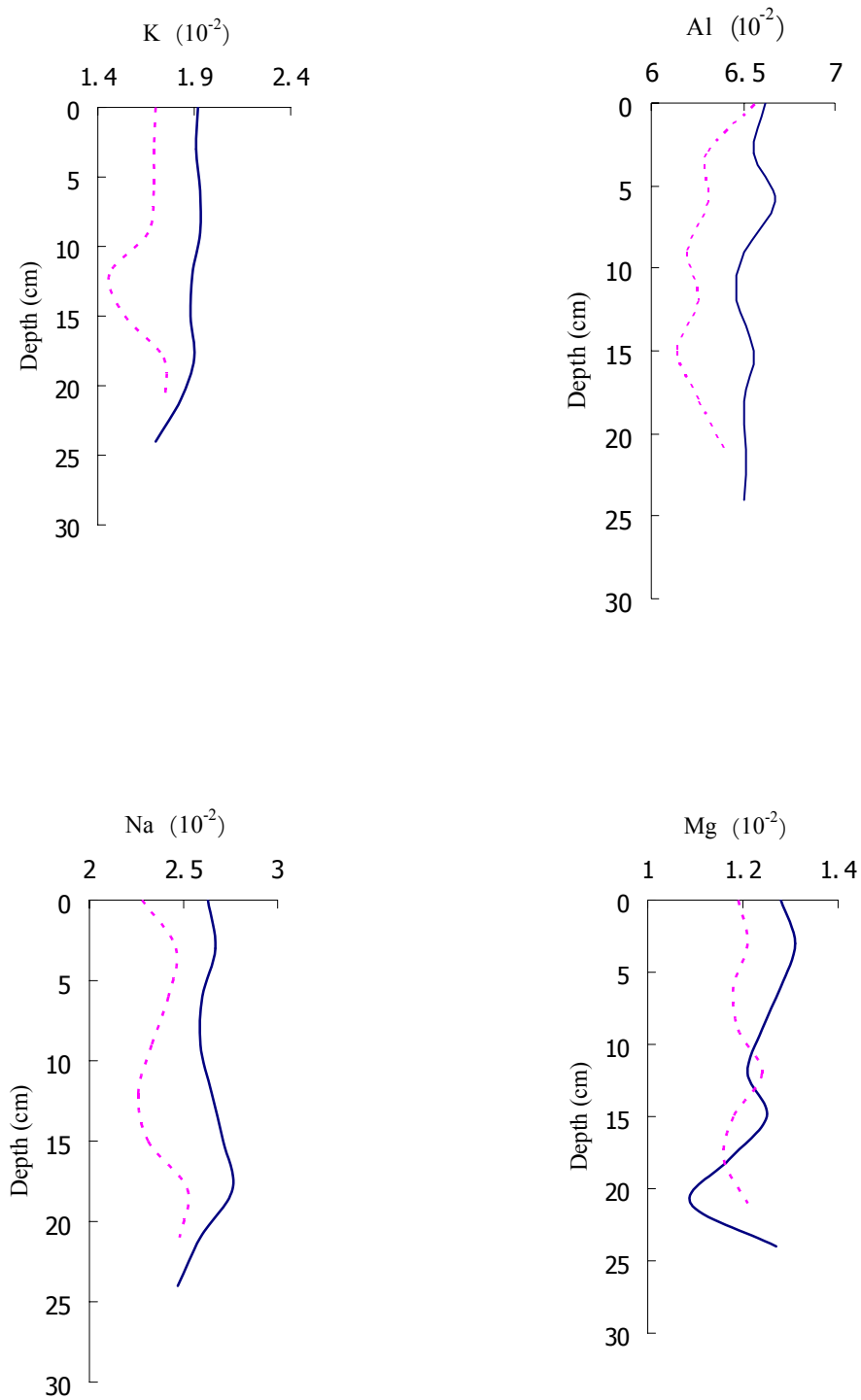


Fig. 3.20 Downcore distribution of the elemental concentrations pc1 continuous lines pc3 dashed lines.

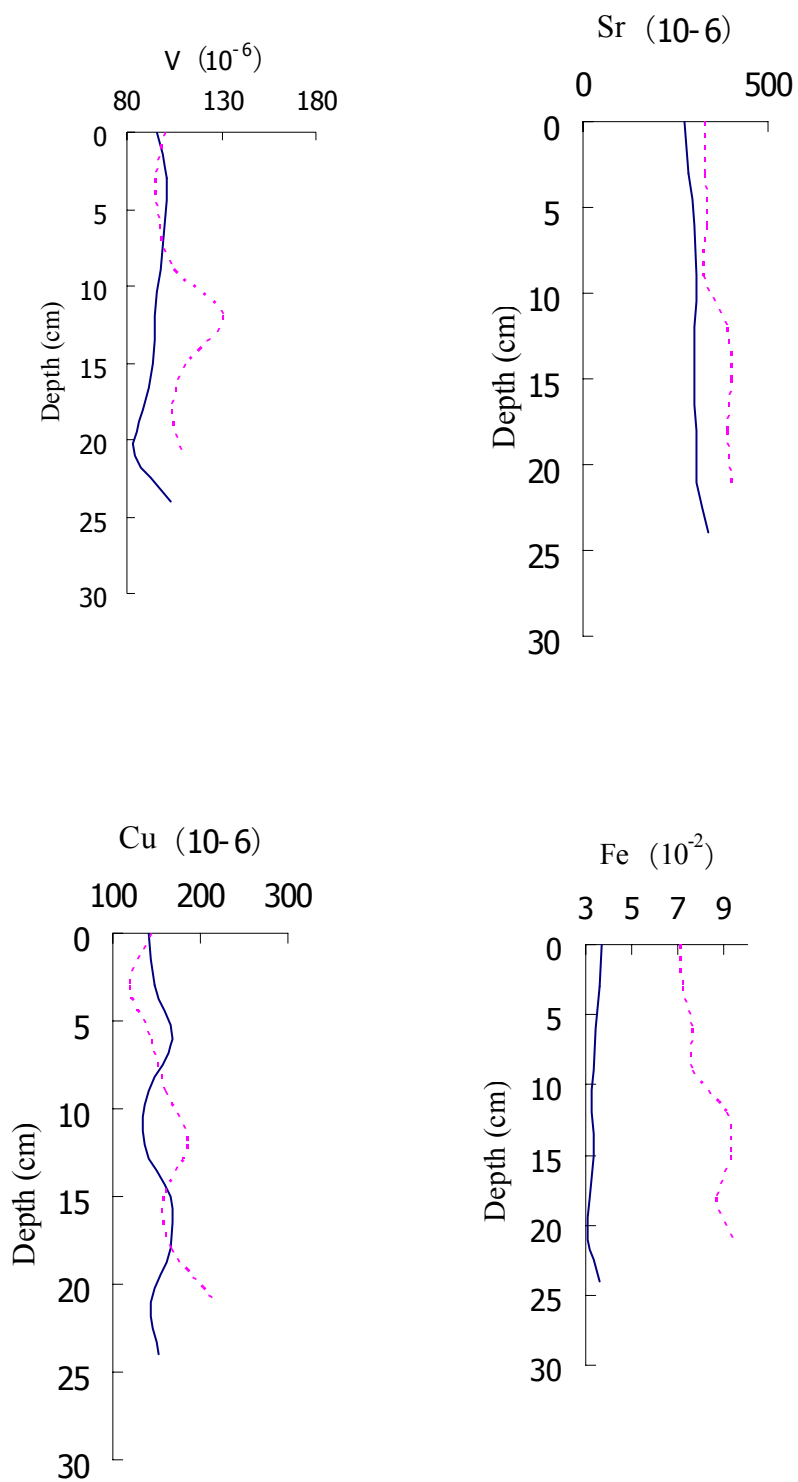


Fig. 3.20 (Continue 1) Downcore distribution of the elemental concentrations pc1 continuous lines pc3 dashed lines.

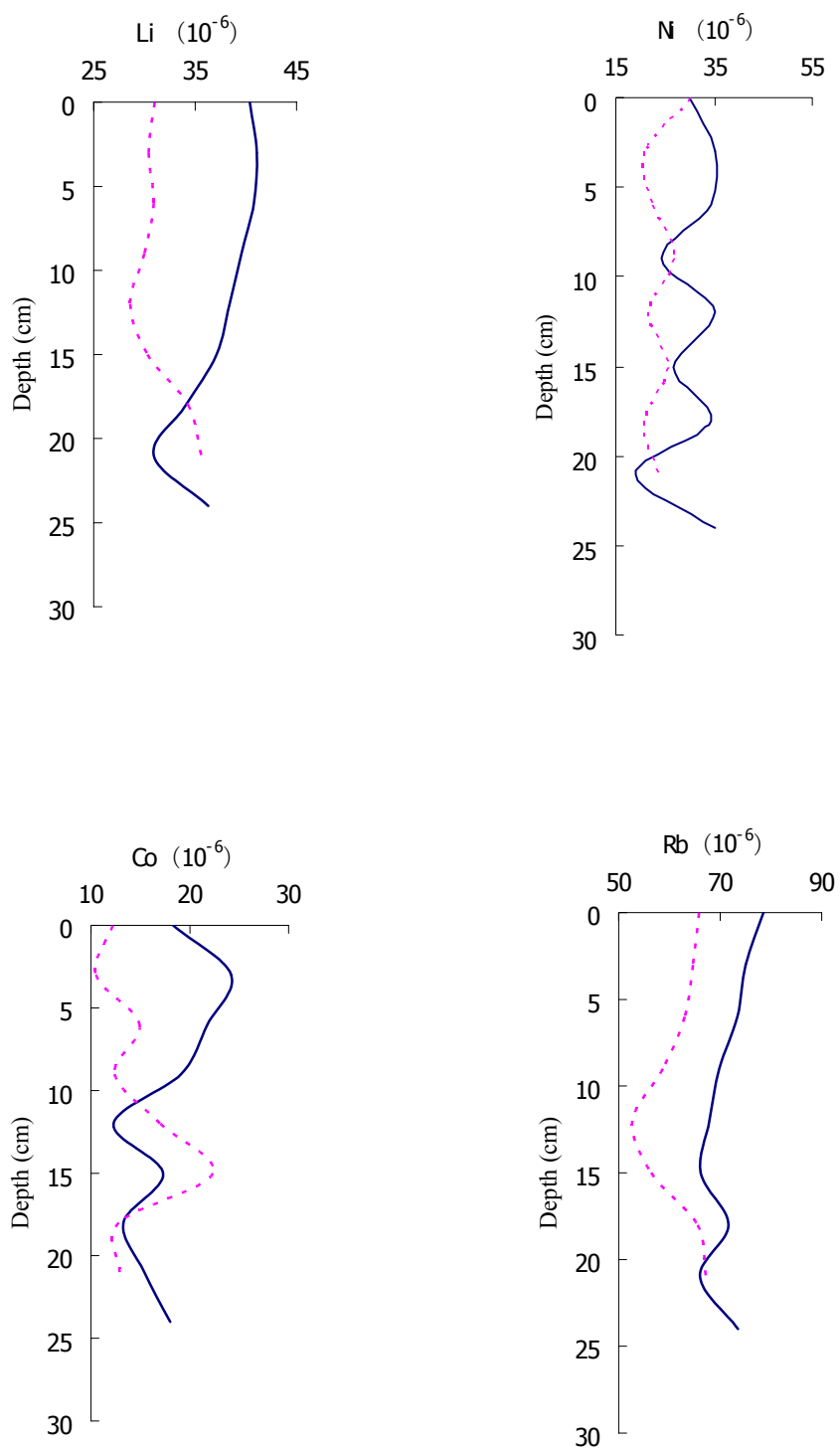


Fig. 3.20 (Continue 2) Downcore distribution of the elemental concentrations pc1 continuous lines pc3 dashed lines.

### 3.6.2 Depth distribution of the elements

Cores PC1 and PC3 lie in the lower part of the Zenisu deep sea channel with water depth of 3400 m and 2560 m, respectively. These depths do not agree with the isobaths in Fig. 3.14. The sediment layers of core PC1 are thick, while those of core PC3 are thin. The lengths of the cores PC1 and PC3 are 30 cm and 27 cm respectively. The downcore distribution of the major elements is shown in Fig 3.20. The contents of Ca, Fe and Sr in core PC3 are higher than those in core PC1, while the contents of Al, Na, K, Li and Rb in PC1 is lower than those in PC3. The lower content of Ca in core PC1 may be attributed to the fact that the water depth at station PC1 is larger than that at station PC3, i.e., it is closer to the CCD and therefore more CaCO<sub>3</sub> can be dissolved. At both sites, the Ca, K, Na, Cu, Ni and V concentrations increase downcore. The Ca range for PC1 is 4.72-6.81 % and for PC3, it is 7.1-9.43 %. The Fe content for core PC1 is within the range of 3.06-3.68 % without any obvious trend from top to bottom, while it increases downcore for PC3. The concentration of Sr is more-or-less constant at both sites. In contrast, the Al, Ti, Mg and Rb contents decrease slightly downcore, the ranges being 6.10-6.67 % (Al), 0.27-0.31 % (Ti), 1.09-1.28 % (Mg), and 62.7-78.5 ppm (Rb) respectively. There is an abrupt increase in the Fe, Ti, Mg, Ni, V, Li and Rb concentrations at 21 cm core depth for core PC1, while the Na and K contents decrease. This corresponds to a change in lithology.

### 3.6.3 Correlation analysis of the elemental concentrations

Table 3.8 shows the correlation matrix of the elements in core PC1. Ca and Sr are notably positively correlated, while they correlate negatively with the other elements, especially K, for which the correlation coefficient reaches  $-0.82$ . Ca and Sr belong to the same group (2A) in the periodic table, their ionic radii are very similar and they can be substituted by each other through allomerism. Sr is derived mainly from the shells of organisms and is associated with carbonates. With sedimentation, the sediment carbonate content decreases because the solubility of carbonate increases as the pressure increases and the temperature decreases. In contrast, the other elemental concentrations change little, thus inducing a negative correlation between them and Sr. This is also the reason why core PC1 has lower Ca and Sr contents than core PC3. Fe shows a strong correlation with Ti, Mg, Ni, V, Co, Li and Rb, suggesting that these elements have the same source. Because Ti in marine sediments is derived mainly from scraping of aluminum silicates (Murray, 1993), so the same source may be assumed for Mg, V, Co, Li and Rb. The correlation between Al and other elements is weak ( $r > 0.5$ ). Because Al is geochemically inactive, it cannot enter the sediment through allomerism. The Al content in the sediment is almost completely controlled by scraping of terrigenous and volcanogenic aluminum silicates such as feldspar and mica, so these elements Al, Ti, Mg, Ni, V, Co, Li and Rb may also be derived from the scraping of terrigenous and volcanogenic aluminum silicates.

Table 3.8 Correlation coefficient of the elements in the core PC1.

Element	Ca	Fe	Al	Ti	Mg	Na	K	Cu	Ni	V	Co	Sr	Li
Fe	-0.40												
Al	-0.61	0.45											
Ti	-0.17	0.84	0.54										
Mg	-0.44	0.90	0.49	0.83									
Na	-0.44	-0.31	0.00	-0.38	-0.14								
K	-0.81	-0.07	0.37	-0.19	0.15	0.65							
Cu	0.09	-0.04	0.45	0.27	0.14	0.31	0.00						
Ni	-0.12	0.54	0.09	0.71	0.59	0.08	-0.04	0.25					
V	-0.13	0.65	0.29	0.84	0.90	-0.48	-0.11	0.01	0.56				
Co	-0.49	0.65	0.64	0.55	0.71	-0.23	0.19	0.14	0.14	0.68			
Sr	0.94	-0.18	-0.43	0.06	-0.22	-0.57	-0.82	0.20	0.05	0.11	-0.26		
Li	-0.65	0.74	0.48	0.65	0.89	-0.02	0.49	-0.07	0.48	0.79	0.64	-0.47	
Rb	-0.55	0.84	0.53	0.66	0.66	-0.16	0.11	-0.02	0.53	0.56	0.52	-0.30	0.59

### 3.6.4 The source of sedimentary material

Submersible observation during cruise 99-09 of the R/V *Yokosuka* show that sediments in the study area consist largely of turbidites, clastics, volcanic ash and biogenic material. Volcanigenics and shells are abundant. The most common volcanigenic material is fluorite and basaltic debris. This material is transported here through allomerism.

Table 9 shows the content of the main elements in the sediments. Compared with deepsea sediments, the Ca content is obviously high, those of Fe, Ti, Mg and K is slightly high, while that of Na is low. This characterizes the sediment source of the study area. Using the correlation coefficients, the major elements may be sorted into two main groups. The first group consists of Sr and Ca, and the second of Al, Fe, Ti, Mg, Ni, V, Co, Li and Rb. Because Ca and Sr are highly positively correlated and Sr is a characteristic product of organisms, the high Ca content suggests that sediments in this area have a large biogenic component as reflected in the abundance of shells in the clastic sediment. Al is not found in shells but occurs mainly in the scraping of terrigenous and volcanigenic aluminum silicates such as feldspar and mica. Fe is abundant in clay minerals and silicate minerals such as pyroxene, hornblende and olivine. Ti is found also mainly in silicate minerals, while volcanigenic silicates are rich in such elements as Fe, Mg, K, Li and Rb, which occur in the crystal lattice of clastic minerals or are adsorbed on the surface of clay minerals. The high correlations between Al, Fe, Ti, Mg, Ni, V, Co, Li and Rb suggest that they are derived from the same source, namely from silicates of terrigenous or volcanigenic material. Thus, large amounts of silicate scrapings of terrigenous or volcanigenic must have been transported to the trough area via deep sea valleys.

Table 3.9 Main elements in the sediments.

Samples	Ca	Fe	Al	Ti	Mg	Na	K
PC1	5.67	3.40	6.55	0.29	1.23	2.63	1.88
PC3	8.22	3.50	6.30	0.29	1.20	2.38	1.65
Pelagic sediments*	0.43	4.55	6.35	0.42	1.39	1.34	1.99

\* Data after Guo (1997).

### 3.6.5 Conclusions from the elemental geochemistry of sediments

(1) Most elemental concentrations change little downcore except Ca which has increases significantly. This suggests that the depositional environment is stable. (2) Ca and Sr are well correlated and they are biogenic in origin. Al, Fe, Ti, Mg, Ni, V, Co, Li and Rb are highly positively correlated; they are terrigenous or volcanigenic in origin. (3) Sediments of this study area have multiple sources: biogenic, terrigenous and volcanigenic.

### 3.7 Seep communities and sedimentary facies

The sediment types and their distributions were mapped by deep-towed camera imagery, sidescan sonar surveying, direct observations as well as sampling from a submersible (Fig. 3.3). Sediment gravity flow, in particular turbiditic flow and debris flow, dominates in the active deep-sea channels. Five sediment facies were distinguished on the slope and basin floor: (1) turbidites with abundant small-scale sandy lobes (levee deposits) on the flat floor of the deep-sea channel; (2) debrites found over steep scarps at the slope base of our study area; (3) hemipelagic deposits composed of fine-grained sediments that occur as a very thin veneer on the slope of the Zenisu Ridge and interbedded with turbidity levee deposits on the basin floor (Fig. 3.3); (4) slump deposits on the lower slope (Fig. 3.1). Numerous steep cliffs outcrop in eroded gullies on the slope of the accretionary wedge and on the northern slope of the Zenisu Ridge. They give rise to hummocky reflections on the seismic profiles and are clearly recognizable in the high-resolution bathymetry; and (5) a calcareous sedimentary facies confined to the frontal fault in the deep-sea channel and to the accretionary slope. Although the distribution of this last facies is very limited, it is important because it provides a substrate for clams and is therefore correlatable to them.

The seep communities observed are fed by seeps of sulfide-rich and methane-enriched fluids from a subducting dewatering source along the thrust fault. Seawater collected immediately above beds of densely concentrated clams are enriched in methane and carbon dioxide (Fujioka, 1989; Henry et al., 1992). Methane has also been reported in bottom waters of the Nankai Trough (Gamo et al., 1992; Ashi, 1997). In addition, heat flow values obtained around the Hatsushima community show positive temperature anomalies ranging from 1.2-2.6° C (Gamo et al., 1992). Thus, there is admixture of deep material. The association of dead and living clams with debris flow deposits or coarse calcareous turbidites in the Nankai Trough and the Zenisu Trough has been confirmed by submersible observations and deep tow survey results. The spatial migration of seep communities not only reflects the migration

of active faulting, but also the relationship between the intensity of fault activity and distance to the thrust fault where fluid expulsion occurs.

Previous geological studies of seep communities show that the geological complexity and tectonically dynamic nature of the continental margins surrounding the Pacific Ocean favor cold seep formation in a variety of geological settings, including fault zones with mud volcanoes, channels, and submarine artesian springs (Barry et al., 1996; Corliss et al., 1979; Fujioka et al., 1989; Greene et al., 1997; Hashimoto et al., 1989; Henry et al., 1989; Kobayashi et al., 1992; Le Pichon et al., 1989; Suess et al., 1998). Here, along active plate boundaries, faults focus fluid migration, enhancing the development and persistence of chemosynthetic communities. The often narrow continental shelf, steep continental slopes and common occurrence of submarine canyons, faulted porous strata, or unconsolidated sediments promote localized upward or outward flow of sulfide- and methane-rich pore water, thereby supporting chemosynthetic communities (Barry et al., 1996; Fujioka et al., 1989; Greene et al. 1997).

The migration of methane-rich fluid to the sites where clam communities are discovered are promoted by two factors: (1) the active thrust fault which provides an important passage way for deep fluid migration to the seafloor along the fault plane or its fractures. The extent of the fault limits the distribution of clams; and (2) the sedimentary facies. Numerous debris lobes and carbonates with a high porosity and a high permeability near the thrust dip gently towards the trough. Fluids therefore flow naturally to the clam sites under normal stratal pressure. In addition, the detachment faults at the frontal fault zone with coarse sediments provide another possible path for fluid migration to the seep community sites (Henry et al., 1992). In the Zenisu Trough, the nascent subducting fault and the distribution of the debrites control the distribution of the cold seep communities (Wu et al., 2000).

### **3.8 Comparison of sedimentary processes between the Nankai Trough and the Zenisu Trough**

A comparison of certain sedimentary features in the Nankai and Zenisu troughs are shown in Table 3.7. Both sedimentary environments are dominated by turbiditic flows, but major differences between the two troughs exist. The Nankai deep-sea channel is characterized by terrigenous detritus derived from the Honshu Island Arc, whereas the Zenisu deep-sea channel is filled predominantly by volcanic detritus originating from the Izu-Ogasawara Island Arc. The seep activity and cold seep communities are also distinct. While seeps and seep communities are widespread on the accretionary slope and floor of the Nankai deep-sea channel because of active faulting and fluid expulsion, only one seep and two kinds of seep communities are found at the base of the Zenisu slope; there is no evidence for such activities at the central channel.

Table 3.10 Comparison of sedimentary features between the Nankai and Zenisu channels.

	Nankai deep-sea channel	Zenisu deep-sea channel
CH <sub>4</sub> -rich sediments	Terrigenous and marine sediments with a moderate organic content	Marine organic sediments with a low organic content
Facies and environment	Channel-levee turbidite complex, debrites	Channel and fan turbidites and debrites
Fault system	Thrust fault exists	Apparently no thrust fault
Carbonate crusts	Commonly occur beneath a thin sandy layer	Not yet known
Deposition and erosion	Erosion or deposition	Erosion
Sediments	Terrigenous detritus	Volcanic detritus

#### 4. Seismic units and facies

By correlating our seismic data acquired during cruise KH96-02 of the R/V Hakuho-maru (Fig. 4.1) and the seismic data collected in the framework of the Kaiko Tokai project (Kaiko Tokai I Research Group, 1986; Tokuyama et al., 1998, also see Fig. 4.1) to ODP Leg 131 site 808 and DSDP sites 582 and 583 (Fig. 1.1, see also Pickering et al., 1993; Taira and Ashi, 1993), the seismic sequences and of the deep-sea channels and adjacent areas as well as their stratigraphy have been established.

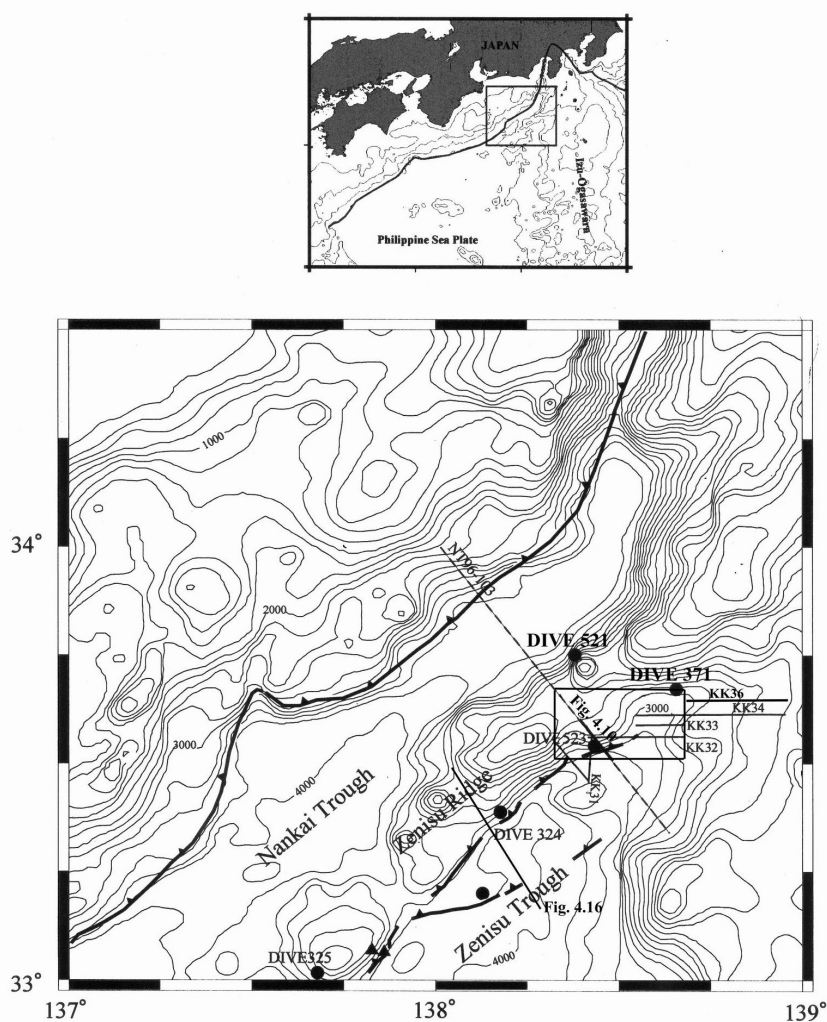


Fig. 4.1 Map of faults and location of single channel seismic lines acquired during cruise *Kaiko-Tokai* (Kaiko I Research Group, 1986). Thick lines with triangles show the subduction zone. Fined solid lines indicate the single channel seismic tracks of the cruise *Kaiko-Tokai*. Bathymetry isobaths are at an interval of 200 m. Dashed line shows the multi-channel seismic line NT96-103.

## 4.1 Seismic sequences and stratigraphic units in the Nankai Trough

The acoustic basement of the Shikoku Basin is recorded on our profiles as discontinuous reflections of a high amplitude (Figs. 4.2 to 4.8). It consists of volcanic debrites and oceanic basalt according to ODP and DSDP drill holes in the western Nankai Trough (Pickering et al., 1993), and represents the rifting sequence formed during the Oligocene and the middle Miocene (Kobayashi et al., 1995). Four post-rift seismic sequences overlie the acoustic basement along the trough axis (Table 4.1).

**Sequence A**, the wedge-shaped upper turbidite sequence, is represented by variable amplitude, transparent to partly transparent, and partly stratified reflections. It onlaps the Zenisu Ridge to the east and is separated from the accretionary wedge by a thrust to the west. Slight, thrust-induced deformations in the form of folds and small reverse faults occur to the east (Figs. 4.4 to 4.7). The thickness is generally 0.5-0.8 sec twt, the maximum being 0.8 sec (profile 901, Fig. 4.4, eastern part of the profile). This corresponds to 720 m if a strata velocity of 1800 m/sec is assumed. Lithologically, the sequence consists of turbidites interbedded with abyssal clay. The eastern part of profile 915 crosses an aggradational turbidity channel with erosion along the channel axis (Fig. 4.8).

**Sequence B**, the lower turbidite sequence, is characterized by a wedge shape, and by continuous reflections of low energy and low amplitude. Its maximum thickness is 0.6 sec twt. It is found at the central trough, and consists probably of mainly turbiditic sand and sandy silt. It onlaps the Zenisu Ridge to the east and is terminated abruptly to west by the thrust. The strata in the west of the trough floor have been involved in the fold-and-thrust system (Fig. 4.9). The lower part of sequence B is characterized by reflections of a low amplitude and moderate continuity, representing turbiditic sands and silts. The more continuous reflections upsequence suggest turbidites interbedded with hemipelagic sediments.

The reflections of **Sequence C** on the Zenisu Ridge have a high continuity and low amplitudes. The thickness of this sequence is 0.3 sec twt and increases in the direction of the ridge, exhibiting onlap terminations beneath the Nankai Trough (Fig. 4.9). This implies that uplift of the Zenisu Ridge is after the deposition of sequence C. The seismic facies is transparent except for some continuous reflectors that mark turbidites, an interpretation which is supported by results from ODP site 808B and DSDP drilling sites 582 and 583 (Pickering et al., 1993; Taira et al., 1993).

**Sequence D**, the Shikoku sedimentary sequence on the Zenisu Ridge, is marked by continuous parallel reflections of moderate energy and moderate amplitudes. Correlation with ODP site 808B shows that it consists of bioturbated hemipelagic mud and volcanic ash, perhaps coarser and with a more significant terrigenous component in our study area because of its closer proximity to the terrigenous source (Pickering et al., 1993).

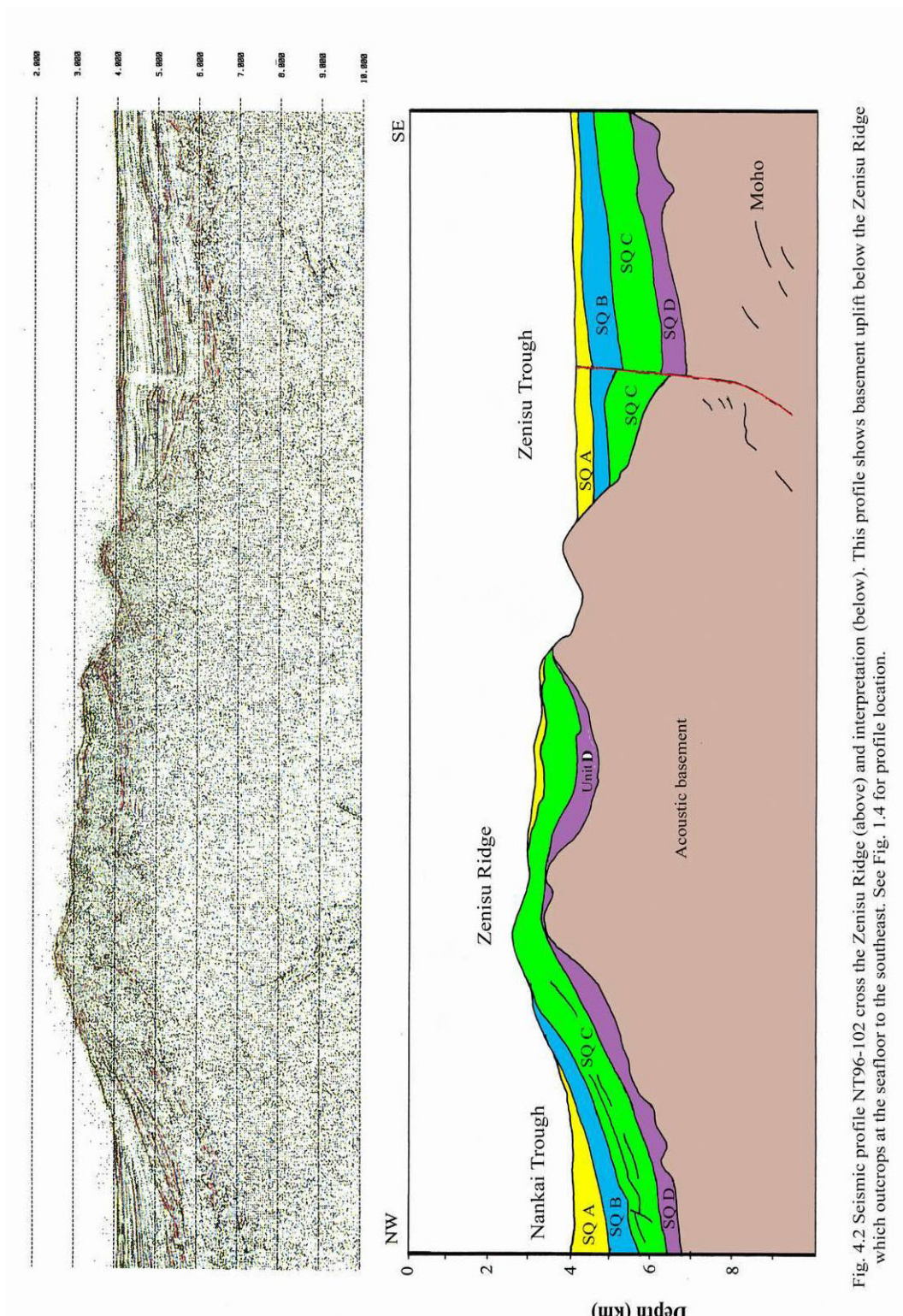


Fig. 4.2 Seismic profile NT96-102 cross the Zenisu Ridge (above) and interpretation (below). This profile shows basement uplift below the Zenisu Ridge which outcrops at the seafloor to the southeast. See Fig. 1.4 for profile location.

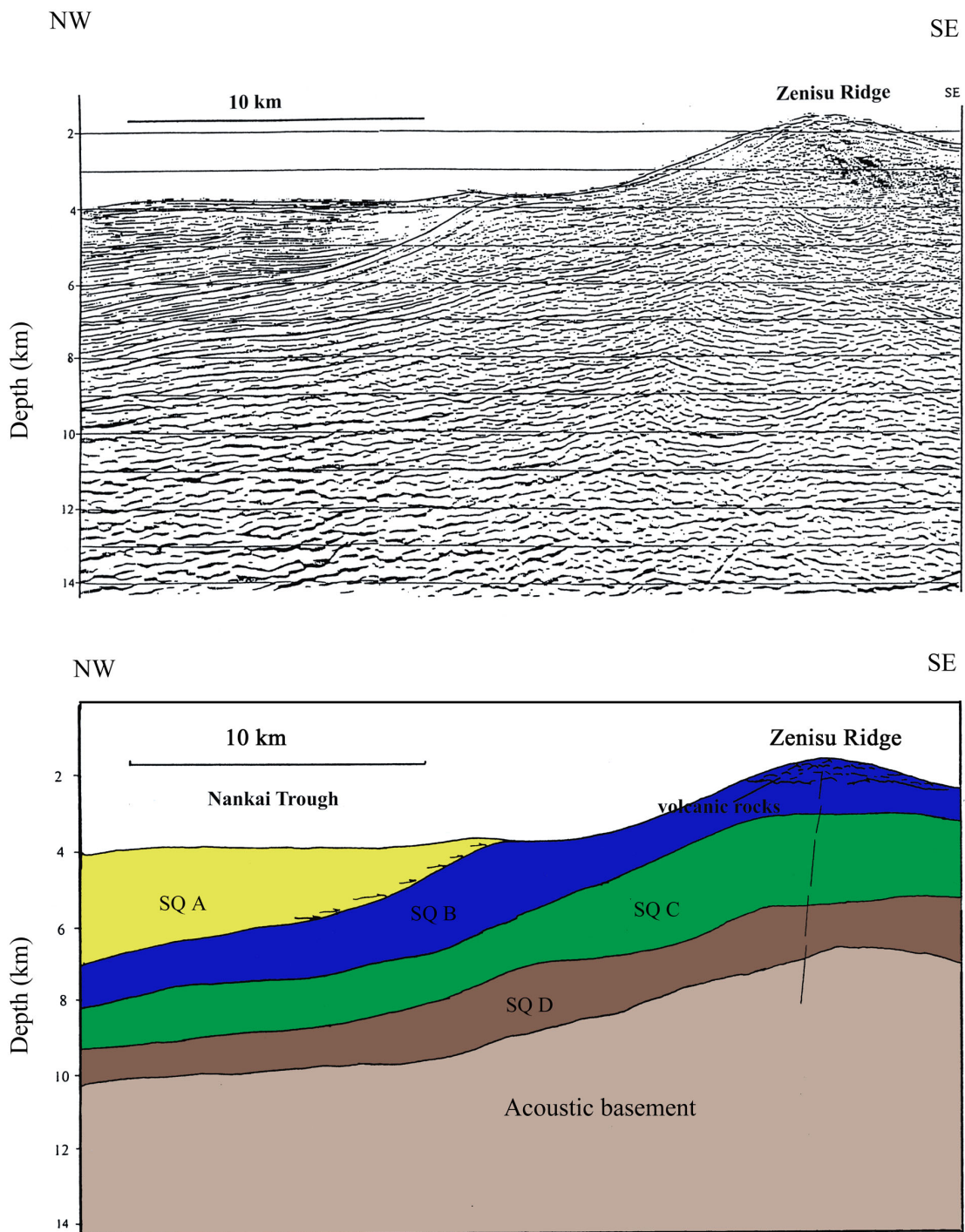


Fig. 4.3 Seismic profile NT96-103 showing the seismic units A, B, C and D. Over 5 km of sediment overlie the acoustic basement on the northern Zenisu Ridge. Units A, B and C consist of thick turbidites. A more important fault may exist dissecting the ridge (right). See Fig. 1.4 for profile location.

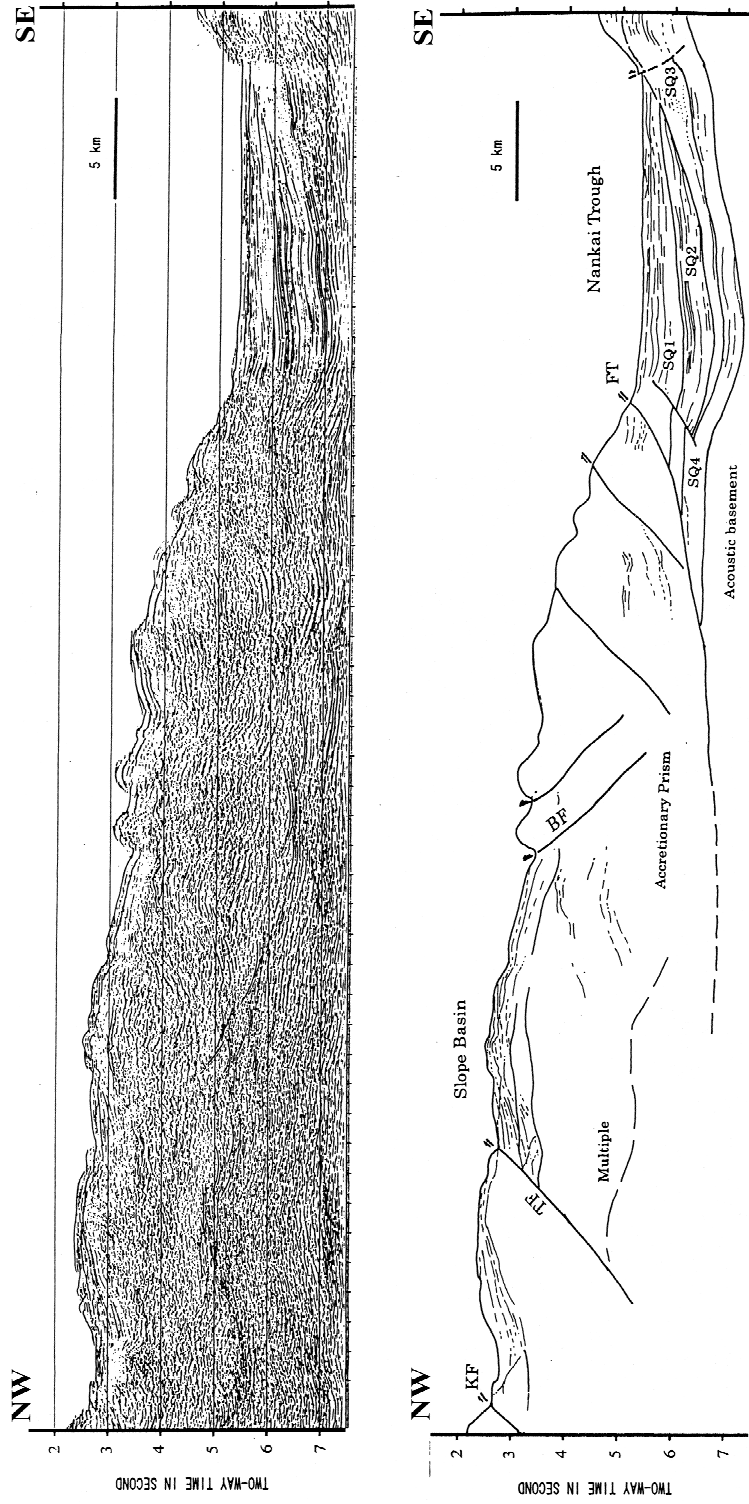


Fig. 4.4 Migrated time section of profile NT96-901 across the Nankai Trough and the slope basin. See Fig. 1.4 for profile location.  
 KF: Kodaiba fault; TF: Tokai thrust fault; BF: back thrust fault; FT: frontal thrust fault.

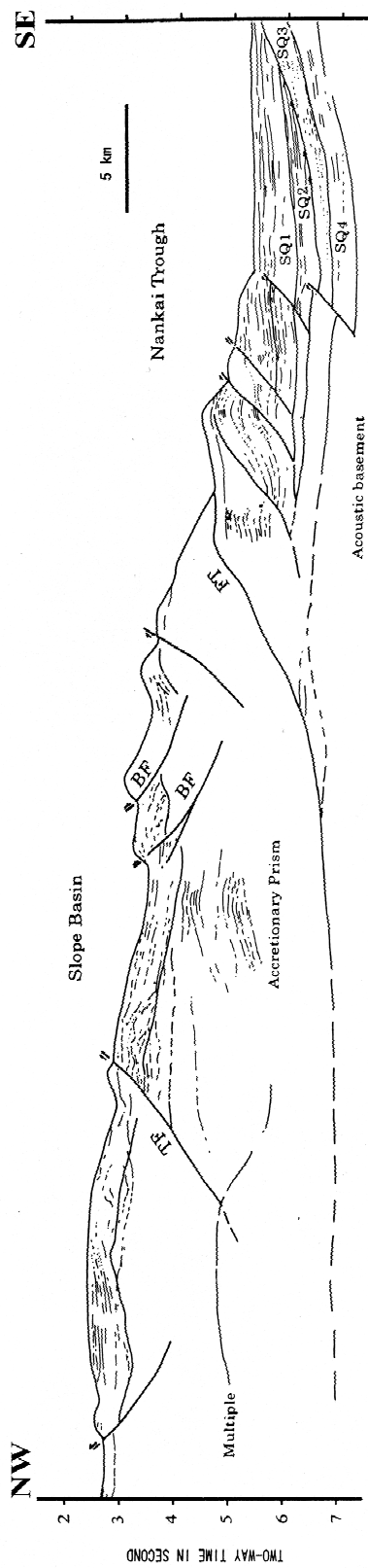
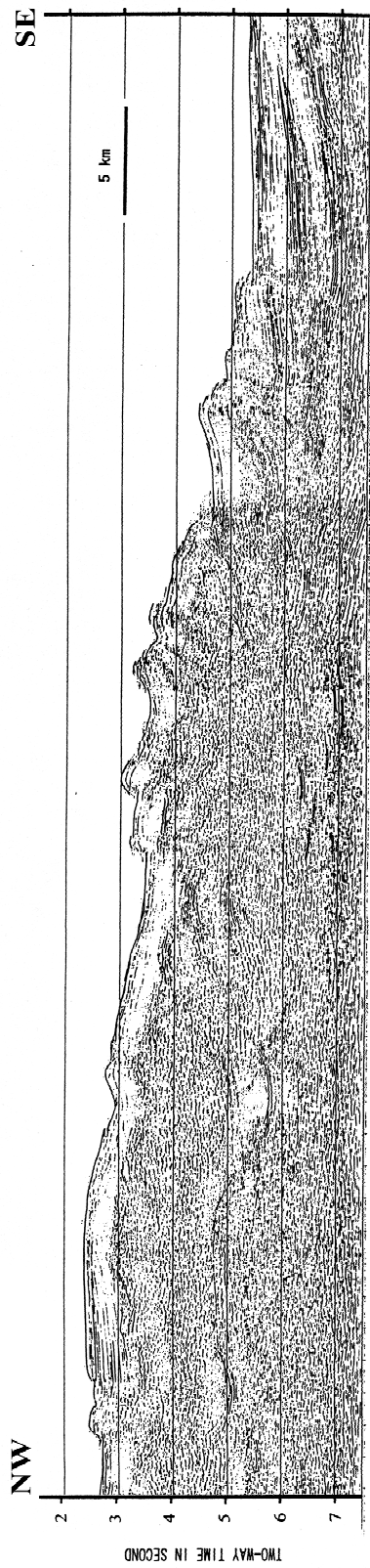


Fig. 4.5 Migrated time section of profile NT96-905. See Fig. 1.4 for profile location.  
 KF: Kodaiba fault; TF: Tokai thrust fault; BF: back thrust fault; FT: frontal thrust fault.

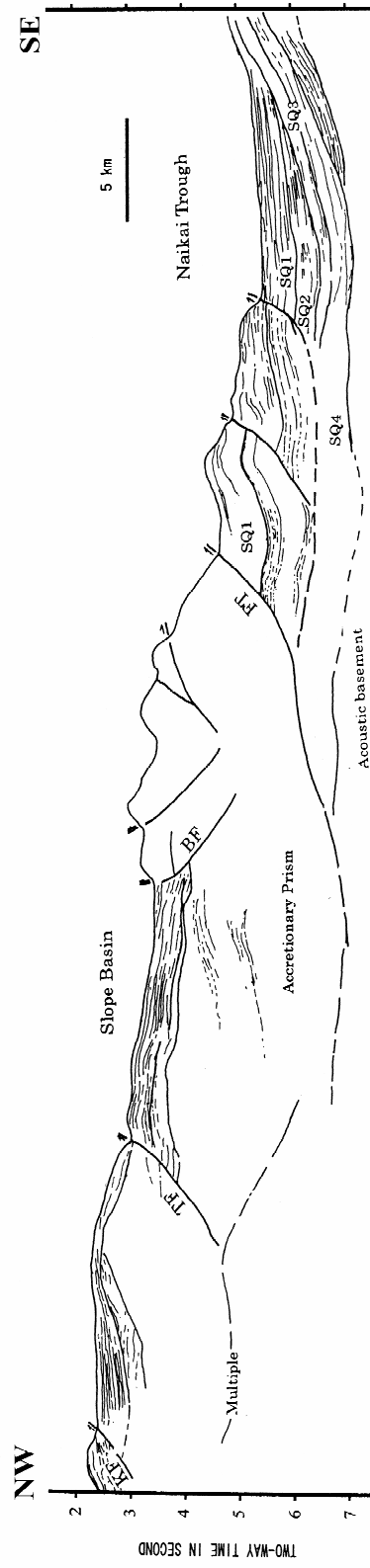
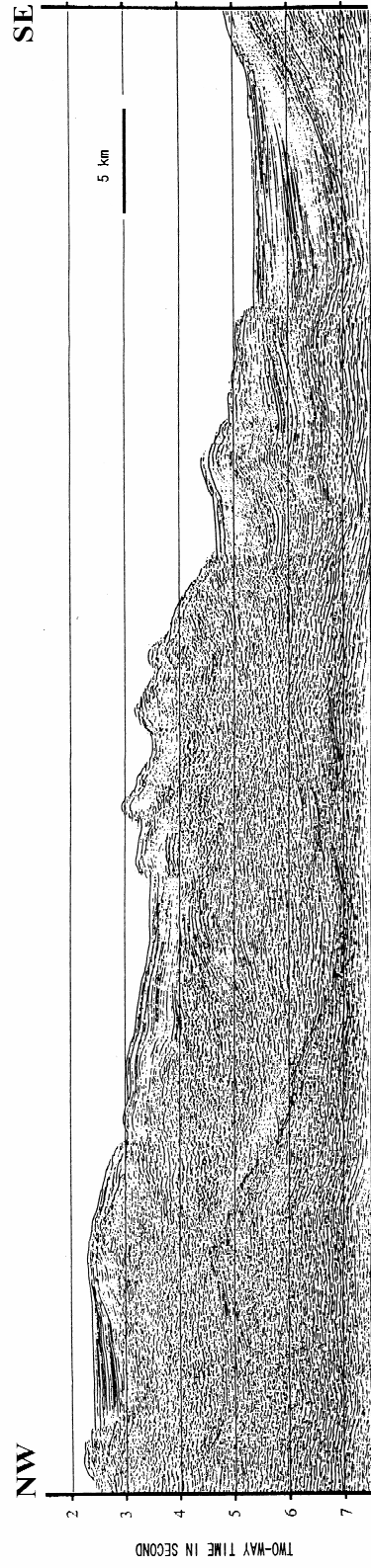


Fig. 4.6 Migrated time section of profile NT96-907. See Fig. 1.4 for profile location.  
 KF: Kodaiba fault; TF: Tokai thrust fault; BF: back thrust fault; FT: frontal thrust fault.

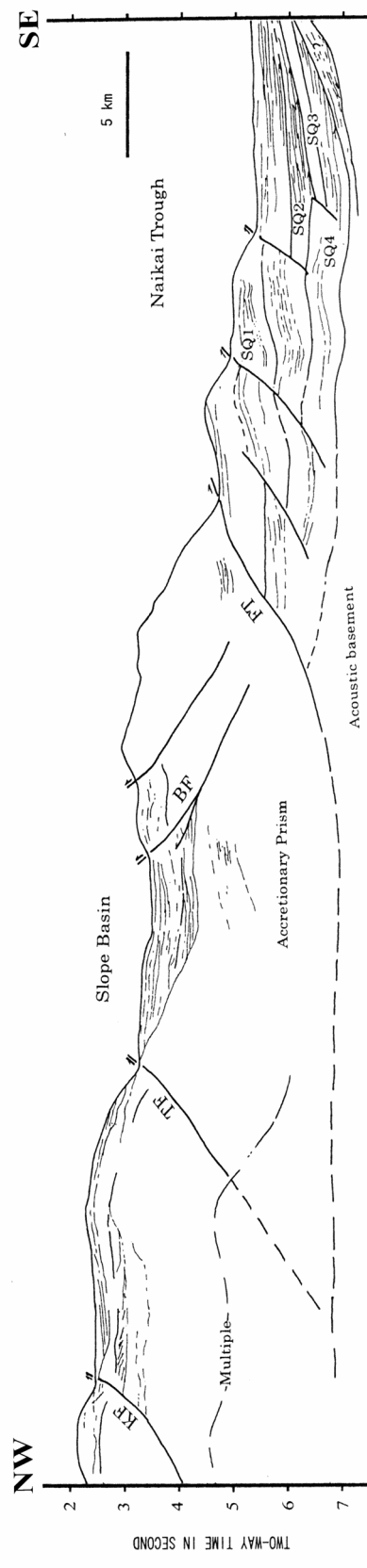
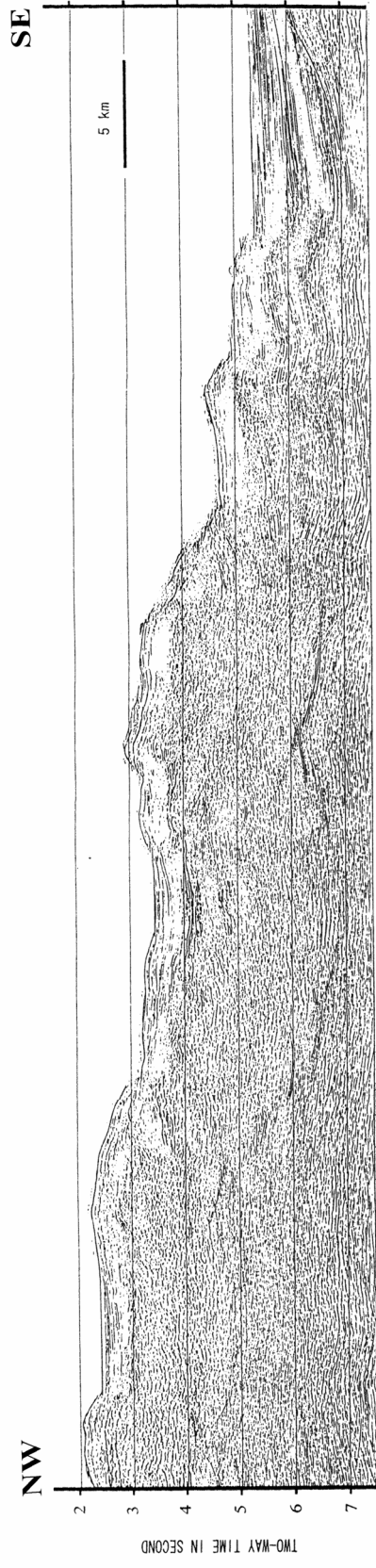


Fig. 4.7 Migrated time section of profile NT96-909. See Fig. 1.4 for profile location.  
 KF: Kodaiba fault; TF: Tokai thrust fault; BF: back thrust fault; FT: frontal thrust fault.

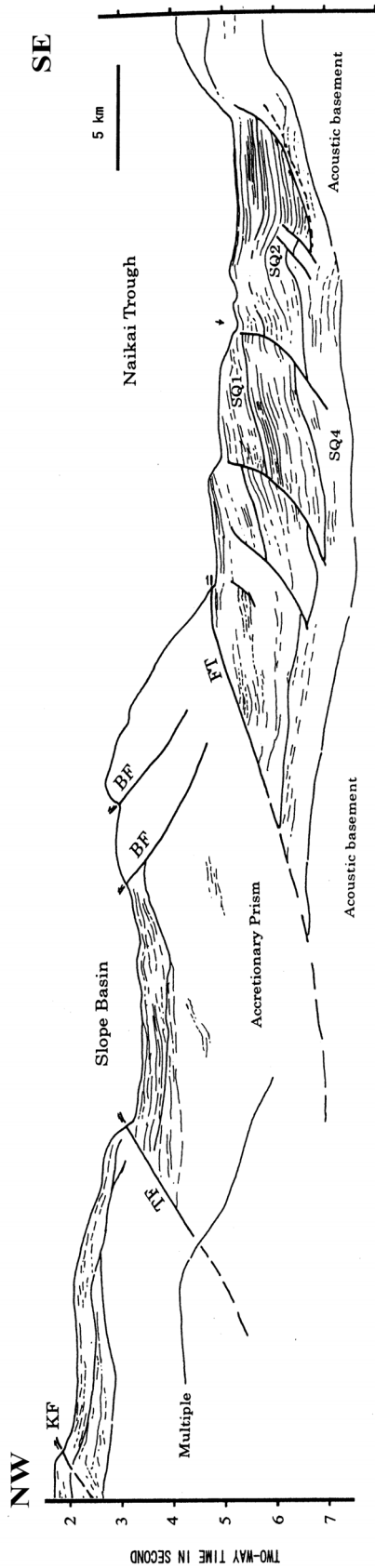
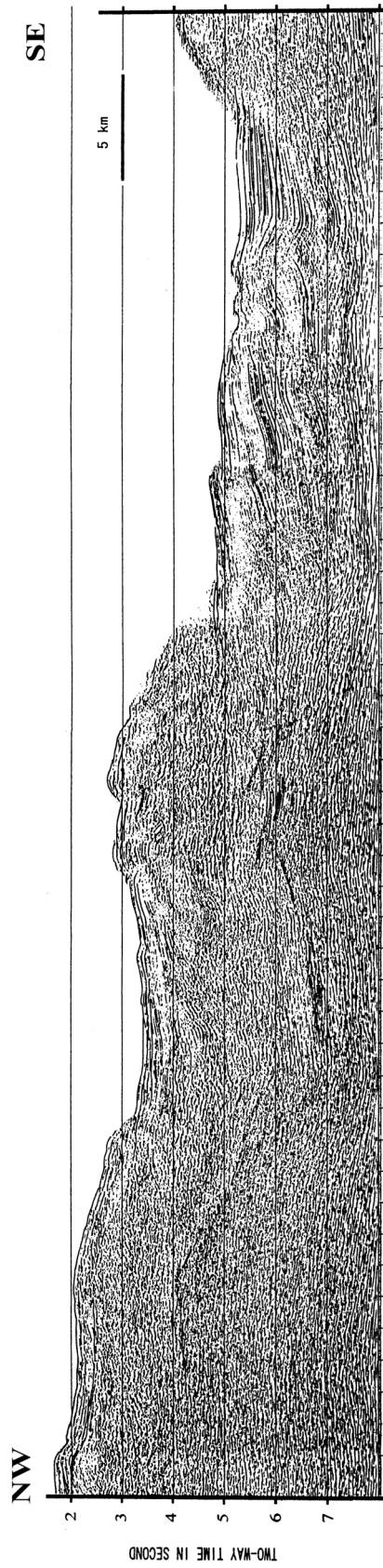


Fig. 4.8 Migrated time section of profile NT96-915. See Fig. 1.4 for profile location.  
 KF: Kodaiba fault; TF: Tokai thrust fault; BF: back thrust fault; FT: frontal thrust fault.

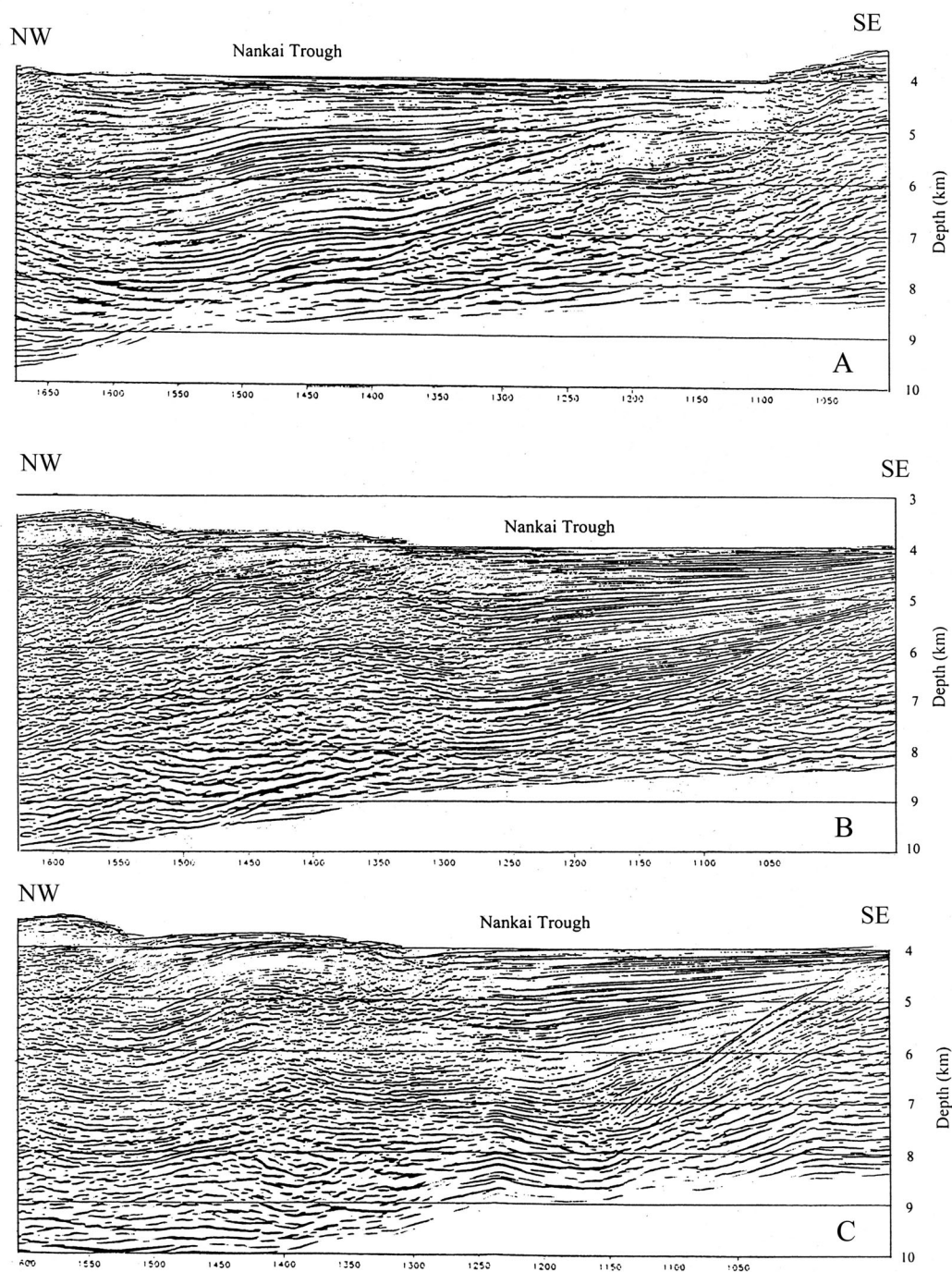


Fig. 4.9 Depth migrated sections showing the sedimentary sequences and deformations of the Nankai Trough axis. A: Depth section of profile NT96-901. B: Depth section of profile NT96-909. C: Depth section of profile NT96-911. See Fig. 1.4 for profile locations.

The strata of the inner accretionary prism on the western trough slope have been faulted and folded, and give rise to characteristically discontinuous reflections of moderate energy and variable amplitudes. The seismic facies of the accretionary prism are complex. The sequence overlying the accretionary prism consists of hemipelagic sediments and deformed accretionary sediments. The Miocene T and K formations of Okuda and Honda (1988) are found along the Tokai thrust fault. The T formation is correlated with the consolidated mudstones dredged at site 362 of the Kumano Basin and is separated from the overlying K formation by an unconformity on the outer accretionary ridge (Inoue, 1980). The K formation consists of forearc terrigenous deposits.

#### 4.2 Seismic sequences and stratigraphic units in Zenisu deep-sea channel

Four seismic sequence units (Unit A, B, C and D) on the northern Zenisu Ridge have been recognized based on the seismic profiles NT96-102 and NT96-103 (Figs. 4.2, 4.3 and 4.10).

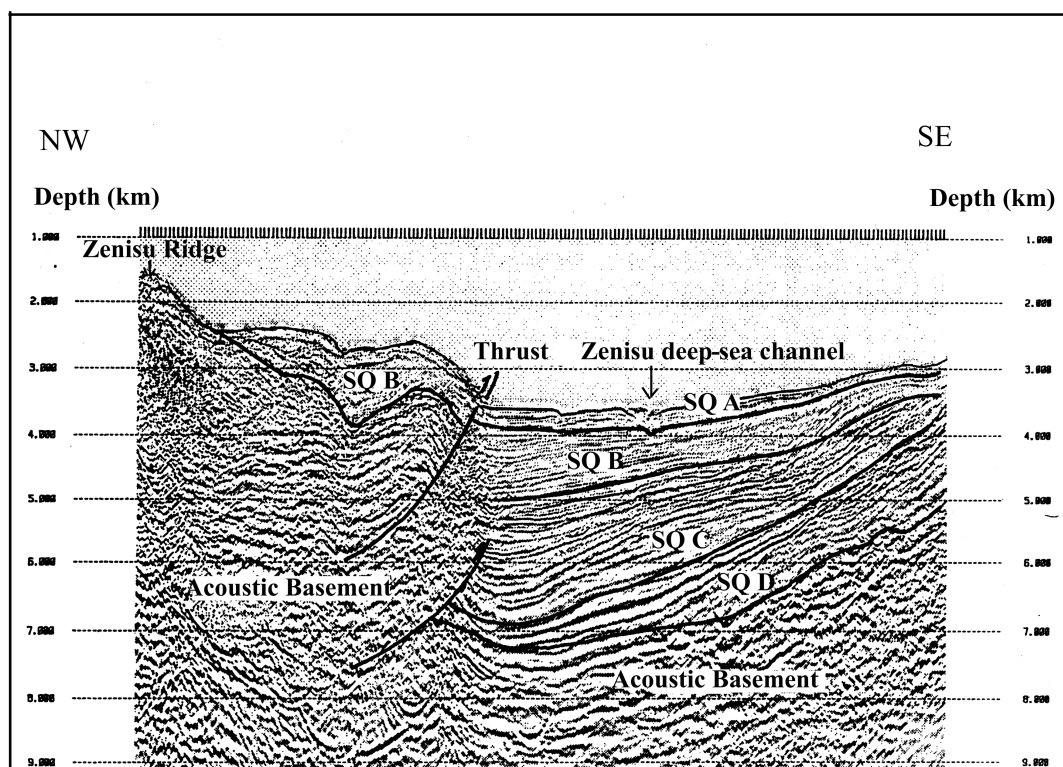


Fig. 4.10 Depth section of profile NT96-103 showing the seismic units A, B, C and D. Sediments over 5 km thick overlie the acoustic basement. SQA, B and C consist of thick turbidites. A channel topography occurs at the central part of the Zenisu Trough. A shallow thrust is interpreted northwest of the Zenisu Trough, but its extension at depth is not clear. See Fig. 1.4 for profile location.

**SQ A** occurs on both sides of the Nankai Trough and the Zenisu Trough. It is characterized by relatively continuous reflections of low energy and variable amplitudes. The sequence onlaps unit B on the Zenisu Ridge. It represents Quaternary channel-fill sediments deposited after uplift of the Zenisu Ridge (Pickering et al., 1993; Taira and Niitsuma, 1986). Unit A is widespread in the central Zenisu Trough (Fig. 4.11, 4.12, 4.13) and represents a levee facies.

**SQ B** consists of relatively continuous, low amplitude reflections. Its thickness varies, but is consistently 500-800 m in the Zenisu area while increasing from south to north (Fig. 4.10). It consists of semi-consolidated turbidites as confirmed by dive 523. We observed the typical graded bedding and wavy and ripple laminated divisions (Wu et al., 2000). Microfossils in the rock yielded a Middle to Late Pliocene age. Outcrops of Unit B also occur on the slope of Zenisu Ridge and on some seamounts (Fig. 4.11).

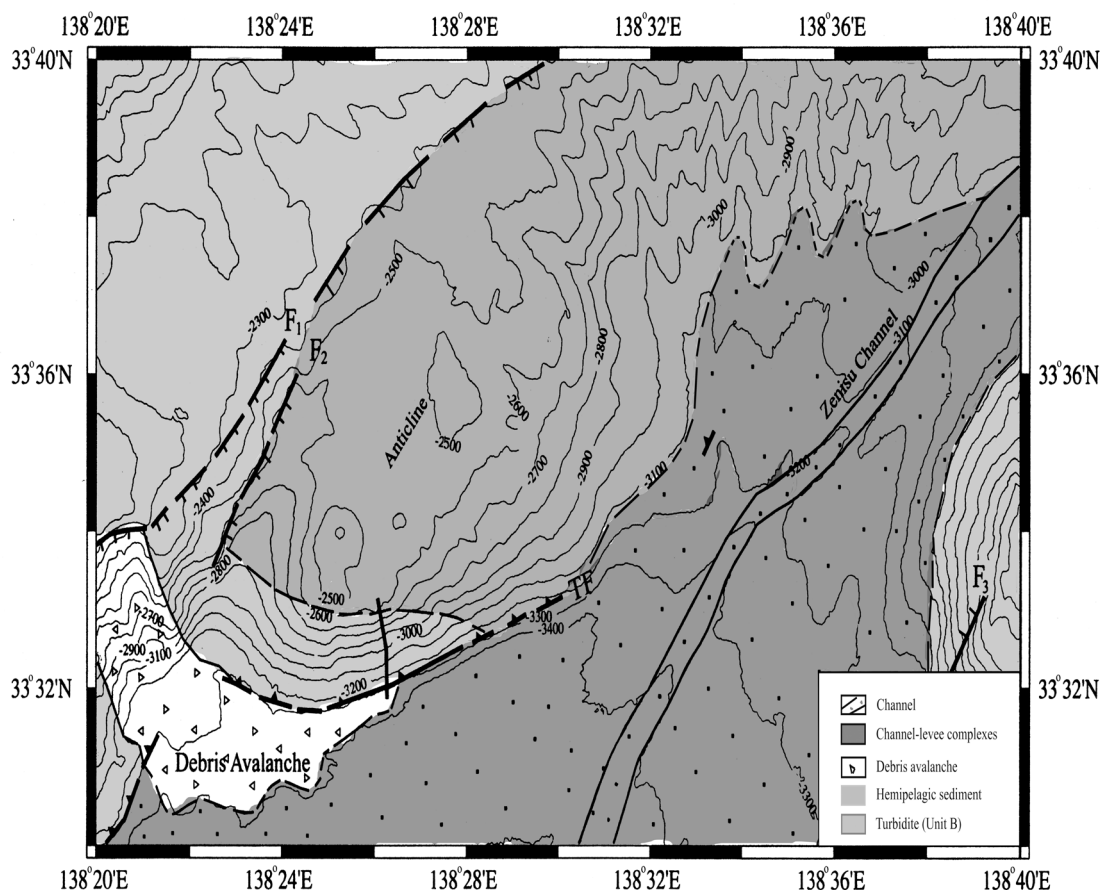


Fig. 4.11 Structural map of the study area, the location of which is shown in Fig. 4.1. Thick lines are faults, of which F1, F2, F3 are normal faults, while TF represents a thrust fault. The distribution of the seismic SQA (turbidites) and B (older turbidites with outcrops) are also shown.

**SQ C** has marked, continuous, parallel reflections of moderate energy and medium amplitude. Its thickness is about 500-900 m on profile NT96-102, increasing to 3000 m northward on profile NT96-103 (Fig. 4.10). This large thickness is a result of rapid subsidence. Unit C is made up probably of bioturbated hemipelagic mudstones and sandstones, volcanic ash and lava as observed during dive 324 (Henry et al., 1997). It represents the strata of the Shikuko Basin, and may be of Late Miocene-Early Pliocene age, although no reliable age data are available.

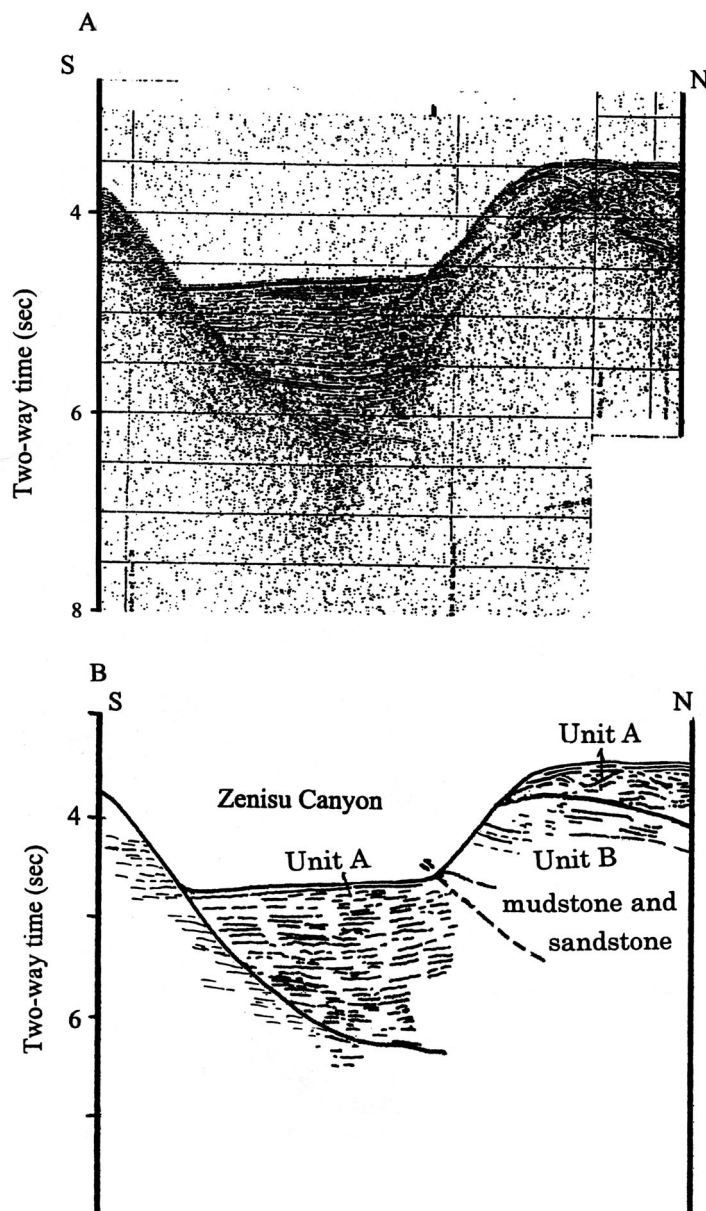


Fig. 4.12 A: Single channel seismic profile KK31 (Kaiko I Research Group, 1986) and B: interpretation. This profile lies very close to dive 523. The dipping strata in the lower part and parallel strata in the upper part of the section have been confirmed by observations from a submersible. Thrust faults are deduced from the observed faulted breccia and steep cliffs. See Fig. 4.1 for profile location.

**SQ D** is marked by high energy, high amplitude reflections. We interpret it to be debris flow deposits derived from proximate submarine volcanoclastic detritus and hemipelagic muds. It may be correlated with the Lower Shikoku Basin strata (Table 4.1) which is of Miocene-Pliocene age (Pickering et al., 1993).

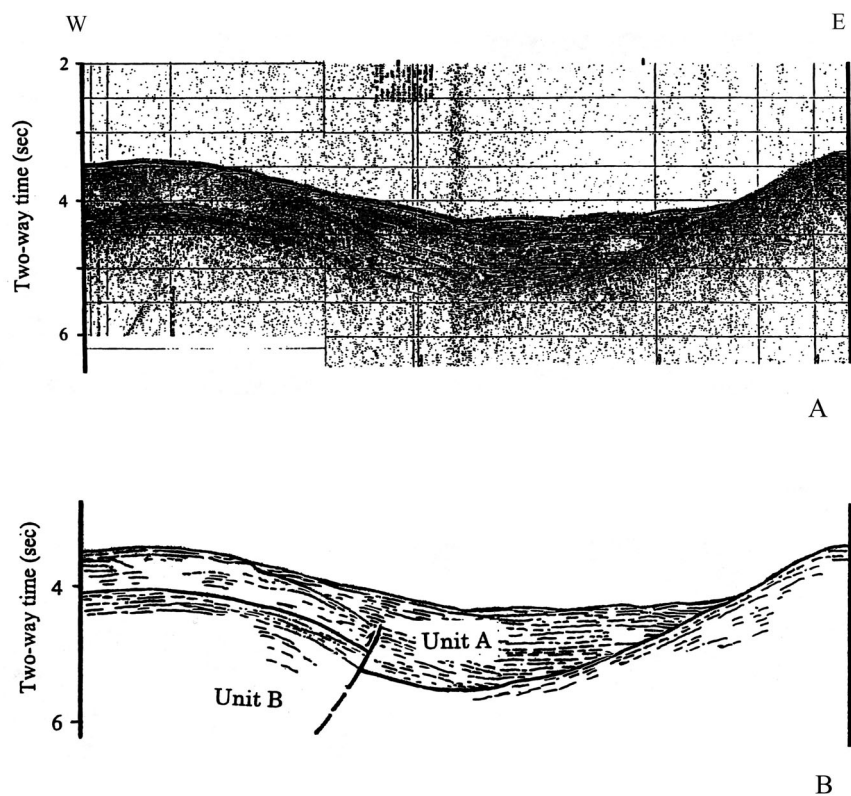


Fig. 4.13 A: Single channel seismic profile KK32 (Kaiko I Research Group, 1986) and B: interpretation. This profile shows a blind thrust and onlap to the east in unit A. See Fig. 4.1 for profile location.

### 4.3 Seismic sequence units of the Zenisu Ridge

The seismic sequences on the Zenisu Ridge were also imaged in seismic profile NT96-102. Three seismic units were recognized on this section while sequence A is lacking because of uplift of the ridge (Figs. 4.2 and 4.14, 4.15, 4.16). Because the basement of this ridge has a pronounced relief, Sequence D is limited to local occurrences. The distribution of all seismic sequences are made more complex by volcanic activity. Sequence B, for example, extends to the trough area in the south (Fig. 4.3).

### 4.4 Correlation and chronology of the seismic sequences

The sedimentary sequences of the Nankai Trough have been drilled during ODP, of which site 808 is the most relevant (Taira et al., 1992; 1993). Pickering et al. (1993) discussed the sequence stratigraphy of the Nankai Trough and correlated it to the major high-frequency variations of the Vail eustatic sea-level curve of the past approximately 14 myr. They did not establish any clear correlation between the major eustatic sea-level lowstands and the time of influx of sandy terrigenous turbidites. The onset of coarse sand accumulation at site 808, about 300 ka, occurred during the last major glacio-eustatic fall in sea level. Therefore, it is reasonable to infer that sea level was a contributing factor, but not the major cause, for deposition of the clastic trough facies (Fig. 4.17).

Assuming that turbidites were emplaced more-or-less instantaneously, we can infer that hemipelagic deposition has taken up most of the time needed for sediment accumulation. If we take the mean values of 30.2 and 6.5 cm as representative thicknesses of turbidites and hemipelagites respectively, then each 6.5 cm-thick hemipelagite section in the lower part of ODP sequence A (Tab. 4.1) and an average of 30 cm of turbidites were deposited every 200 years. Given that the average recurrence time of large historic earthquakes off southwestern Japan is on the order of 100-200 years, a relationship between turbidite deposition and major seismic events may be speculated on (Ikehara, 1999).

Tokuyama et al. (1998) divided the trough-fill into two seismic sequences on the southern Zenisu Ridge (Fig. 4.17). The unit overlying reflector c (Fig. 4.16) represents volcanoclastic turbidites and hemipelagic sediments laid down during the past 1 myr based on tectonic analysis. The sequence between the reflectors b and c is probably hemipelagic. Underlying reflector b are sediments 20-1 Ma in age deposited after rifting of the Shikoku Basin. The Tenryu turbiditic fan system developed since 1 Ma from sediments delivered via the Tenryu deep-sea channel. This implies that the channel came into existence at that time. Tokuyama (1998) suggested that if the subsidence rate is 3 cm/yr, then the 3 km thickness of sediment fill would represent about 1 myr, a value that is in agreement with the independent estimate above.

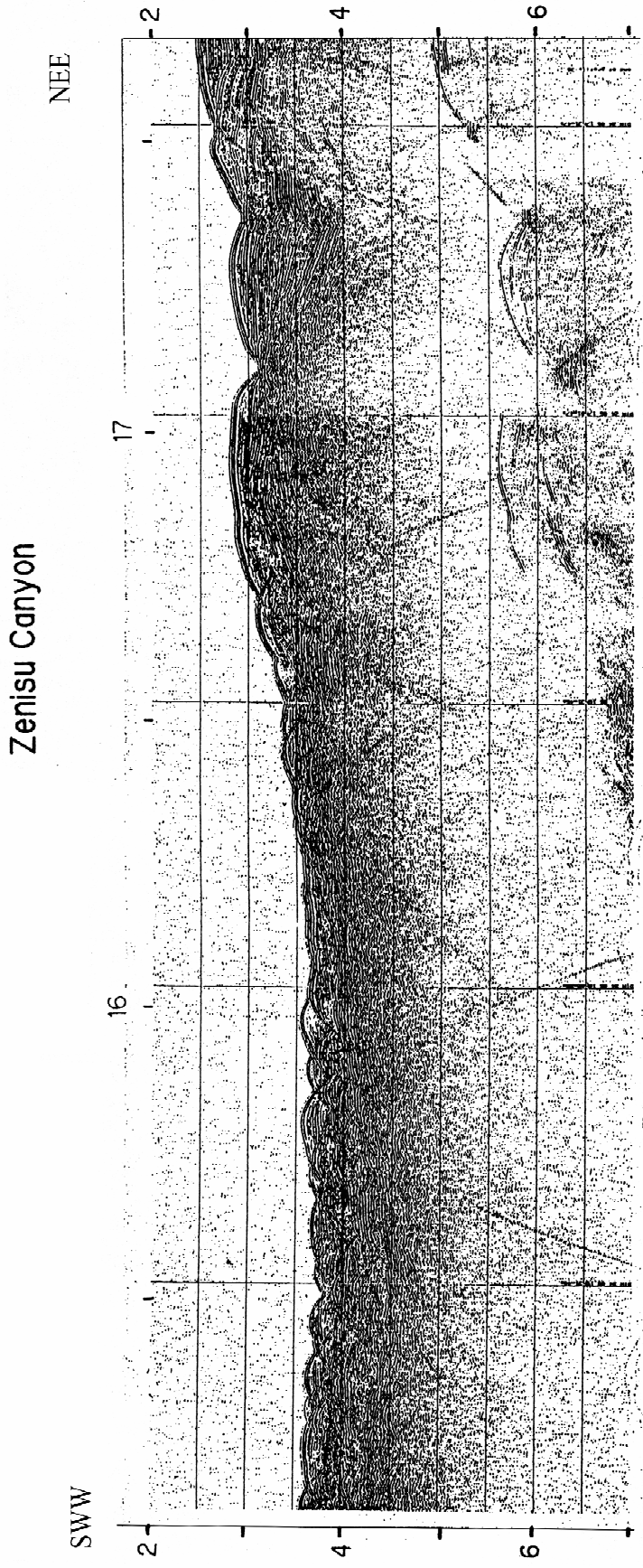


Fig. 4.14 A: Single channel seismic profile KK36 (Kaiko I Research Group, 1986). This profile shows channel-levee sediments (SQA) of the upper part of the trough-axis channel. Fig. 4.1 for profile location.

Tab. 4.1 Seismic sequences and stratigraphic units in the Nankai Trough and the Zenisu area.

					Quaternary	Pliocene	Miocene
					ODP site 808 in the Nankai Trough (Pickering et al., 1993)		
		Zenisu area (Nakanishi, 1998)			Unit I-III, Nankai Trough facies	Unit III-IVa, Upper Shikoku Basin strata, volcanic ash, tuff, bioturbated hemipelagic muds	Unit IVb, Lower Shikoku Basin strata, bioturbated hemipelagic sediment
		Zenisu area (Tokoyama et al., 1998)			Layer 1, P-wave velocity 1.7-2.0 km/s	Layer 2, P-wave velocity 2.5-3.0 km/s	Volcaniclastic sediments
					Upper sequence	Lower sequence I	Igneous basement
					channel-levee turbidites	fan turbidites	
					Interpretation of sedimentary facies	interbedded turbidites and hemipelagic muds	
					discontinuous to continuous, low energy, variable amplitude reflections onlapping the underlying strata	interbedded hemipelagic muds and turbidites	
					continuous reflections, low energy and low amplitude	interbedded hemipelagic muds and turbidites	
					reflection of a variable amplitude and energy	interbedded hemipelagic muds and turbidites	
					discontinuous reflections with variable amplitude and moderate to high energy	interbedded hemipelagic muds and turbidites	
					discontinuous, high energy reflections, top is an important unconformity	igneous basement (possibly volcanic rocks)	
					Basemnet		Basalt
					SQA	SQB	SQC
					SQD		

A schematic stratigraphic column for ODP site 808 based on detailed shipboard core description, sedimentary facies interpretations and microfossil control is shown in Fig. 4.17 (Pickering et al., 1993; Taira et al., 1993). Five stratigraphic sequences overlying SQ VI, the basaltic igneous basement, are evident. SQ V is made up of volcanoclastic rocks. SQ IV represents bioturbated hemipelagic mud with a higher content of volcanic ash and tuff in the upper section. SQ III corresponds to sediments of the trench-basin transition. The initiation of outer trench-wedge sedimentation can

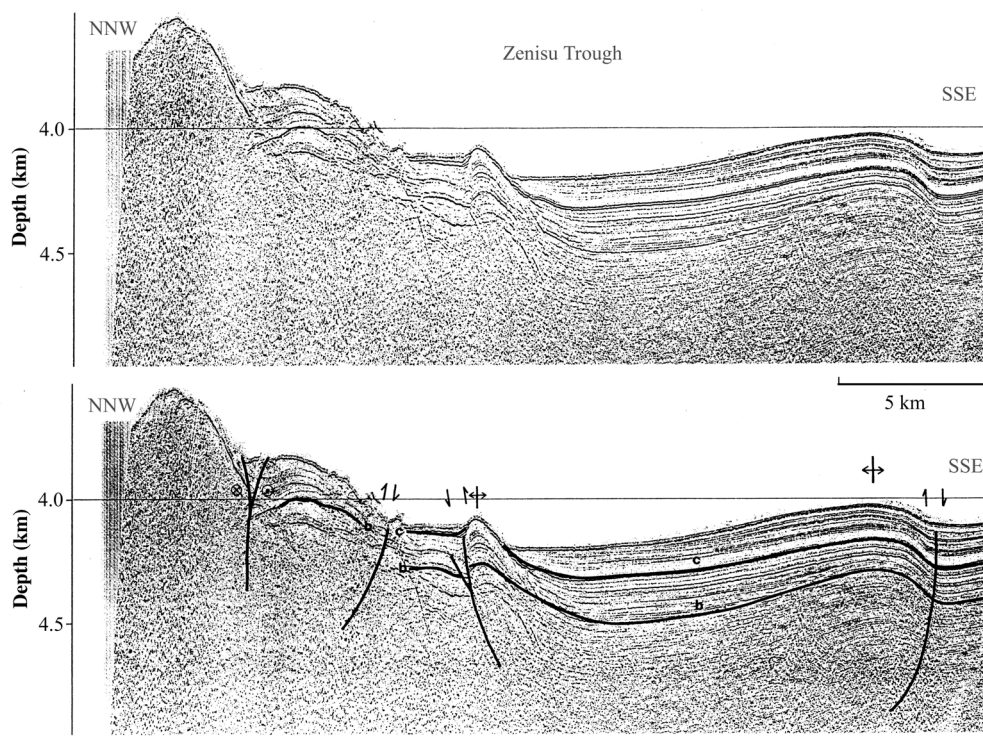


Fig. 4.16 Profile across the Zenisu Trough (upper) and interpretation (lower) (after Tokuyama et al., 1998). See Fig. 4.1 for profile location.

be recognized by the first appearance (moving upsection) of silty terrigenous turbidites at a depth of about 620 mbsf (Fig. 4.17). These turbiditic layers typically display base-absent Bouma sequences complete with ripple cross-lamination. In contrast, the deposits of the Shikoku Basin are dominated by bioturbated hemipelagic mud. SQ II consists of trench-wedge silty turbidites and hemipelagic mud, and is a coarsening-upward sand/silt sequence. SQ I represents a thin, silty or sandy debris slide. These trench sediments from site 808 are early Quaternary in age. Accordingly, we assume by correlation that the sequences of the eastern Nankai Trough are of the same age.

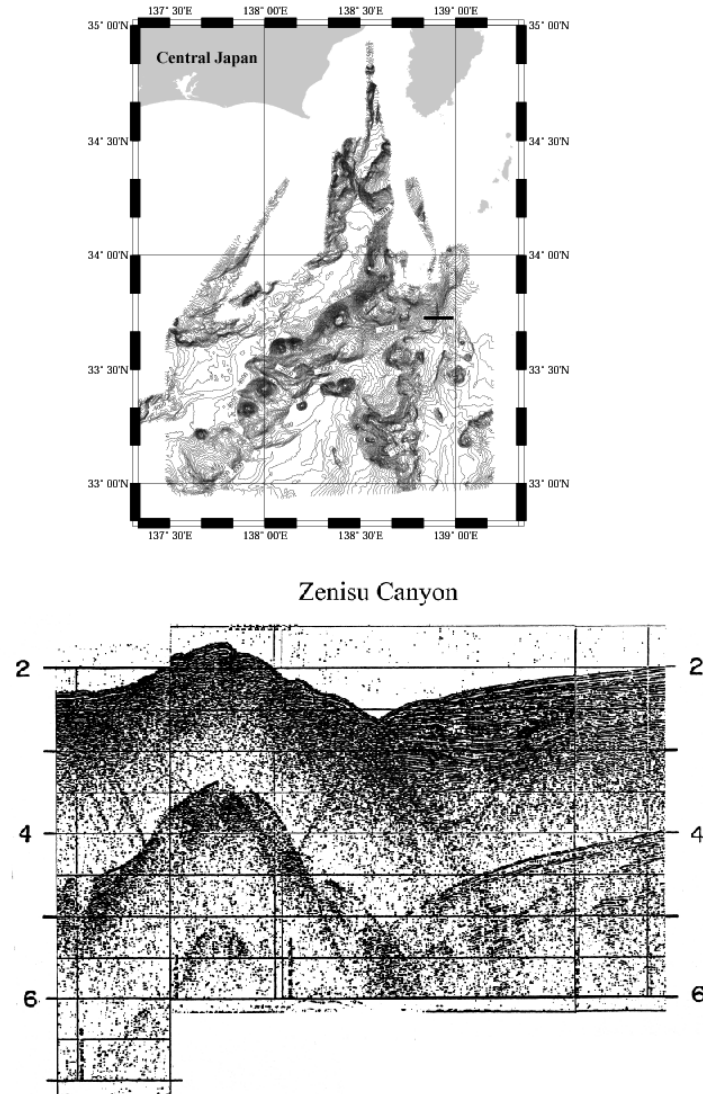


Fig. 4.15 Single-channel seismic profiles KK42 (Kaiko I Research Group, 1986) which shows the morphology and fill sediment of the Zenisu Canyon. See upper map for profile location.

## 5. Structure of the eastern Nankai Trough

A total of 454 km of G-gun seismic data were acquired during cruise KH96-02 of the R/V *Hakuho-mura* (Fig. 1.4) to study the detailed structure and evolution of the Nankai deep-sea channel developed in the eastern Nankai Trough just external to the

subduction zone (Aoki et al., 1982; Moore et al., 1993; Nakanishi et al., 1998; Okuda and Honda, 1988; Tokuyama, 1998).

The Nankai Trough has been a major site of subduction until Recent time, when a nascent subduction zone developed at the southern Zenisu Ridge. Evidence for this

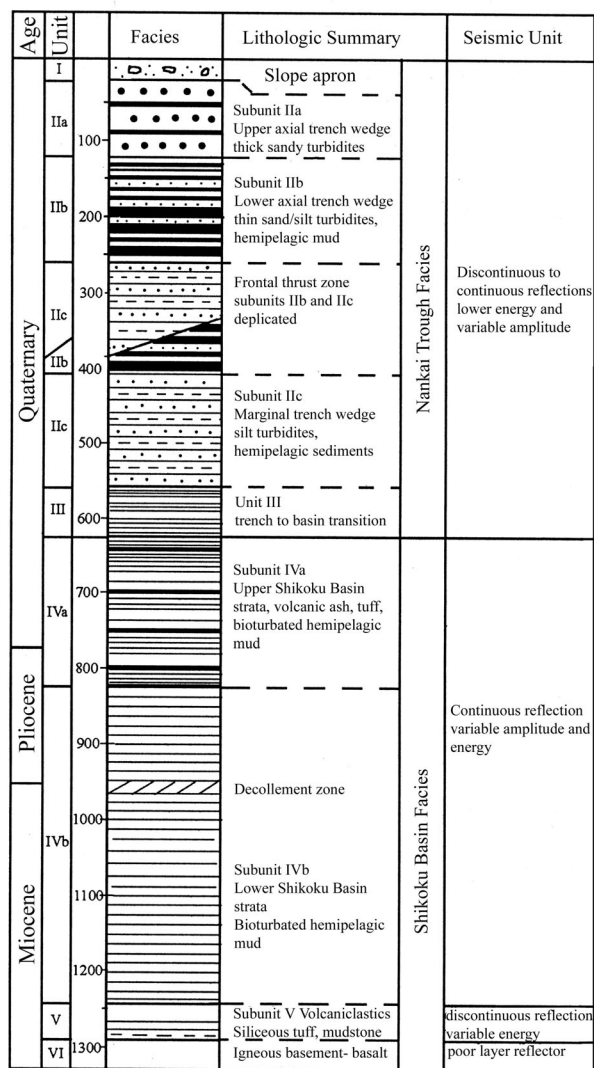


Fig. 4.17 The stratigraphy, lithology, facies and correlation to the seismic units of ODP site 808C of the western Nankai Trough based on shipboard core descriptions, sediment interpretation and microfossil control (modified after Pickering et al., 1991).

nascent subduction is provided by the intra-oceanic plate thrust fault extending from the southern Zenisu Ridge northward to the Izu-Bonin Arc (Fig. 5.1), as well as uplift of the basement and possible dewatering processes on the southern Zenisu Ridge. Thus, the Nankai Trough and surroundings provide a rare opportunity to study the process of

subduction zone jump and formation of a new subduction zone and hence to elucidate the dynamic processes of subduction. In the following, we shall discuss the deformation, nascent subduction zone and subduction jump in the study area based on seismic data and submersible surveys.

### 5.1 Structural elements of the Nankai Trough

In our study area, six tectonic units have been recognized from the continental slope to the Zenisu Ridge based on geomorphology and deformation style (Fig. 5.2): (1) forearc basin, (2) accretionary wedge, (3) Nankai Trough, (4) Zenisu Ridge, (5) Zenisu Trough and (6) Izu-Ogasawara Arc. The forearc basin is located north of the Tokai thrust fault. The accretionary wedge includes the rigid backstop, the slope basin and the lower slope prism. The rigid backstop is an old accretionary complex located west

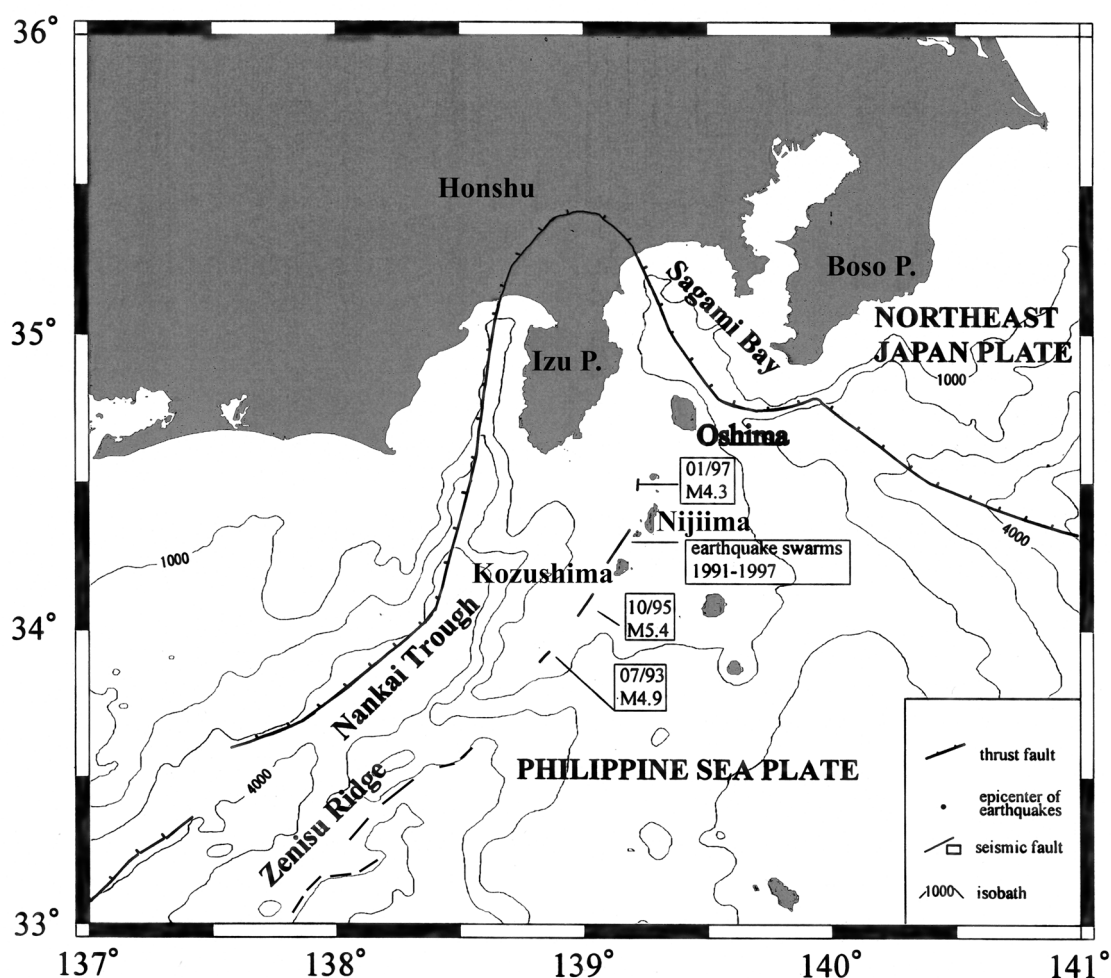


Fig. 5.1 Schematic regional tectonic map showing the nascent subduction zone and earthquake occurrences.

of the Tokai thrust (TF), which is an important zone of seismicity (Tokuyama, 1988). The slope basin lies between the Tokai thrust fault (TF) and backthrust fault (BF) and is marked by folds, listric thrusts and sediments derived from the uplifted subduction complex (Dickinson and Seely, 1979; not labelled in Fig. 5.2 for the sake of clarity). The accretionary wedge is bounded by the frontal thrust. The major deformational characteristics of the subduction zone from west to east based on seismic data (MCS reflection profiles of Figs. 4.4-4.10) and submersible surveys will now be discussed.

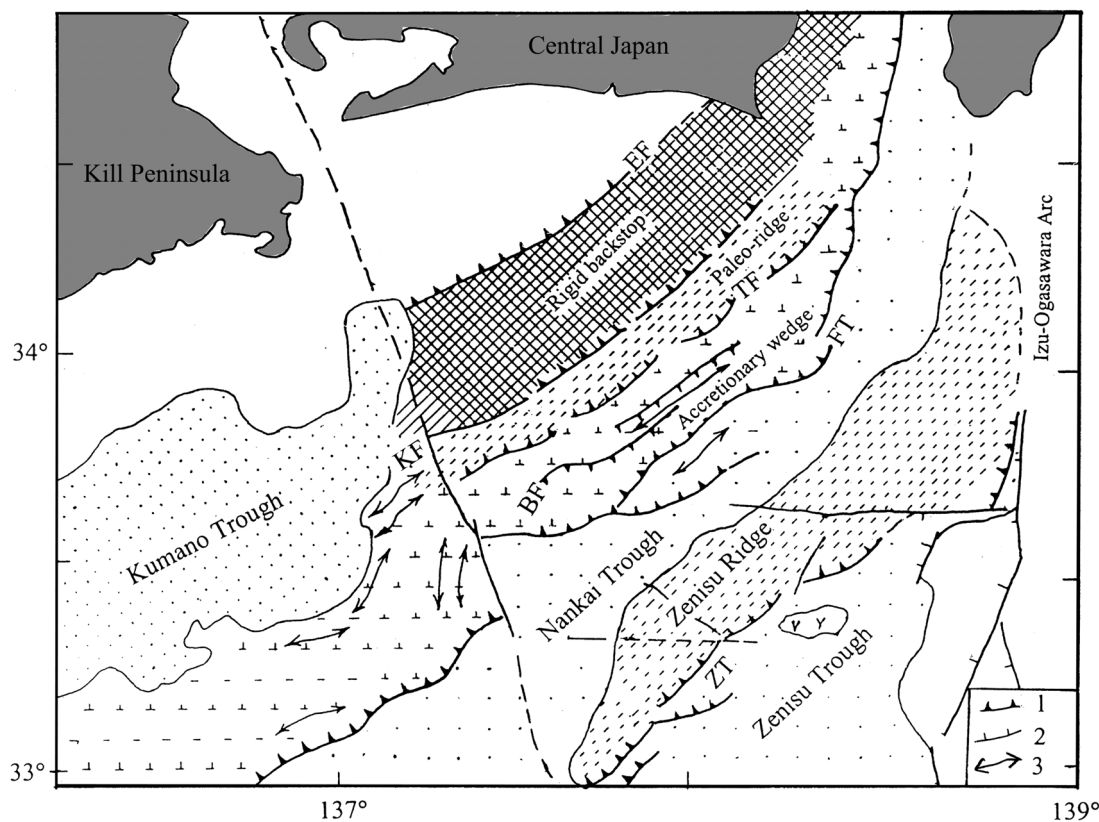


Fig. 5.2 Geological map of the eastern Nankai Trough accretionary prism derived from swath bathymetry and submersible data. The six tectonic units of the area are: Kumano Trough (densely dotted), accretionary wedge (rigid backstop, paleo-Zenisu Ridge, new accretionary wedge), Nankai Trough, Zenisu Ridge (dashed), Zenisu Trough and Izu-Ogasawara Island Arc. 1: thrust fault, 2: shear fault, 3: fold, EF: Enshu thrust fault, KF: Kodaiba thrust fault, TF: Tokai thrust fault, BF: backthrust fault, FT: frontal thrust fault, ZT: Zenisu thrust fault.

### 5.1.1 Forearc basin and accretionary wedges

The upper slope prism (Kumano Basin and rigid backstop) is part of the outer ridge. It is represented by discontinuous reflections of a moderate amplitude, and consists of Neogene sediments probably of Miocene age (the M formation of Okuda and Honda, 1988). Rock samples from the uppermost sedimentary layers yielded ages of 5.6-8.2 Ma. Two important thrust faults, the Enshu thrust fault and the Tokai thrust fault, existed at the inner and eastern boundaries of the forearc basin respectively (Fig. 5.2).

The Tokai thrust system is located at the margin of the rigid backstop where there is a step morphology and recent sediments are lacking. This fault is an expression of the most recent tectonic activity, whereby old slope sediments thrust over Quaternary deposits as seen on many profiles (Figs. 4.4 to 4.8). Abundant talus have been observed during submersible dives (Ashi, 1997); its concentration is used as an indicator of the degree of activity of the TF. Deformation of the footwall is suggested by the inclined stratification of the gravity flow deposits on the upper section, while complex folding and faulting characterize the underlying sedimentary section on profiles 909 and 915 (Figs. 4.6 and 4.7). On the profiles 909 and 915 (Fig. 4.7 and 4.8), two listric reverse faults occur beneath the inclined strata. These faults have small throws and extend to the surface at the fringes of folds. They cannot be readily followed at depth because of multiples (Fig. 5.6).

The Kodaiba Fault (KF) observed during several submersible dives (Mazzotti et al., 1996; Le Pichon et al., 1994; Thoue et al., 1995) is an active listric thrust which strikes NE-SW and extends for more than 70 km but does not reach the acoustic basement. Strata outcropping on its hanging-wall block are most probably Lower-Middle Miocene in age (Okuda et al., 1983; Okuda and Honda, 1988). Large talus accumulations are found at the footwall of the fault as well as along the fault plane.

The slope basin is located between the TF and the BF. It is a compressional basin bounded by thrust faults, a characteristic sedimentary basin that accompanies subduction. The basinal fill consists of a stratified sequence (sequence B) overlain by a transparent sequence (sequence A) and can be contrasted with the trough fill. In general, sequences A and B comprise a thick, intensively compressed sedimentary section with reflections of moderate to high amplitude, low continuity and moderate energy. On the hanging-wall of the TF, sequence B probably represents the Middle Miocene to Early Pliocene accretionary prism sediments (Taira and Ashi, 1993). The rugged acoustic basement occurs at a depth of about 6 km below sea level and can be correlated directly with that beneath the Zenisu Ridge (profile 96-102, Fig. 4.2).

The accretionary prism is located on the lower slope, bounded by the frontal thrust faults (FT) and the back thrusts (BF). The FT form a major fault zone with thrust faults

commonly extending to the decollement surface (Figs. 4.4 to 4.7 and 4.9). The thrust surfaces are wavy, suggesting that different lithologic units are involved. On the landward slope, several very low angle thrusts developed over the older sequence SQ4 of the Quaternary slope fan. The backthrusts have moderate dip angles as seen on seismic profiles and during submersible observations (Le Pichon et al., 1992).

### 5.1.2 Deformation of the trough axis and the decollement

The Nankai Trough can be subdivided into: (1) an area west of the trough axis, with a protothrust system which is characterized by box-folds and two high-angle thrusts in the trough-fill sequences (Fig. 4.10), and two thrusts which reach the seafloor and bound the folds; and (2) the area east of the trough axis where the sediments are undeformed. The boundary between the Nankai Trough and the Zenisu Ridge is unclear because it is masked by numerous slumps. It is interpreted as a reverse fault on profile 901 (Fig. 4.4). The basement is not involved in these deformations. Within the sedimentary section of the Shikoku Basin (most likely within its hemipelagic layers) as well as in the trough fill sequences is an apparent decollement.

The Nankai Trough (NT) was assumed to be formed in the Late Pliocene (Shimamura, 1988). Before that time, the region of the Nankai Trough was an old swell, because SQ4 increases from 0.5 sec in thickness under the Nankai Trough to 0.8 sec under the lower accretionary wedge. Structurally, it was probably similar to a swell like the recently uplifted Zenisu Ridge.

The decollement has been drilled through at hole 808C of ODP Leg 131. It is represented by a 19.2 m thick zone of intense faulting and brecciation (Moore et al., 1992; Park et al., 1999). On seismic profiles in the western Nankai Trough, the decollement under the NT accretionary prism is imaged as a high-amplitude, reverse-polarity reflection (Aoki et al., 1982; Moore and Shipley, 1993; Moore et al., 1990). In the eastern NT, it occurs at 5-6 sec twt on our seismic time sections (Figs. 4.4 to 4.7). It is ca. 5 km below the sea surface at the lower prism, but plunges slowly to 6 km below the Tokai thrust (Fig. 5.3). The decollement dips slightly to the west. It is imaged clearly beneath the lower prism, but is indistinct and perhaps undulating near the Tokai thrust because of the effect of multiples. The undulating decollement was affected by a complex, highly deformed subducting ridge under the lower accretionary wedge (Lallemant et al., 1992; Le Pichon et al., 1996).

### 5.1.3 Structure of the Zenisu Ridge from seismic and geochemical data

The Zenisu Ridge has been suggested to be a nascent subduction zone (Segawa, 1998). Seismic profiling has demonstrated the occurrence of shallow reverse faults (Aoki et al., 1982; Okuda and Honda, 1988), while thrusts have been directly observed from submersibles on its eastern flank (Le Pichon et al., 1987; Lallemand et al., 1989, Tokuyama, et al., 1998). From our data, folds are absent on the western ridge flank, while gentle folds perhaps accompanied by overthrusting occur on the eastern margin (profile 102, Fig. 4.2). Additional evidence for the nascent subduction zone character of the Zenisu Ridge may be found in the negative free-air gravity anomalies at the southeastern base of this ridge, as well as in earthquake activity in the same area (which is the highest in the Tokai area; Takahishi et al., in press). In addition, GPS measurements since 1994 show that the Zenisu Ridge is moving northwestwards at a velocity of 2.5 cm/yr (Segawa, 1998). Although a deep-sea trench and a seismically active Wadati-Benioff zone typical of a subduction zone do not exist at the present time, we suggest that the Zenisu ridge-trough complex will develop into the major compressional zone that accommodates the collision between the Izu-Bonin and Honshu arcs.

More than 90 % of the seismic energy in subduction zones are released in thrust type earthquakes with the axis of maximum compression oriented transverse to the subduction zones. This is consistent with the convergence of the lithospheric plates in these zones. Despite this geotectonic configuration, it is not obvious that generally the stress regime of the lithosphere in a subduction zone is characterized by horizontal compression. It is well known that the lithosphere in a subduction zone can undergo tension and, moreover, the convergence itself can be driven by the gravitational sinking of the subducting plate into the mantle. Nevertheless, to form the subduction zone and to start the convergence and sinking of the plate into the mantle, large compression of the lithosphere is probably necessary. It seems that there is no other physically realistic way to cause failure of the plate and to initiate subduction other than application of large compressive stresses to the lithosphere.

Two examples of lithospheric failure and subduction zone jump exist (Platt, 1990; Shemenda, 1994). One is related to a cessation of subduction resulting from large-scale continent-continent collision. The India-Eurasia collision caused an increase in compression of the Indo-Australian plate. The compressive stresses probably reached the yield strength of the oceanic lithosphere south of Hindustan and produced an intensive intraplate deformation in the central basin of the Indian Ocean. If the convergence continues, a new convergent plate boundary might form in this area resulting in a jump of the subduction zone over a large distance, namely nearly 3000 km. Another case of subduction zone jump occurs in the East Pacific Ocean within the subducting oceanic lithosphere in a flexural sag behind the outer rise due to strong

resistance against the subduction. Along with the very low density of the subducting plate, such a resistance can be caused by subduction of an extensive plateau with a thick crust, by high viscosity of the mantle, or by presence of obstacles (Cande et al., 1987; Schemenda, 1994).

On the southern Zenisu Ridge, failure within the oceanic crust has been confirmed by submersible and OBS data. Le Pichon et al. (1987) reported for the first time the occurrence of surface thrust faults and geophysical and geochemical data have demonstrated the typical oceanic character of the crust in this area. Nakanishi et al. (1998) studied the P-wave velocity and crust structures of the Zenisu Ridge. Their OBS profile P6 obtained during cruise KH96-1 of the R/V *Hakuho-maru* (Fig. 5.3) shows oceanic crust with little thickness increase eastward. The position of OBS's are shown by red lines on the upper right of Fig. 5.3.

Magnetic anomalies across the Zenisu Ridge are generally negative; they are superposed on the short-wavelength anomaly (40-50 nT) caused by the ridge topography. Basaltic and andestic rocks have been dredged from the middle segment of the Zenisu Ridge. They are not of oceanic origin, but are similar to the rocks on Nijima Island (Research Group of the 1992 Cruise to the Zenisu Ridge Area, 1994). Analyses of our rock samples obtained during dive 521 and Dolphin dive 445 are consistent with this result.

## 5.2 Thrust faults on the southern slope of the Zenisu Ridge

### 5.2.1 Thrust faults revealed by seismic data

On profile NT96-103, we mapped two parallel thrusts along the boundary between the Zenisu Trough and the Zenisu Ridge (Fig. 4.10). The crest of the thrust ramp rises ca. 900 m from the deep seafloor. Deep-water turbidites onlap the back of the ramp, where the crest may undergo erosion, with the progradation of a denudation complex basinward from the front of the thrust.

On seismic profile KK31, possible evidence for thrusting also exists. At the base of the ridge slope, the strata change their dip and reflections from a fault may be discerned (Fig. 4.12). Profile KK32 shows a blind thrust and the accompanying anticlinal structures (Fig. 4.13).

Within the south Zenisu Trough, a thick turbiditic sequence (Units A, B, C) with a drape fold was deposited (Le Pichon et al., 1987; Takahashi et al., 1999; Tokuyama et al., 1988). The contact between the uplifted acoustic basement of the Zenisu Ridge and

the infilling turbidites is possibly a reverse fault. The accompanying fold observed during our dive and by Le Pichon et al. (1987) also support this interpretation. It suggests a blind thrust and drape on the fault (Lallemant et al., 1989; Le Pichon et al., 1987), but the same configuration also results when the fault reaches the seafloor (seismic profile NT96-103, Fig. 4.10).

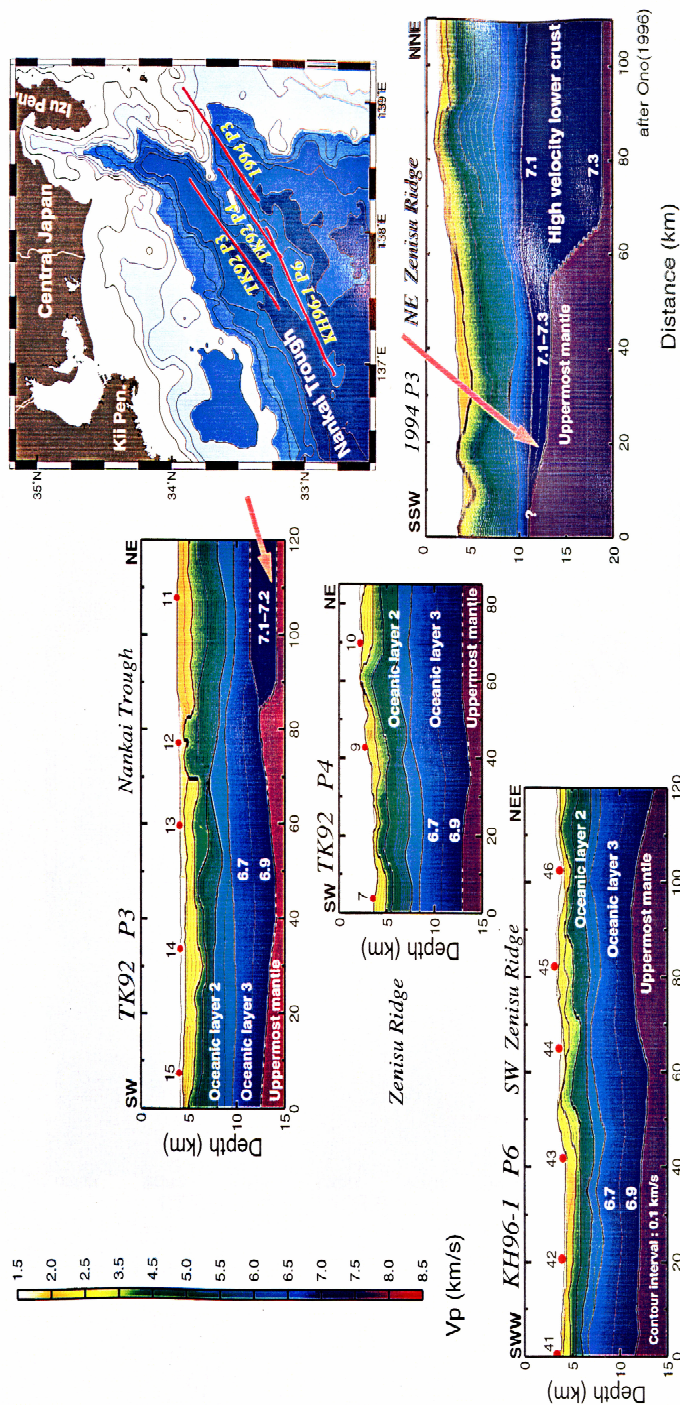


Fig. 5.3 Results of OBS refraction profiles along the Zenisu Ridge and Nankai Trough which show the velocity-depth structures of the Zenisu Ridge and the central Nankai Trough. Profile KH96-1 in the southwest shows typical oceanic crust, while profile 1994 P3 of Ono (1996) in the northeast shows transitional crust. Upper right shows the location of the profiles (after Nakanishi et al., 1998).

The regional extension of the fault could also change its nature. Soh et al. (1998) suggested that the fault extends northward as the Zenisu-Oki Tectonic Line (Zenusu-Oki TL, Fig. 5.4), which involves shortening within the Izu-Ogasawara Arc. Note that the subduction boundary has migrated gradually with time (Fig. 5.4).

### 5.2.2 Deformations observed from a submersible

Amid the fractures seen from a submersible, it is not always possible to recognize joints and faults. A simple criterion we used is based on the density and continuity of the fractures and on the existence of tectonic breccia. Joints usually end abruptly on bedding planes or as they meet another joint, whereas faults show more continuity, density and are accompanied by breccia. However, large joints may appear locally to consist of several fractures. For this reasons, our fault observations are not always definitive.

The first part of dive 523 covered the southeastward-dipping lower scarp from 3400 to 3200 m water depth. The track started from the flat seafloor of the Zenisu Trough at 3380-3390 m where erosion or non-deposition dominated. Then the debris flow sediments or avalanche breccia covering the base of the slope were investigated. At dive time 11:43 to 11:45, a few clam shells were observed (Fig. 3.10, photo I). The last time we observed clams was at 12:00:25. Among them appeared be living specimens. Poorly consolidated mudstones crop out over the entire lower slope. We collected the rock sample SP1 which consists of mudstones and sandstones (Figs. 3.10, photos II, III and IV). High-density fractures were observed along the track (Fig. 3.10, photo IV). The strike of the fractures is either northwest (normally  $298^{\circ}$ - $323^{\circ}$ ) or northeast ( $60^{\circ}$ - $84^{\circ}$ ). The rocks were brecciated (Fig. 3.10, photo II), suggesting that we encountered a fault zone, namely the thrust TF mapped on seismic profiles NT96-103 and KK31 (Fig. 4.11). This thrust may have reached the seafloor because of the observed breccia and dipping stratifications.

After leaving the thrust, the slope gradient became more gentle. Fine hemipelagic sediments sampled by push core no. 2 predominated. There was a large mudstone outcrop on the upper scarp. It dips very gently in the down-slope direction. The rocks were completely fractured. At dive time 14:14:53, we observed two conjugate fracture systems, *viz.*  $331^{\circ}/60^{\circ}$  and  $239^{\circ}/70^{\circ}$ , with the WNW-trending system dominating. To the northeast, an anticline induced by the second fold was observed along the track, but the dive track crossed only its eastern flank. For a detailed geometry of this anticline, the reader is referred to the discussion of the seismic profiles KK32 and NT96-103.

### 5.3 Neotectonics and the regional stress field of the Nankai Trough

Methods of stress measurement include the analysis of earthquake focal mechanism, well-bore enlargements and other *in situ* stress measurements, as well as the analysis of faults and fractures. In this study, we reconstruct the stress field by using natural deformations such as fractures and folds.

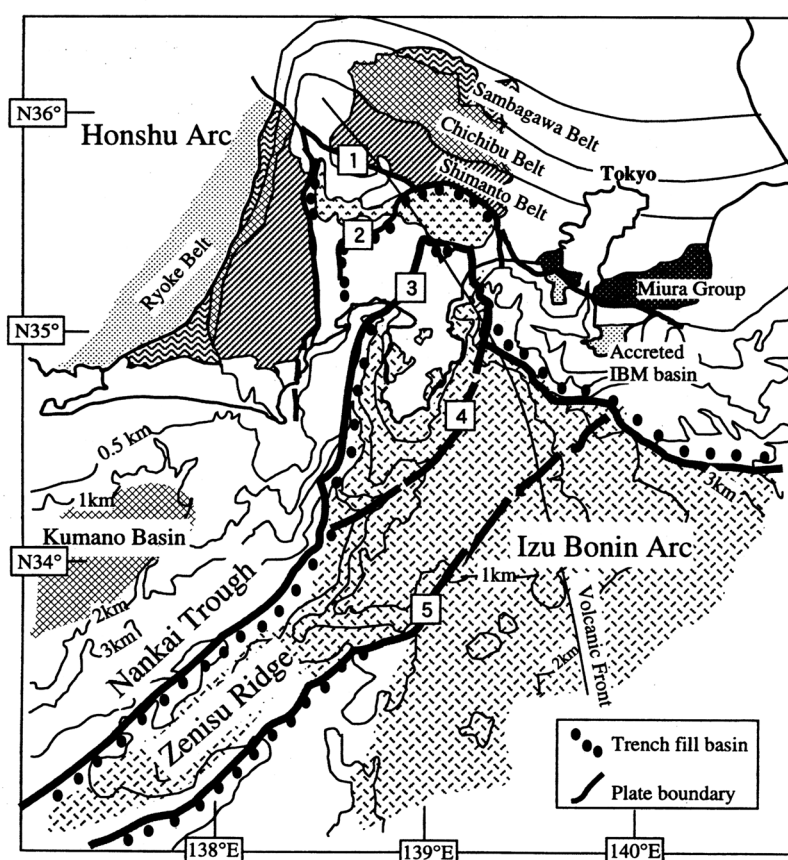


Fig. 5.4 General tectonic setting of the Izu collision zone. Numbered lines represent plate boundaries (trenches) with ages ranging from the Middle Miocene to the present. The Ashigara Basin is located around the label '3'. Noteworthy is that the plate boundary has migrated step-by-step with time from north to south. 1: Mineokia/Tonoki-Aikawa/Itoigawa-Shizuoka Tectonic Line (TL). 2: Tonoki-Aikawa/Nishikatsura/Minobu TL. 3: Kouzu-Matsuda/Kannawa TL. 4: Izu-Toho TL. 5: Zenisu-Oki TL (after Soh et al., 1998).

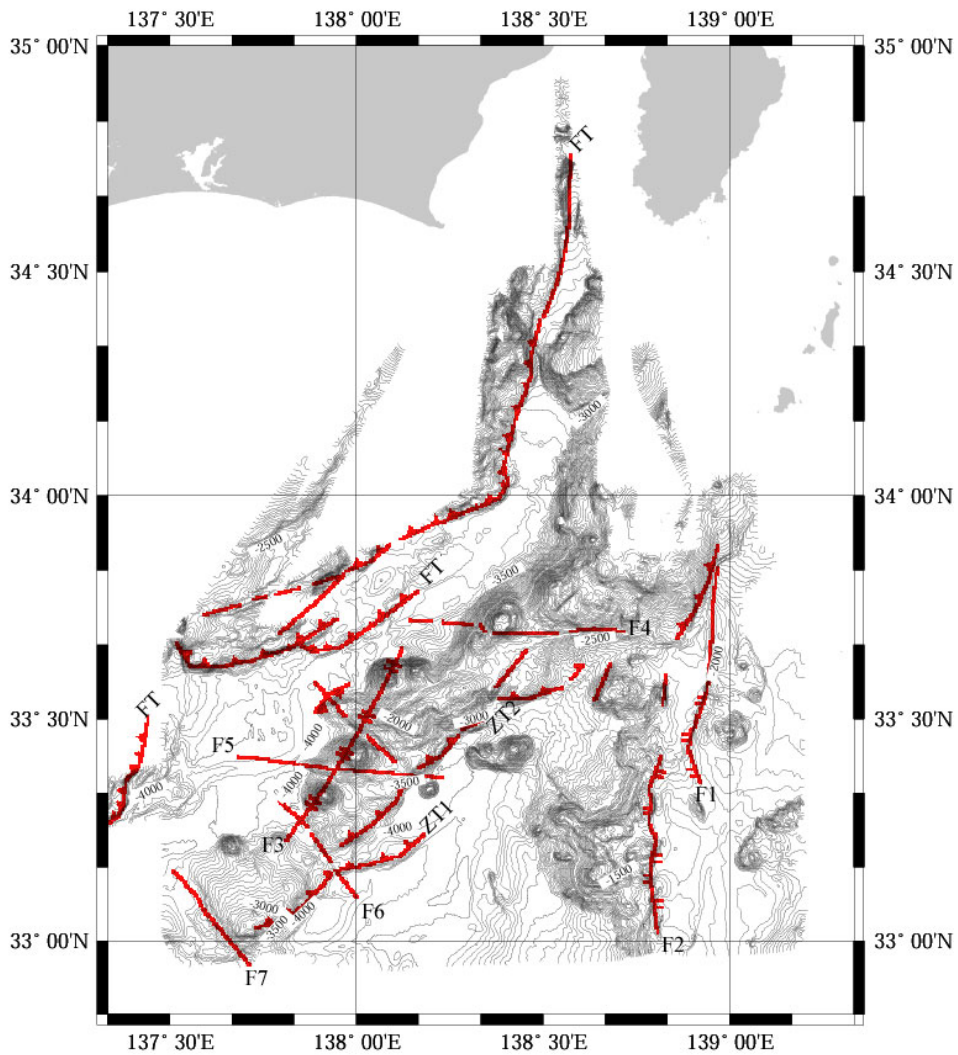


Fig. 5.5 Structural interpretation of the Zenisu Ridge from swath bathymetry in combination with seismic data and field observations. Only major faults are shown in the map. FT is frontal thrust, ZT1 and ZT2 are thrust faults in the southern Zenisu Ridge, F1, F2 and F3 are shear extensional faults, F4 and F5 are transcurrent faults. F6, F7 are sinistral strike-slip faults.

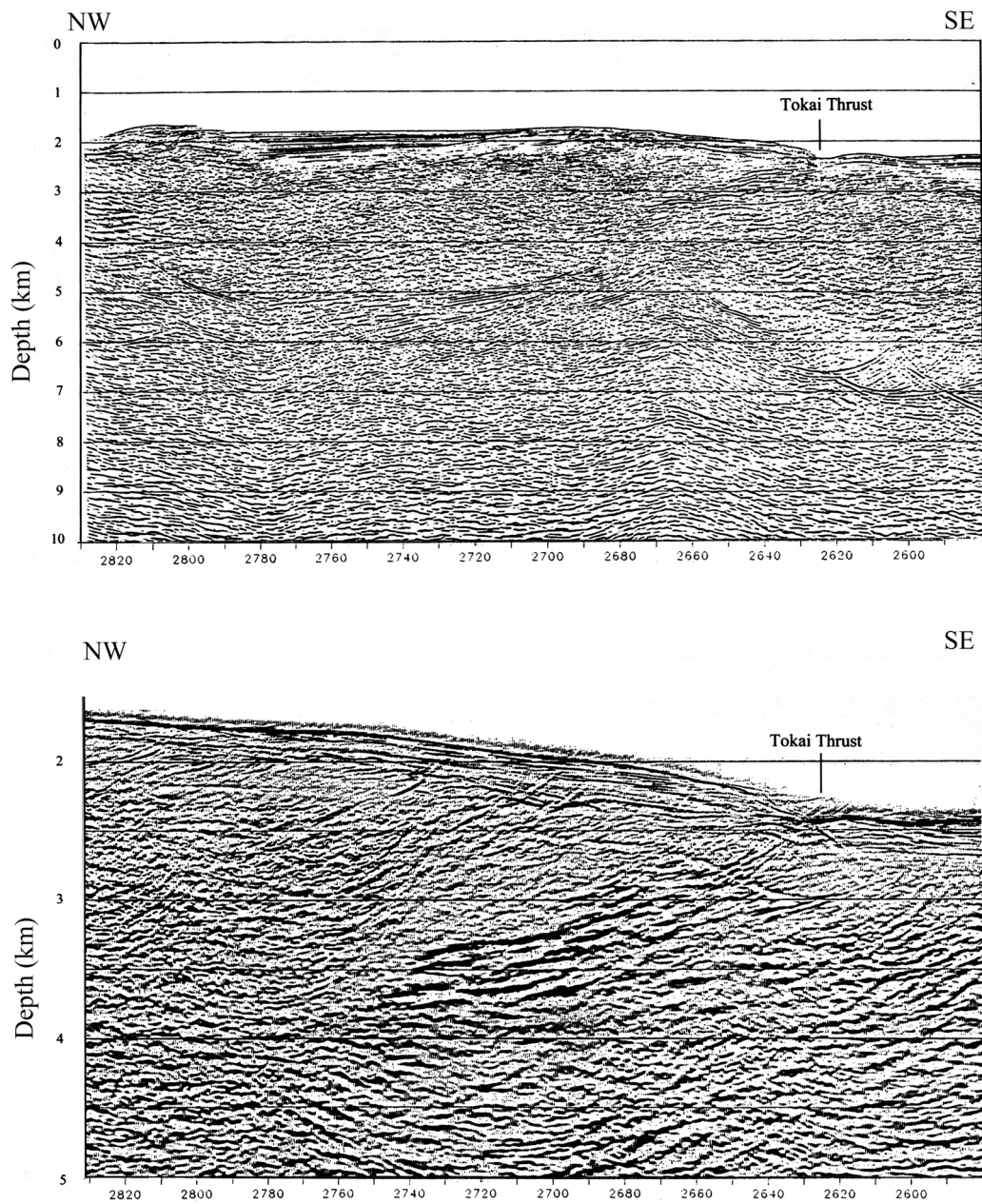


Fig. 5.6 Seismic profiles 909 (upper) and 905 (below) showing the Tokai thrust fault.

The frontal thrusts are oriented normal to the maximum stress axis. The thrust faults in the Zenisu Trough strike about  $44^\circ$ , so the main compressional stress must be in the direction of  $N\ 316^\circ\ W$ . The extensional directions of the frontal thrusts in the Nankai Trough vary greatly (Fig. 5.5). We observed two conjugate fracture systems during dive 523, *viz.*  $331^\circ/60^\circ$  and  $239^\circ/70^\circ$ , with the WNW-trending system dominating and corresponding to the maximum wrench stress field. Therefore,

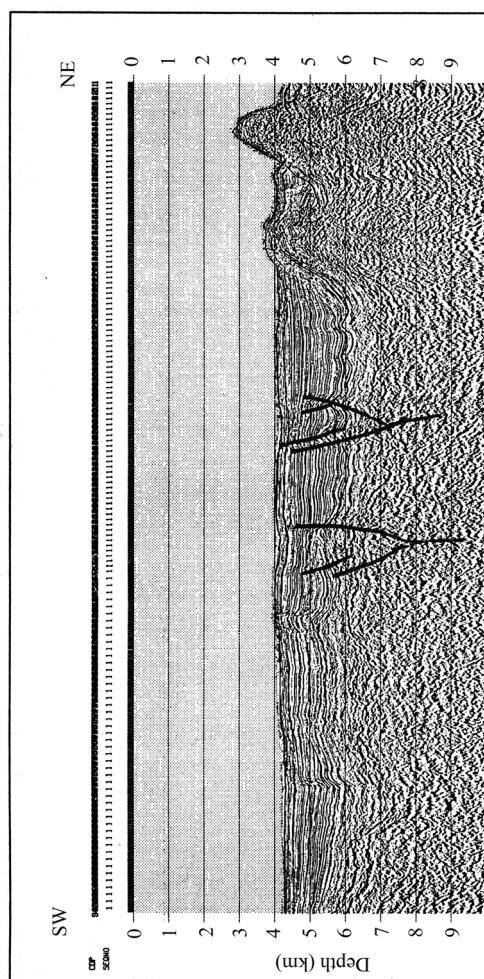


Fig. 5.7 Depth section of seismic profile NT96-202 showing flower structures in the Nankai Trough. See Fig. 1.4 for profile location.

NW-oriented strike-slip faults must have developed on the Zenisu Ridge (Fig. 5.5). The N-S striking faults are very straight and they control the sedimentation process. They are wrench faults associated with an extensional stress field. The E-W directed faults control the geomorphology and are expressed as flower structures on the seismic

profile NT96-202 (Fig. 5.7). Such structures often accompany strike-slip faults (Harding and Lowell, 1979).

#### **5.4 Evolution of the accretionary prism**

Several models on the evolution of the accretionary prism adjacent to the Nankai Trough have been published (Honza and Murakami, 1985; Okuda and Honda, 1988; Kagami, 1985). This is an important issue because the prism deformation is complex and the deep structures are poorly known. The accretionary wedge northwest of the Nankai Trough has the following specific characteristics in our study area: (1) it has a significantly steeper regional slope; (2) its orientation varies from 50°N to 70°N; (3) it has a tight style of folding; (4) it has been strongly eroded, leaving behind huge scars; and (5) it is extremely narrow. All these characteristics can be explained by ridge subduction, namely subduction of the paleo-Zenisu Ridge below this wedge during the past 2 million years.

The upper slope accretionary prism consists of Miocene strata (Okuda and Honda, 1988) and was the site of major subduction since the Early Pliocene. It continues to be active as an internal thrust of the prism. Volcanic activity of the arc on Honshu Island and subduction of the Shikoku Basin beneath the Honshu Island since the Miocene (Kobayashi et al., 1995) suggest that another subduction zone must have existed when modern subduction began in the Late Pliocene. Where was this paleo-subduction zone? Many scientists suggest that the TF marks the subduction zone at this stage. The key to this problem lies in the slope basin of the accretionary wedge. We believe that the sediments here represent a Miocene to Early Pliocene trough. The TF continued to be active during the Quaternary as an internal thrust of the prism, while major frontal thrusting shifted to the FT which extended down to the detachment fault.

The second tectonic stage, namely ridge subduction, began at 2 Ma (Le Pichon et al., 1996). With the subduction of the paleo-Zenisu Ridge beneath the prism, compression is expected in front of it, uplift over it and erosion behind it. For this reason, the TF is still active today, while the accretionary prism is uplifted and extensively eroded. Development of the frontal fault along the trough axis started in the Late Pliocene based on the age of the strata involved. The eastern Nankai Trough is located in a region undergoing intense compression between two colliding arcs. The subduction angle is low, so that the main subduction zone is transferred backward from the TF to the FT. The steeper frontal slope of the accretionary prism is evidence for backthrusting, the sharp slope break is thus a result of past ridge subduction (Lallemant et al., 1989; Le Pichon et al., 1996).

## **5.5 Neotectonics and sedimentation**

### **5.5.1 Active fault and nascent subduction zone**

A primary result of dive 523 is the documentation of active compressional deformation. ENE-WSW trending faults were observed along the scarp of the southeastern flank of the Zenisu Ridge. Uplift of the Zenisu massif took place along this fault, the offset of which is generally 2-3 km on our seismic profiles, but reaches 4 km on the Kaiko profiles (Le Pichon et al., 1987). We interpret this thrust fault to be a nascent subduction zone, an interpretation which is consistent with gravity, earthquake and crust structure data already discussed (Lallemant et al., 1989; Le Pichon et al., 1987; 1989; Tokuyama et al., 1998).

Shemenda (1994) demonstrated experimentally that subduction zone jumps are possible and that they are likely at locations of lithospheric failure, especially in the flexural sag behind the outer rise caused by subduction of a ridge or by strong resistance from the mantle. The Zenisu Ridge lies on the outer rise of the Nankai Trough and the paleo-Zenisu Ridge presumably existed under the eastern Nankai prism (Lallemant et al., 1992; Le Pichon et al., 1996). Therefore, large resistance to subduction exists in the region and this may have led to failure along the southern Zenisu Ridge. The tectonic line can thus extend northward and become a shortening zone between the intra-oceanic crust in the south and the arcs in the north (Soh et al., 1998).

### **5.5.2 Characteristics of the sedimentary units and their implications for the formation of the Zenisu Ridge**

Units C and D of the Zenisu Ridge are comparable to the corresponding strata of the Shikoku Basin, but are richer in turbidites in the northern part of the ridge because of its closer proximity to the source area. They are overlain conformably by thick deep-sea turbidites (Unit B) of Middle to Upper Pliocene age. Thus, there is no evidence that the Zenisu Ridge was uplifted before the Quaternary. The Zenisu area is subjected to intense compression as a result of subduction of the Philippine Sea plate. The high tectonic stress leads to failure of the lithosphere along the Zenisu Ridge and with it the initiation of a new subduction zone. The sedimentary thickness, amount of basement uplift and deformational style of the different segments of the Zenisu massif are different; they are controlled most probably by the NW-SE striking transcurrent faults (Lallemant et al., 1989).

The basement at the southern Zenisu Ridge is uplifted to within 1-2 km of the seafloor on profile NT96-102 (Fig. 4.2; Takhashi et al., 2000), but it is buried at least 5 km below the seafloor on profile NT96-103 (Fig. 4.3). Thick turbidites (units A, B, C) overlie the basement, which at the southern Zenisu Ridge transits to turbidites of the Shikoku Basin as suggested by many authors (Lallemant et al., 1989; Le Pichon et al., 1987; Tokuyama et al., 1998). OBS data support the interpretation that the basement of the Zenisu Ridge is oceanic in nature but is thicker than normal oceanic crust (Nakanishi et al., 1998). We consider that the same acoustic basement possibly extends northward to 33° 40' N where an east-west oriented fault exists. However, island arc basalts (IAB) have been recovered from the overlying sediments between 33° 20' N and 33° 40' N. Although such volcanic rocks formed during the Quaternary (Lallemant et al., 1989), they may also indicate that the basement of the Zenisu Ridge is not typically oceanic. The origin of the IAB between 33°20'-33°40' N is still a matter of debate.

### 5.5.3 Ridge subduction: the Zenisu and paleo-Zenisu ridges

The Zenisu Ridge has been considered a site of intra-oceanic subduction by many authors (Le Pichon, 1987; Chamot-Rooke and Le Pichon et al., 1989; Lallemant et al., 1989). In the past, such a ridge (now buried beneath the eastern Nankai Trough prism) has been postulated in order to explain some of the characteristics of the eastern Nankai accretionary prism (Lallemant et al., 1992). Le Pichon et al. (1996) demonstrated using geomagnetic, gravity and OBS velocity structure evidence that this ridge, referred to as the paleo-Zenisu Ridge, existed beneath the eastern Nankai prism.

The Zenisu Ridge is an area of important thrust tectonics. Our seismic data show that the Pliocene sequence D comprises parallel reflections with a gentle geomorphology, suggesting that this ridge has been undergoing uplift only since the Late Pliocene. In addition, the hemipelagic layer in the Nankai Trough is clearly thinner than that beneath the prism, which may imply the existence of old trough-fill sediments beneath the prism. Faulting in the thicker sediments requires a higher tectonic stress, so that instead, folds formed in the former trough-fill deposits as a result of compression.

The nature of the Zenisu Ridge varies along-strike. The southern Zenisu Ridge consists of oceanic basalt sampled during *Shinkai 6500* dive 325, while in the central Zenisu Ridge, transitional arc basalts or andesites were retrieved during dive 521 and *Dorphan 3k* dive 445 (Tables 5.1 and 5.2). Fig. 5.8 shows a plot of total alkali content vs. SiO<sub>2</sub> for five rock samples retrieved from the Zenisu Ridge during submersible dives 521 and 445. This TAS diagram shows that the samples may be classified as basalts (B) or basaltic andesites (O1).

Whether Zenusu Ridge is a nascent subduction zone or simply an intraplate thrusting phenomenon is still being debated. The key question is the existence and evolution of the paleo-Zenusu Ridge. This ridge if it existed must have played an important role in the evolution of the accretionary prism. Profile NT96-102 shows a ridge-like structure at the footwall of the Tokai thrust which is characterized by low amplitude, weak energy reflections and may be interpreted as the paleo-Zenusu Ridge (Fig. 4.2).

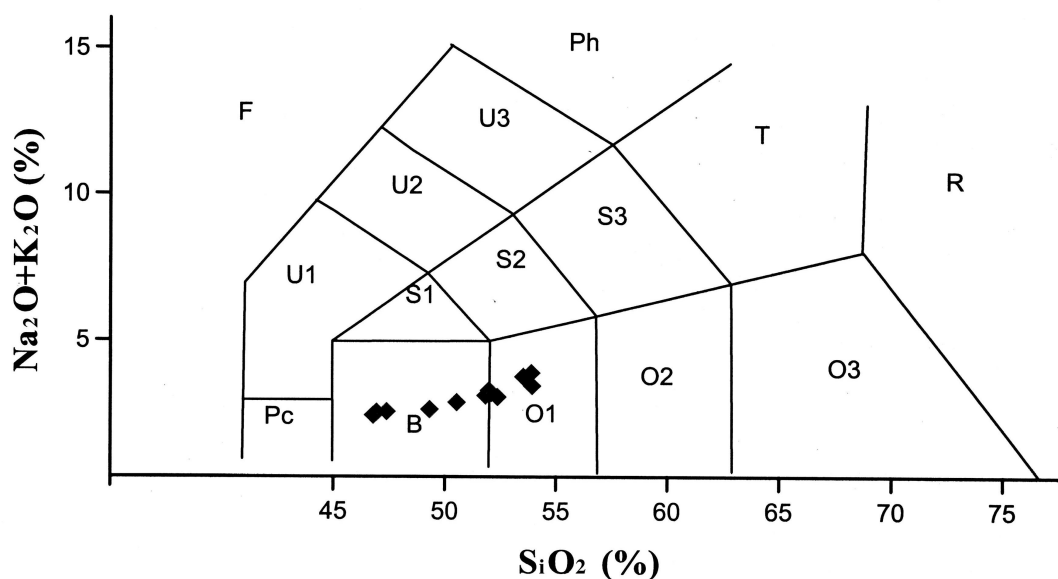


Fig. 5.8 Plot of total alkali content vs.  $\text{SiO}_2$  for five rock samples retrieved from the Zenusu Ridge during submersible dives 521 and 523. This TAS diagram classifies rock samples into basalt (B), basaltic andesite (O1), andesite (O2), dacite (O3), rhyolite (R), trachydacite (T), trachyandesite (S3), basaltic trachydacite (S2), trachybasalt (S1), basaltic tephrite (Pc), tephrite (U1), nephelinite (U2), nephelinite (U3), phonolite (Ph) and fassalite (F) respectively. Our samples are located in the basalt (B) and basaltic andesite (O1) fields.

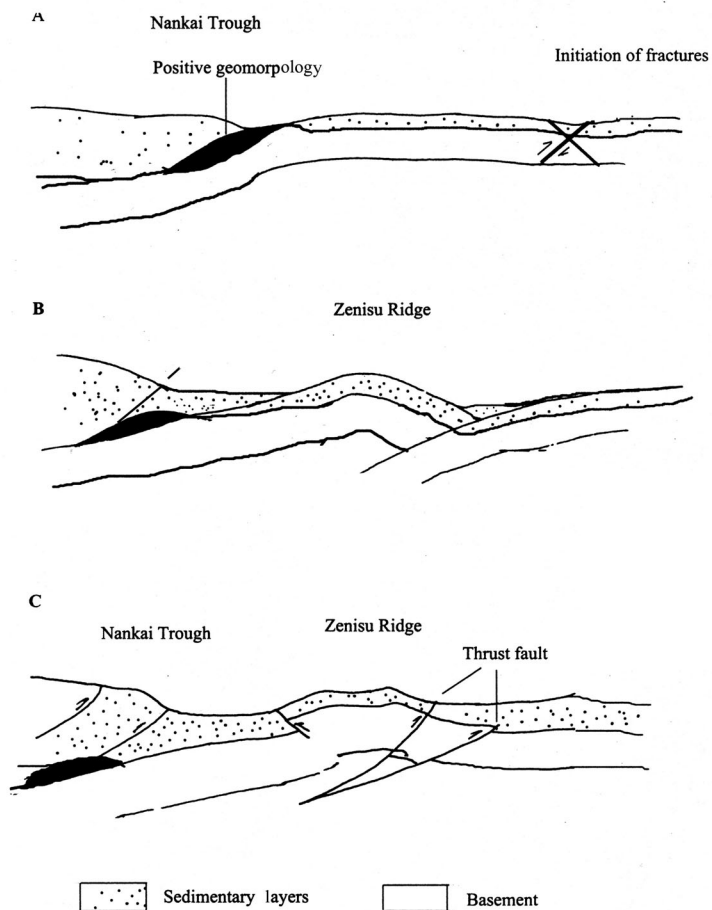


Fig. 5.9 Tectonic evolution of the Zenisu Ridge. A: Initiation of fractures in the Zenisu Trough accompanying the activity of the Nankai subduction zone. B: Uplifting of the Zenisu Ridge. C: Formation of the frontal thrusts and back thrusts since 1 Ma.

## 6. The tectonic development and evolution of the deep-sea channels

### 6.1 Tectonics and evolution of the Nankai deep-sea channel

The Nankai deep-sea channel apparently vanished from the trough floor in the

central Nankai Trough off the Kii Peninsula. The undulations of the trough floor that reflect the deformation of the trough-fill layers become gentle in the central and western Nankai Trough in concert with the disappearance of a marked channel topography. Although the reasons for the differing degrees of deformation of the trough-fill in the western Nankai Trough are undoubtedly important, another factor that could have played a role is the strong turbidity current activity. It is possible that this channel was formed by bottom current activity. However, the average current velocity in the trough region studied is only 2-7 cm/sec, and the currents are not steady (Taira and Teramoto, 1985). We suggest that the Nankai deep-sea channel was formed by sedimentary gravity flow, in particular turbidity currents, and that its course may be controlled by geology and/or tectonics. This channel has been regarded as a passageway for terrigenous sediments into the Suruga and Nankai troughs by turbidity flow (Taira and Niitsuma, 1986; Soh, et al., 1986), and results of ODP drilling and piston coring on many cruises support this idea (Kagami et al., 1985; Shimamura et al., 1988). The morphologic features and lateral grading along the Nankai deep-sea channel as described above may be regarded as additional evidence.

If fluid action alone resulted in the formation of a deep-sea channel in an area without any structural restrictions, the channel may have a freely meandering pattern. Although such a pattern of the Nankai deep-sea channel has been recognized in the junctional area between the Suruga and Nankai troughs, the Nankai deep-sea channel shows incised meandering and straight channel patterns with marked erosional features. In general, the formation of such channel patterns is strictly controlled by tectonic movements (Schumm, 1977). The channel pattern, channel position, relief and other features are controlled by the structure of the trough-fill layers, and therefore it appears that almost all of the Nankai deep-sea channel may be regarded as a subsequent channel. It is related to plate subduction, and the easternmost part of the channel is related to the ridge collision between the Japan Islands and the Izu-Ogasawara Arc, which causes intense uplift of the land and a high sedimentation rate in the trough such as that off Shikoku (maximum rate 2 m/yr; Taira and Niitsuma, 1985). Growth of the Nankai deep-sea channel in the Nankai Trough with high sedimentation rates near collisional plate boundaries took place in four stages (Fig. 6.1a, b and 6.2a, b).

The plate boundary extends from the Nankai Trough to the coast of Shizuoka Prefecture, and functions as the pathway of sediment transport to the Nankai Trough. Kobayashi et al. (1995) suggested that the Nankai Trough did not exist during the period 5-3 Ma, and pointed to the breakdown of subduction as the cause. They also proposed a subsequent resumption of plate subduction and a reconstruction of the trench which corresponds to the initial form of the present-day Nankai Trough. During the first stage 3 myr ago when breakdown of subduction occurred, a turbidite current must have travelled down the continental shelf and slope through the deep-sea canyon and reached as far as the deep-sea basin because a trench morphology was absent. Assuming that there were no tectonic restrictions acting as obstacles in the deep-sea basin, the channel must have had a freely meandering pattern such as the Amazon

deep-sea channel (Damuth et al., 1988).

The second stage began at 2 Ma with the formation of the outer ridge by subduction of the oceanic plate and hence the formation of a trench morphology. Active ridge collision occurred since the Pliocene and the Tazawa Block collision in the Early Pliocene (Fig. 5.5, Soh et al., 1998). As a consequence of the collision which began about 2 Ma (Fig. 6.1b; Tokuyama et al., 1998), a steep drainage system formed along the strike-slip faults, providing coarse clastic sediments, creating a major fan-delta system at the river mouth (Soh et al., 1995) and forming a deep-sea channel along the axis of the trough. Because this sediment yield was too rapid to be subducted, an accretionary prism formed at the base of the inner trench (Taira and Niitsuma, 1986). At approximately the same time, the deep-sea channel changed its course along the trench axis.

Table 5.1 Whole-rock chemical analyses of the rock samples retrieved during dives 521 and 445 (in %)

Sample	SiO <sub>2</sub>	TiO <sub>2</sub>	Al <sub>2</sub> O <sub>3</sub>	Fe <sub>2</sub> O <sub>3</sub>	MnO	MgO	CaO	Na <sub>2</sub> O	K <sub>2</sub> O	P <sub>2</sub> O <sub>5</sub>	Total
445R3-1	51.99	0.95	18.27	7.90	0.14	5.49	11.76	2.31	0.97	0.22	100.00
445R1-2	49.32	0.85	16.84	9.85	0.19	9.00	11.04	2.04	0.63	0.23	100.00
445R1-1	53.92	0.90	18.05	9.84	0.20	4.33	9.12	2.69	0.74	0.21	100.00
445R2-1	50.53	0.84	16.56	9.56	0.15	8.02	11.27	2.04	0.83	0.20	100.00
521R1-2	53.53	0.82	18.15	9.96	0.19	4.00	9.30	2.65	1.10	0.29	100.00
521R3-2	51.84	0.89	19.44	10.10	0.17	4.10	10.14	2.39	0.71	0.22	100.00
521R3-1	52.36	0.91	19.63	9.34	0.18	4.06	10.27	2.35	0.70	0.20	100.00
521R4-1	46.94	0.95	18.9	12.74	0.25	5.16	12.19	2.17	0.35	0.33	100.00
521R4-4	46.78	0.96	18.91	12.85	0.27	5.88	11.75	2.02	0.40	0.18	100.00
521R3-3	52.09	0.89	19.09	10.06	0.17	4.16	10.12	2.43	0.76	0.24	100.00
521R1-1	53.89	0.82	18.25	9.60	0.19	3.92	9.20	2.72	1.15	0.26	100.00
521R5-1	47.39	0.95	18.78	12.64	0.21	5.06	12.01	2.17	0.38	0.41	100.00

Table 5.2 Trace element composition of the rocks retrieved during dives 523 and 445 (in ppm).

Sample	521R5-1	521R1-1	521R3-3	521R4-4	521R4-1	521R3-1	521R3-2	521R1-2	445R2-1	445R1-1	445R1-2	445R3-1
<b>Sr</b>	516.00	420.00	324.00	516.00	524.00	323.00	322.00	414.00	334.00	310.00	346.00	377.00
<b>Rb</b>	8.00	21.00	16.00	8.00	3.00	15.00	16.00	21.00	18.00	14.00	9.00	16.00
<b>Ba</b>	47.00	149.00	70.00	43.00	54.00	68.00	67.00	144.00	104.00	80.00	110.00	121.00
<b>Nb</b>	1.70	2.40	2.20	1.90	1.80	3.30	2.20	2.40	3.80	2.10	3.00	3.50
<b>Zr</b>	55.00	66.00	66.00	55.00	55.00	60.00	64.00	66.00	59.00	65.00	60.00	68.00
<b>Y</b>	25.00	23.00	21.00	21.00	22.00	21.00	21.00	23.00	20.00	24.00	21.00	22.00
<b>Yb</b>	2.54	2.81	2.41	2.24	2.48	2.49	2.42	2.60	2.14	2.57	1.76	1.83
<b>Nd</b>	15.80	14.50	13.40	15.20	16.70	13.60	13.90	13.80	12.90	14.10	9.59	9.65
<b>Co</b>	46.90	40.70	44.20	41.60	40.60	43.30	48.60	39.80	50.20	44.50	55.80	41.70
<b>Cr</b>	21.7	8.60	37.3	18.6	19.9	37.5	39.1	8.30	666.	28.7	563	546
<b>Cu</b>	106.00	39.00	100.00	120.00	114.00	122.00	123.00	39.00	67.00	29.00	76.00	80.00
<b>Ni</b>	23.00	4.00	21.00	26.00	24.00	20.00	21.00	4.00	141.00	11.00	139.00	88.00
<b>Rh</b>	8.00	21.0	16.0	8.0	3.0	15.0	16.0	21.0	18.0	14.0	9.0	16.0
<b>Zn</b>	91.00	68.00	75.00	80.00	81.00	75.00	76.00	70.00	65.00	76.00	65.00	63.00

During stage 3 (Fig. 6.2a), plate subduction temporarily ceased because of ridge collision and collision with the Izu Block in the Middle Pleistocene. This resulted in intense uplift and erosion. Abundant clastic material was produced and transported by sediment gravity flow into the trench; it filled up the trench and formed the accretionary wedge. The deep-sea channel at this time had a more pronounced channel morphology.

During stage 4, subduction of the oceanic plate resumed and the trench-wedge began to deform. As the deformation front and other tectonic lines formed in the course of subduction, the channel course became regulated along these structures. The deep-sea channel thus acquired a straight channel pattern.

## **6.2 Tectonics and development of the Zenisu deep-sea channel**

Over the past two decades, models based on the sequence stratigraphic concept have been used widely to predict and locate submarine fan reservoirs in deep-sea basins. These models assume that the growth and deposition of deep-sea fan systems are intimately tied to a cycle of eustatic or relative sea-level change. Early sequence stratigraphic models envisaged fan development to be related to eustatic sea-level fall, when the base level falls below the offlap break and bypass of coarse-grained clastic sediment into the deep-sea basin can take place (Mitchum et al., 1977; Nichols, 1999; Posamentier and Vail, 1988; Posamentier et al., 1988). Early lowstand fan models largely ignored the role played by tectonics, sediment type and sedimentation rate in influencing the growth of the fan, especially on convergent margins (Kolla and Macurda, 1988; Reading et al., 1996; Soh et al. 1990).

The Zenisu deep-sea channel, however, originated from the Izu-Ogasawara Arc (IOA) which is an area of active uplift, so the source area of the IOA has been supplying sediments to the channel during the entire Quaternary. The deep-sea channel therefore functions as an active conduit also during sea-level highstands and turbiditic sedimentation is still active during this time. During dive 371, turbidity current activity was observed even though we have the Holocene sea-level highstand. Thus, clastic input overwhelms any potential eustatic signature and results in a direct and substantial input of coarse-grained clastics into ancient deep marine basins (Mitchum, 1985).

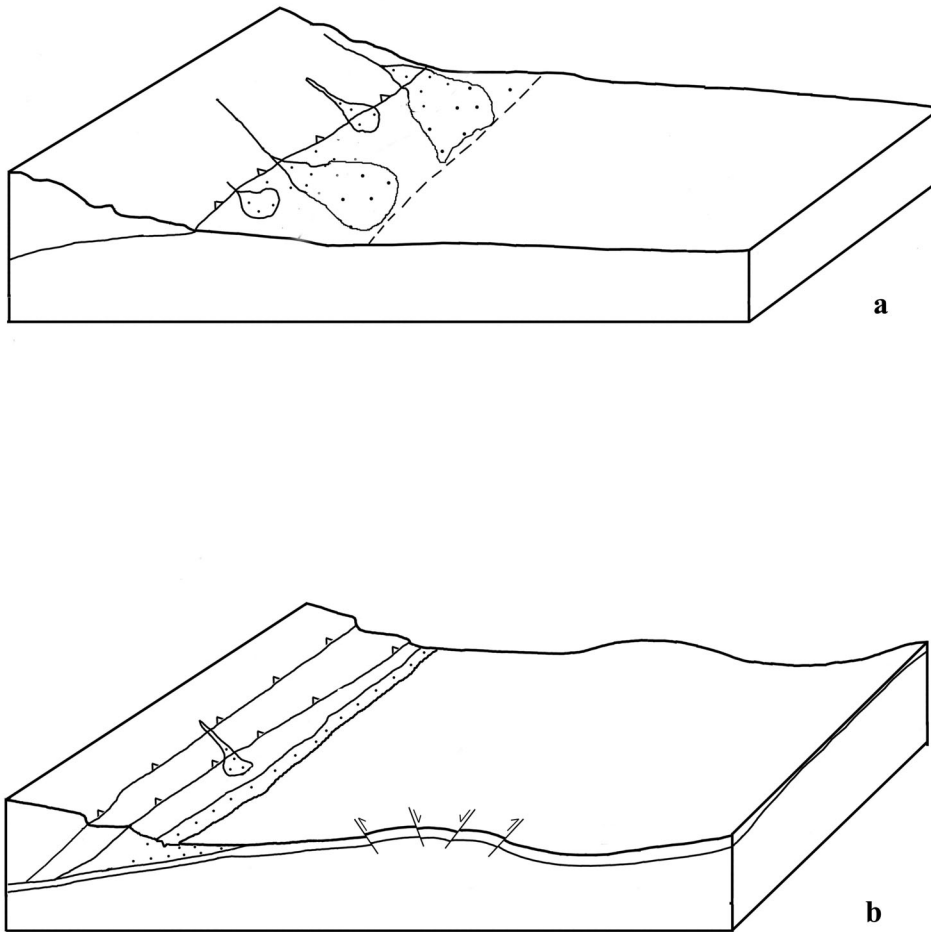


Fig. 6.1 Development of the Nankai deep-sea channel. a: Slope fan before the formation of the Nankai deep-sea channel. b: Sedimentation model after formation of the Nankai deep-sea channel since 2 Ma.

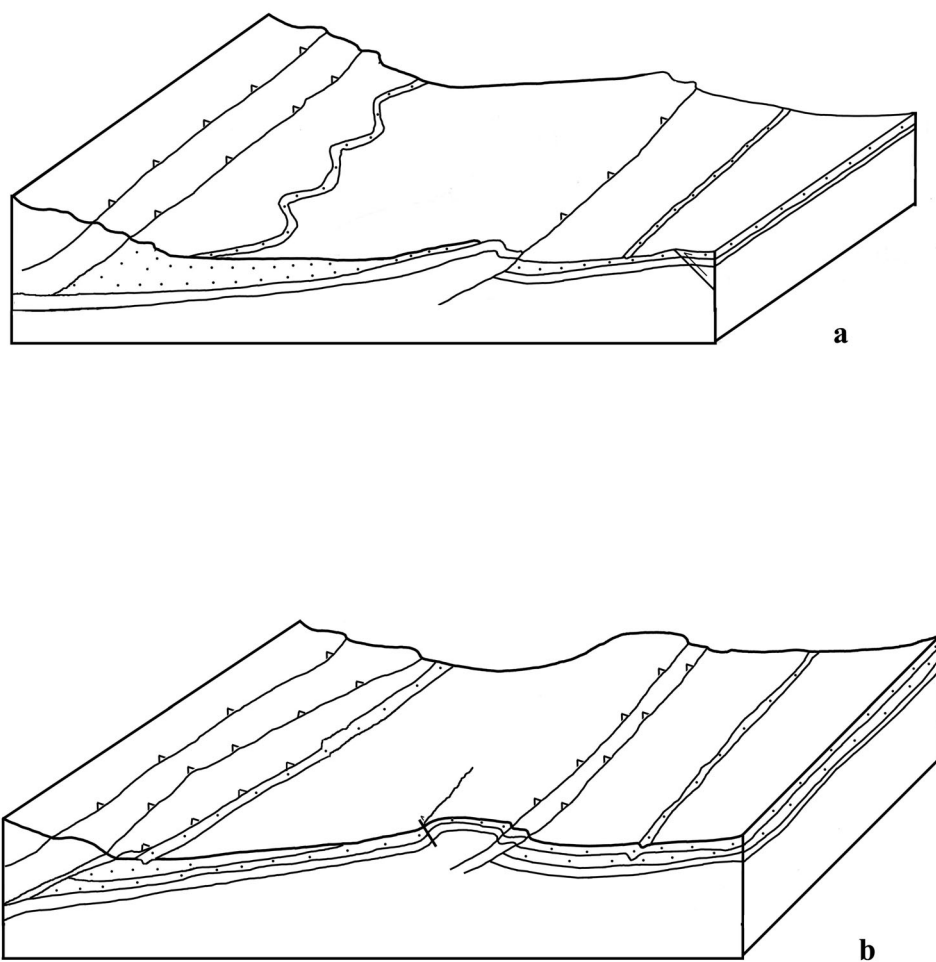


Fig. 6.2 Development of the Zenisu deep-sea channel. a: More pronounced channel morphology of the Nankai deep-sea channel before the formation of the Zenisu trough axis channel. b: Formation of the Zenisu trough-axis channel since 1 Ma after uplift of the southern Zenisu Ridge.

Even though recent syntheses of submarine-fan sedimentology emphasize multiple controls on the fan character, the primary control is still the tectonic setting (Shanmugam and Muiola, 1988). Our scenario for the formation and development of the Zenisu Canyon since 1 Ma is controlled by tectonics (Fig. 6.2a).

The upper part of the canyon developed along a N-S oriented shear fault or fault zone which formed the faulted graben and controlled subsidence of the Zenisu Trough as well as uplift of the Izu-Ogasawara Arc. The geometry of the fault can be seen in the seismic sections KK36, KK40 and KK42 (Figs. 4.14 and 4.15). The high-resolution bathymetric map (Fig. 2.1) shows very straight and steep fault scarps, as well as a horst and graben topography.

The middle segment of the E-W fan channel marks a E-W tectonic boundary which is also the boundary between the Shikoku Basin and the Izu-Ogasawara Arc. OBS refraction profile 1994 P3 (Fig. 5.3) shows the different velocity-depth structures at the two sides of the fault F4 (Fig. 5.5), and SeaBeam bathymetric data demonstrate that the morphology along the fault is steep (Fig. 5.5).

The lower segment (the trough-axis channel) is apparently controlled by uplift of the Zenisu Ridge and subsidence of the adjacent Zenisu Trough. Catuneanu et al. (1997) demonstrated that changes in accommodation over the forebulge are in the opposite sense to those in the foredeep. During active crustal loading when the Zenisu Ridge undergoes uplift, the Zenisu Trough is deeper.

Our data on the northeastern continuation of the proposed thrust zone along the Zenisu Ridge yield only weak evidence for thrusting and deformation of the ridge. Compressive deformation, however, exists. Its weaker development might be understood in terms of the difference in nature of the basement rocks. The subduction zone is involved in the Izu collision zone. The northern segment of the Zenisu Ridge is formed by the Izu-Ogasawara volcanic ridge, as opposed to the southern Zenisu Ridge where it is probably formed from the crust of the Shikoku Basin by thrusting over itself. Therefore, the present plate boundary is likely located along the southern margin of the Zenisu Ridge and the Zenisu Canyon (Le Pichon et al., 1987; Nakanishi et al., 1998; Soh et al., 1998; Taira, et al., 1992; Tokuyama et al., 1998). The difference in nature of the crust might explain the different styles of deformation, which change from intense reverse faulting to diffuse strike-slip faulting as observed to the northeast including on the Izu Peninsula (Nakamura et al., 1987).

## 7. Conclusions

(1) An important result obtained during dive 523 is the existence of active compression on the southern scarp of the central Zenisu Ridge. The first discovery of dead clams and living deep-sea biological communities and active fault at the base of the slope may reflect dewatering processes. This interpretation is consistent with the structural regime derived from seismic profiles. The compression suggests that the Zenisu Ridge is a product of intra-plate shortening. This shortening is presently active and has resulted in the formation of a nascent subduction zone. We suggest that the shortening takes place along two crustal faults, each accounting for about half of the total offset of 2-3 km.

(2) Four sediment types have been mapped using bathymetric and sidescan data and submersible observations in the eastern Nankai and Zenisu troughs. Turbidity currents have been observed at the base of the slope even during times when it was seismically quiescent. Immediately after an earthquake, more pronounced turbidity currents are expected to occur both on the upper and lower slopes. Small-scale turbidites were found at the base of the slope. Debrisites dominate the western slope and are closely related to the distribution of seep communities which are controlled by sediment facies and active faulting. Thick turbidites were observed both along the dive track and on seismic profiles. Unit B of the turbiditic sequence is younger than Late Pliocene. Since it overlies conformably the underlying strata, deformation and hence uplift of the Zenisu Ridge must be post-depositional relative to Unit B, i.e., no earlier than Late Pliocene or Pleistocene (after 2.65 Ma).

(3) Four seismic sequences have been recognized in the Nankai Trough and the Zenisu Trough (Figs. 4.2 and 4.10). Sequences A and B consist of trough-fill turbidites and hemipelagic sediments. They were laid down during the Late Pleistocene and the Holocene. Sequences C and D represent upper turbidite sequences and hemipelagic deposits in the Shikoku Basin. The accretionary wedge has a very complex internal geometry and was formed during the Miocene and the Early Pliocene.

(4) The study area may be divided into five tectonic units, each with its characteristic deformations and structural evolution. They are: accretionary slope, Nankai Trough, Zenisu Ridge, Zenisu Trough and Izu-Ogasawara Island Arc. There are three major thrust zones, namely the Tokai thrust zone, the frontal thrust zone and the Zenisu thrust zone. The first episode of subduction began during the Miocene when major subduction occurred along the Tokai fault. The second subduction phase started in the Pliocene, when another major subduction thrust formed. Ridge subduction occurred in the eastern Nankai Trough. This led to the deposition of a thick accretionary wedge and significant intraplate faulting. The subduction jump from the Tokai thrust fault via the Nankai subduction zone to the South Zenisu subduction zone occurred since the Miocene.

## 8. Summary

The convergent margin off central Japan is characterized by numerous deep-sea channels such as the Nankai and Zenisu channels which are closely related to the subduction process. The geomorphology, sedimentation processes and tectonic development of these deep-sea channels were studied using swath bathymetry, submersible observations, as well as sidescan and seismic data.

The Nankai deep-sea channel starts from Suruga Bay and apparently vanished from the trough floor in the middle Nankai Trough off the Kii Peninsula. The undulations of the trough floor that reflect the deformation of the trough-fill deposits become gentle in the middle and western Nankai Trough in concert with the disappearance of a marked channel morphology. The existence of this remarkable deep-sea channel is closely related to its geological and/or tectonic development. The primary cause for the formation of a deep-sea channel may be fluid flow at the seafloor and active tectonics. One possibility for such a fluid flow is bottom current. However, the average current velocity measured in the eastern Nankai Trough region is only 2 to 7 cm/sec and the bottom flow is not steady (Taira and Teramoto, 1985). More probable are turbiditic flows, according to which the Nankai deep-sea channel may be regarded as a passageway for terrigenous sediments into the Nankai Trough. Our high resolution bathymetric data, submersible observations and seismic profiles provide detailed information for a better understanding of deep-sea sedimentation processes and the tectonic evolution of subduction in the Nankai deep-sea channel. Turbidity currents have been observed at the base of the slopes of the Nankai Trough even during times when this trough was seismically quiescent. Small-scale turbidites were found at the base of the slope. Debrisites dominate the western slope and are closely related to the distribution of seep communities which are controlled by sediment facies and active faulting.

The Zenisu deep-sea channel is situated south of Kozushima Island and Miyashima Island of the Izu-Ogasawara Arc. Its geomorphology and the associated sedimentation processes are constrained by tectonic activity as well as the supply of volcanic debris as revealed by SeaBeam bathymetry and observations from manned submersible dives (*Shinkai 6500* dives 371, 523, 555 and 556). Morphologically, the Zenisu deep-sea channel consists of three segments: the Zenisu Canyon, the E-W Channel and the Trough Axis Channel.

Several bottom sediment types were identified on the basis of observations from a submersible and acoustic imaging. Very thin, fine layers drape the slopes of the accretionary wedge and the Zenisu Ridge, while debris flow deposits and turbidites dominate the floor of the deep-sea channels. At the base of the slope of these channels, large slumps and rock outcrops with associated clam communities occur amid

abundant small-to-large scale debrites. Sampling of vesicomid white clams seen during dive 523 of 1999 was successfully carried out in 2000. Two species were recovered, the hitherto unknown large form *Calyptogena sp.* (Wu et al., 2000) and a form common to the recently described species *Calyptogena (Archivesica) tsubasa* collected from the Tenryu Canyon area (Fujioka and Taira, 1989).

The occurrence of dense beds of *Calyptogena* bivalves, buccinid snails and white galatheid *Munidopsis sp.* provides unequivocal supporting evidence for nascent subduction and concomitant seepage at the base of the southern flank of the Zenisu Ridge.

In the Zenisu Trough, four seismic sequences with distinct external geometries and internal configurations were recognized. Sequences A and B are trough-fill turbidites. Age dating suggests that unit B is younger than Late Pliocene and uplift of the Zenisu Ridge probably occurred since the Late Pliocene or the Pleistocene (after 2.65 Ma). The discovery of dead clams and living deep-sea biological communities at the base of the slope point to active faulting and sediment dewatering.

To study the development of these deep-sea channels, a total of 454 km of G-gun seismic data were acquired during cruise KH96-02 of the R/V *Hakuho-mura*. Six structural zones were recognized in the study area according to their deformational style and sediment architecture. These are: forearc basin, accretionary prism, trough axis, Zenisu Ridge, Zenisu Trough and Izu-Ogasawara Arc. The Tokai Thrust which marks the southeastern boundary of the forearc basin is considered an important regional tectonic element that has decisively influenced the lithofacies distribution. The strata of the footwall of this fault consist of slope basin deposits and terrigenous components. A more active imbricated thrust system exists on the lower slope since the Late Pliocene. Backthrusts and extensive erosion occur at the Yukie Ridge on the lower accretionary slope. The southern segment of Zenisu Ridge is considered the site of a nascent subduction zone by many authors (Le Pichon et al., 1987; Lallemand et al., 1989), and is marked by several compressional fractures in its upper layers. During our dives 523 and 556, a similar thrust fault has been found along the middle segment of the Zenisu Ridge. Northward extensions of the thrust faults have been mapped using direct observations from a submersible and seismic reflection profiling on the southern slope of the Zenisu Ridge. These data show that shortening occurs at least in the middle segment of the Zenisu Ridge and has resulted in the formation of a nascent subduction zone.

The Nankai deep-sea channel exhibits an incised straight channel pattern with marked erosional features and is controlled by E-W, N-S and NNE-SSW-trending faults. The channel pattern, channel position, relief and other characteristics are dependent on the structural style of the trough-fill. The morphology of the Nankai deep-sea channel reflects the subduction of an oceanic plate. Its easternmost segment is related to the collision between the Honshu and Izu-Ogasawara island arcs which resulted in intense uplift of the Izu-Ogasawara Arc and a high erosional rate in the

adjacent trough.

The growth of deep-sea channels at this convergent margin took place in several stages. The initial stage in the development of the Nankai deep-sea channel ended by the breakdown of subduction at about 5-3 Ma (Kobayashi et al., 1995). During this time, turbidity currents travelled down the continental shelf and slope, incised a deep canyon, and reached the deep basin because of the lack of a trench morphology. Assuming that there were no tectonic elements acting as obstacles in the deep basin, the channel must have had a freely meandering pattern such as the Amazon today (Damouth, 1988). During stage 2, subduction of the oceanic plate and hence the formation of a trench morphology took place 15–12 Ma (Kobayashi et al., 1995). At approximately the same time, the Nankai deep-sea channel changed its course along the trench axis. In stage 3, subduction temporarily ceased due to collision between the Japan Island Arc and the Izu-Ogasawara Arc in the east which resulted in intense uplift and erosion in central Honshu (Soh et al., 1998). Abundant clastic material was produced and transported by gravity flow into the trench, filling it up and forming the trench wedge. The deep-sea channel at this time had a freely meandering pattern. During stage 4, probably at 1 Ma when the deformation front and the NE-SW and E-W striking fault systems were formed in the course of subduction, the channel course became confined to these orientations. Thus, the deep-sea channel exhibited a straight channel pattern. These stages constituted a major cycle that began with oceanic subduction and ended in the breakdown of the subducted slab.

Development of the Zenisu deep-sea channel is closely related to uplift of the Zenisu Ridge as a result of the extensive collision between the Japan Island Arc and the Izu-Ogasawara Arc. It is therefore tectonically controlled. Nascent thrust faults formed during the latest Pliocene or the Pleistocene, and the channel grew thereafter. The trough morphology formed at this time (at ca. 2.0 Ma). The sedimentary sequence in the deep-sea channel of the Zenisu Trough has a thickness of about 100 m in the south (sequence 1a of Tokuyama et al., 1998). Using an average sedimentation rate of 1 cm/yr (Takayama et al., 1998), this implies that the deep-sea channel started to form about 1 myr ago. During Recent times, the northern segment of the channel developed along a N-S trending transtensional fault, while the southern segment was under the control of a nascent thrust.

### **Acknowledgement**

My most sincere thanks go to my dissertation adviser, Prof. Dr. H. K. Wong, who encouraged me to finish my Ph. D. and guided my research work both in the Institute of Biogeochemistry and Marine Chemistry of the University of Hamburg and abroad. Thanks are due also to Dr. Thomas Lüdmann for his kind help during my stay in

Hamburg. I would also like to thank friends that have stood by me throughout the years, including Philipp Konerding, Jair Weschenfelder, and Christiane Haft.

The research project leading to this dissertation was supported by the Japan Marine Science and Technology Center and the Japan International Science and Technology Exchange Center. I am indebted to the pilots and support crews of the submersible Shinkai 6500 during cruises YK99-09 Leg 2 and YK00-06 Leg 1 of the R/V Yokosuka, as well as those of the ROV Dorphin 3K and of cruise 445 of the R/V Natsushima. My thanks also go to pilots Mr. K. Iijima and Mr. H. Higuchi, and the captain of the R/V Yokosuka, Mr. Tanaka, as well as to my good friends and colleagues Dr. Izumi Sakamoto, Dr. Narumi Takahashi, Dr. Toshiya Kanamatsu, Mr. Masayuki Toizumi and Dr. Toshiya Fujiwara, who helped me to finish the field surveys. In addition, thanks are due to the executive director of the Japan Marine Science and Technology Center, Dr. Hajimu Kinoshita, and director of the Department of Deep Sea Research, Dr. Suyehiro, who provided the opportunity for me to work in the research center and to make two dives with the submersible Shinkai 6500.

Unforgettable to me is Mrs. Eva-Maria Hongsernant from the German Federal Ministry of Education, Science, Research and Technology. She provided me the needed financial support as well as encouragement for the two years I stayed in Hamburg.

Last but not least, my thanks go to the Director, Mr. Xiong Jianhai and colleagues of the Institute of Oceanology, Chinese Academy of Sciences, who made it possible for me to finish my dissertation. I would like to thank specially Mr. Qin Yunshan for his encouragement. My deepest gratitude goes to my family, my parent and my wife.

## References

- Aoki Y., Tamano, T. and Kato S. (1982): Detailed structure of the Nankai Trough from migrated seismic sections. *Am. Assoc. Pet. Geol. Mem. No. 34*, 308-322.
- Ashi J. and Taira A. (1992): Structure of the Nankai accretionary prism as revealed by IZANAGI sidescan imagery and multichannel seismic reflection profiling. *The Island Arc*, 1, 104-115.
- Ashi J., Segawa J., Le Pichon X., Lallement S., Kobayashi K., Hattori M., Mazzotti S. and Aoike K. (1996): Distribution of cold seepage at the Ryuyo Canyon off Tokai: 1995 Kaiko Tokai Shinaki 2000 dives. *JAMSTEC J. Deep-sea Res.* 13, 159–166.
- Ashi J. (1997): Distribution of cold seepage at the fault scarp of the eastern Nankai accretionary prism. *JAMSTEC J. Deep-sea Res.* 13, 495–501.
- Barry J.P., Greene H.G., Orange D.L., Baxer C.H., Robinson B.H., Kochvar R.E.,

- Nybakken J.W., Reed D.L. and McHugh C.M. (1996): Biologic and geologic characteristics of cold seeps in Monterey Bay, California. *Deep-sea Research* 43(11-12), 1739-1762.
- Blondel P. and Murton B.J., 1997. *Handbook of Seafloor Sonar Imagery*. John Wiley-Praxis, Chichester, 314 pp.
- Cande S.C., Leslie R.B., Parra J.C. and Hobert M. (1987): Interaction between the Chile Ridge and Chile Trench: geophysical and geothermal evidence. *J. Geophys. Res.* 92, 495-520.
- Carter R.M. (1988): The nature and evolution of deep-sea channel system. *Basin Research* 1, 41-54.
- Catuneanu O., Beaumont C. and Waschbusch P. (1997): Interplay of static loads and subduction dynamics in the foreland basins: reciprocal stratigraphies and the missing peripheral bulge. *Geology* 25, 1087-1090.
- Chamot-rooke N. and Le Pichon X. (1989): Zenisu Ridge: mechanical model of formation. *Tectonophysics* 160, 175-193.
- Clark J.D. and Pickering K.T. (1993): Architectural elements and growth patterns of submarine channels: application to hydrocarbon exploration. *Bull. Am. Ass. Petro. Geol.* 80, 194-221.
- Damuth J.E., Flood R.D., Kowsmann R.O., Belderson R.H. and Gorini M. (1988): Anatomy and growth pattern of Amazon Deep-sea fan as revealed by long range sidescan sonar and high resolution seismic studies. *Am. Assoc. Petrol. Geol. Bull.* 72, 885-911.
- Damuth J.E., Flood R.D., Pirmez C. and Manley P.L. (1995): Architectural elements and depositional processes of Amazon deep sea fan imaged by long-range side-scan sonar (GLORIA). Bathymetric swath-mapping (SeaBEAM), high resolution seismic, and piston core data. In: *Atlas of Deep Water Environments: Architectural Style in Turbidite Systems* (ed. By Pickering K.T., Hiscott R.N. Kenyon N.H., Ricci Lucchi F). Chapman and Hall, London, 105-121.
- Davis E.E., Hyndman R.D. and Villinger D. (1990): Rates of fluid exclusion across the northern Cascadia accretionary prism: constraints from new heat flow and multichannel seismic reflection data. *J. Geophys. Res.* 95, 8869-8889.
- Demets C., Gordon R.G., Argus D.F. and Stein S. (1990): Current plate motion. *Geophys. J. Int.* 101, 425-478.
- Dickson W.C. and Seely D.R. (1979): Structure and stratigraphy of forearc regions. *AAPG Bulletin* 63(1), 2-31.
- Flood R.D., Manley P.L., Kowsmann R. O., Appi C. J. and Pirmez C. (1991): Seismic facies and late Quaternary growth of Amazon submarine fan. *Seismic Facies and Sedimentary Processes of Submarine Facies and Turbidity Systems*. Springer-

- Verlag New York. Inc. 415-433.
- Flood R.D. and Damuth J.E. (1987): Quantitative characteristics of sinuous distributary channels on the Amazon Deep-sea Fan. *Geological Society of American Bulletin* 98, 728-738.
- Fujioka K. and Taira A. (1989): Tectono-sedimentary settings of seep biological communities: a synthesis from the Japanese subduction zone. In Taira A. and Masuda F. (eds.), *Sedimentary Facies in the Active Plate Margin*. Terra Scientific Publishing Company, Tokyo, 1989.
- Gamo T., Ishibashi J., Shiatshima K., Kinoshita M., Watanabe M., Nakayama E., Sohrim Y., Kim W.-S., Masuzawa T. and Fujioka K. (1989): Anomalies of bottom CH<sub>4</sub> and trace metal concentrations associated with high heat flow at the Calyptogena community off Hatsushima Island, Sagami Bay, Japan: a preliminary report of Tansei-Maru KT88-1 cruise, leg 1. *Geochemical Journal* 22, 215-223.
- Gamo T., Sakai H., Ishibashi J.I., Shitashima K. and Boulegue J. (1992): Methane, ethane and total inorganic carbon in fluid samples taken during the 1989 Kaiko-Nankai project. *Earth Planet. Sci. Lett.* 109, 383-390.
- Greene H.G., Barry J.P., Hashimoto J., Fujiwara Y., Kochevar R.E. and Robinson B.H. (1997): A submersible-based comparison of cold-seep regions in Sagami and Monterey bays. *JAMSTEC Journal of Deep-sea Research* 13, 395-423.
- Guo J. (1997): *Chemical Oceanography*, Xiamen University Press, Xiamen, pp 370.
- Harding T.P. and Lowell J.D. (1979): Structural styles, their plate-tectonic habitats and hydrocarbon traps in petroleum provinces. *AAPG Bulletin* 63, 1016-58.
- Hashimoto J., Ohta S., Tanaka T., Hotta H., Matsuzawa S. and Sakai H. (1989): Deep-sea communities dominated by the giant clam *Calyptogena* along the slope foot of Hatsushima Island, Sagami Bay, central Japan. *Palaeogeog., Palaeoclim., Palaeoecol.* 71, 179-192.
- Henry P., Foucher J.P., Le Pichon X., Sibuet M., Kobayashi K., Tarits P., Chamot-Rooke N., Furuta T. and Schultheiss P. (1992): Interpretation of temperature measurements from the Kaiko-Nankai cruise: modeling of fluid flow in clam colonies. *Earth Planet. Sci. Lett.* 109, 355-372.
- Henry P., Mazzotti S., Maury R., Robert C., Lallemand, S.J. (1997): Uplifted oceanic crusts on Zenisu Ridge. *JAMSTEC J. Deep Sea Res.* 13, 509-520.
- Honda E. and Marukami F. (1985): Accretion in the Nankai Trough. In Nasu, N., Kobayashi, K., Uyeda, S., Kushiro, I. and Kagami, H. (eds.), *Formation of Active Ocean Margins*, Terra Scientific Publication Company, Tokyo, 343-364.
- Hyndman R.D., Foucher J.P., Yamano M., Fisher A. and Scientific Team of ODP 131 (1992): Deep sea bottom-simulating reflection: calibration of the hydrate stability field as used for heat flow estimates. *Earth and Planetary Science Letters* 109,

289-301.

- Ikeda Y. and Yuasa M. (1989): Volcanism in nascent back-arc basins behind the Shichito Ridge and adjacent areas in the Izu-Ogasawara arc, northwest Pacific: evidence for mixing between E-type MORB and island arc magmas at the initiation of back-arc rifting. *Mineralogy and Petrology* 101, 377-393.
- Ikewara K. (1999): Earthquake-triggered turbidites around Japan. In Saito Y. et al. (eds.), *Land and Sea Link in Asian, Proceeding of an International Workshop on Sedimentary Transport and Storage in Coastal Sea-Ocean System*, Japan Geological Survey, Tsukuba, 393-398.
- Ishi T., Watanabe M., Ishizuka T., Ohta S., Haramura H., Shikazono N., Togashi K., Minai Y., Tominaga T., Chinzei K., Horikoshi M. and Matsumoto E. (1988): Geological study with the 'Shinkai 2000' in the west Sagami Bay including Calyptogenia colonies. *JAMSTEC Journal of Deep-sea Research* 4, 157-175 (in Japanese).
- Ito M., Nishikawa T. and Sugimoto H. (1999): Tectonic control of high-frequency depositional sequences with durations shorter than Milankovitch cyclicity: an example from the Pleistocene paleo-Tokyo Bay, Japan. *Geology* 27, 763-766.
- Kagami H. (1985): Internal structures of the accretionary wedge in the Nankai Trough off Shikoku, southwestern Japan. In Nasu, N., Kobayashi, K., Uyeda, S., Kushiro, I. and Kagami, H. (eds.), *Formation of Active Ocean Margins*, Terra Scientific Publication Company, Tokyo, 193-219.
- Kaiko I Research Group (1986): Topography and structure of the Trench around Japan: Data Atlas of French-Japan Kaiko Project, Phase I., University of Tokai Press, pp. 136.
- Kato S., Sato T. and Sakurai M. (1983): Multi-channel seismic reflection survey in the Nankai, Suruga and Sagami troughs. *Rep. Hydrogr. Res., Maritime Safety Agency of Japan*, 18, 1-23.
- Kidd R.B., Lucci R.G., Gee M., Woodside J.M. (1998): Sedimentary processes in the Stromboni Canyon and Marsili Basin, SE Tyrrhenian Sea: results from side-scan sonar surveys. *Geo-Marine Letters*, 1998, 18:146-154
- Kinoshita M. and Yamano M. (1995): Heat flow distribution in the Nankai Trough region. In *Geology and Geophysics of the Philippine Sea*, edited by H. Tokuyama, Shcheka S.A., Isezaki N. et al., Terra Scientific Publishing Company (Terrapub), 77-86.
- Kobayashi K, Ashi J, Boulegue J. and Kaiko Scientific Crew (1992): Deep-tow survey in the Kaiko-Naikai cold seepage area. *Earth and Planetary Science Letters* 109, 347-354.
- Kobayashi K., Kasuga S. and Okino K. (1995): Shikoku Basin and its margins. In Taylor, B. (ed.) *Backarc Basin: Tectonics and Magmatism*. Plenum Press, New

York, 381-405.

- Kolla V. and Macurda D.B. (1988): Sea-level changes and timing of turbidity current events in the deep sea fan systems. In *Sea-Level Changes: An Integrated Approach* (ed. by C.K. Wilgus, B.S. Hastings, G.St.C. Kendall, H.W. Posamentier, C.A. Ross and J.C. Van Wagoner). Special Publication, SEPM, Tulsa, U. S. A., 42, 381-392.
- Kuijpers A., Hansen B., Huhnerbach V., Larsen B., Nielsen T., Werner F. 2002 Norwegian Sea overflow through the Faroe-Shetland gateway as documented by its bedforms. *Marine Geology* 188: 147-164.
- Lallemant S.E., Malavieille J. and Calassou S. (1992): Effects of oceanic ridge subduction on accretionary wedges: experimental modeling and marine observations. *Tectonics* 11, 1301-1313.
- Lallemant S., Chamot-Rooke N., Le Pichon X. and Rangin C. (1989): Zenisu Ridge: a deep intra-oceanic thrust related to subduction off southwest Japan. *Tectonophysics* 160, 151-174.
- Langseth M.G. and Moore J.C. (1990): Introduction to special section on the role of fluids in sediment accretion, deformation, diagenesis and metamorphism in subduction zones. *J. Geophys. Res.* 95, 8737-42.
- Leeder M. (1991): *Sedimentology and Sedimentary Basins from Turbulence to Tectonics*. Blackwell Science Ltd., 591 pp.
- Le Pichon X., Iiyama T., Boutegue J., Charvet J., Faure M., Kano K., Lallemant S., Okada H., Rangin C., Taira A., Urabe T. and Uyeda S. (1987): Nankai Trough and Zenisu Ridge: a deep-sea submersible survey. *Earth and Planetary Science Letters* 87, 285-299.
- Le Pichon X., Kobayashi K. and Kaiko-Nankai Scientific Crew (1992): Fluid venting activity within the eastern Nankai Trough accretionary wedge: a summary of the 1989 Kaiko-Nankai results. *Earth and Planetary Science Letters* 109, 303-318.
- Le Pichon X., Lallemant S.J., Thoue H., Huchon P. and Henry P. (1996): Structure and evolution of the backstop in the eastern Nankai Trough arc (Japan): Implications for the soon-to-come Tokai earthquake. *The Island Arc* 5, 440-454.
- Lewis K.B. (1994): The 150-km-long Hikurangi channel: trench-axis channel that escapes its trench, across a plateau, and feeds a fan drift. *Geo-Marine Letters* 14, 19-28.
- Lowe D.R. (1979): Their classification and some problems of application to natural flows and deposits. In Doyle L.J. and Pikey O.H. (eds.), *Geology of Continental Slopes*. Spec. Publ. Soc. Econ. 27, Tulsa, 75-82.
- Lowe D.R. (1982): Sedimentary gravity flow II: depositional models with special reference to the deposits of high density turbidity currents. *J. Sedimentary*

- Petrology 52, 279-297.
- Maslin M., Mikkelsen N., Vilela C. and Haq B. (1998): Sea-level- and gas hydrate-controlled catastrophic sediment failures of the Amazon fan. *Geology* 26 (12), 1107- 1110.
- Matsumoto R., Lu H., Hiroki Y., Waseda A., Baba K., Yagi, M. and Fujii, T. (1998): Gas hydrate drilling in the Nankai Trough offshore Cape Omaezaki, central Japan. Abstracts, Gas Hydrates Symposium, *Geoscience* 98 (Keele, U.K.), p. 13.
- Mazzotti S., Le Pichon X. and Lallemand S. (1996): Tectonics of eastern Nankai accretionary prism, in situ study of the Kodaiba fault central scarp (October 1995, 'Shinkai 2000' Dive Report). *JAMSTEC J. Deep-sea Res.* 12, 167-173.
- McHugh C.M.G. and Ryan W.B.F. (2000): Sedimentary features associated with channel overbank flow: examples from the Monterey Fan. *Marine Geology* 163, 199-215.
- Middleton G.V. and Hampton M.A. (1973): Sediment gravity flows: mechanics of flow and deposition. In: *Turbidites and Deepwater Sedimentation* (ed. By G.V. Middleton & A.H. Bouma). Society of Economic Paleontologists and Mineralogists, Los Angeles, pp. 1-38.
- Middleton G.V. and Hampton M.A. (1976): Subaqueous sediment transport and deposition by sediment gravity flows. In Stanley D.J. and Swift D.P. (eds.), *Marine Sediment Transport and Environmental Management*, Wiley, New York, 197-218.
- Minshull T.A. and White R.S. (1989): Sediment compaction and fluid migration in the Makran accretionary prism. *J. Geophys. Res.* 94, 7387-7402.
- Mitchum R.M., Vail P.R. and Thompson S. (1977): Seismic stratigraphy and global changes of sea-level, Part 2: The depositional sequence as a basic unit for stratigraphic analysis. In Payton C.E. (ed.), *Seismic Stratigraphy: Application to Hydrocarbon Exploration*. AAPG Mem. 26, Tulsa, 53-62.
- Mitchum R.M. (1985): Seismic expression of submarine fans. In: *Seismic Stratigraphy II - An Integrated Approach* (edited by O.R. Berg & D.G. Woolveton). AAPG Memoir 39, Tulsa, 116-136.
- Moore G. F., Shipley T.H., Stoffa P.L. and Karig D.F. (1990): Structure of the Nankai Trough accretionary zone from multichannel seismic reflection data. *J. Geophys. Res.* 95, 8753-8765.
- Moore G.F. and Shipley T.H. (1993): Character of the decollement in the Leg 131 area Nankai Trough. Hill I.A., Taira A., Firth J.V. et al., *Proceedings of the Ocean Drilling Program, Scientific Results Vol. 131*, 73-82.
- Murray R W, Leinen W, Chemical transport to the seafloor of the equatorial Pacific ocean across a latitudinal transect at 135°W: tracking sedimentary major trace and

- rare elements fluxes at the equator and the equator and the intertropical convergence zone. *Geochimistry Cosmochimistry Acta*, 1993, 57: 141-163.
- Nakajima T., Satoh M. and Okamura Y. (1998): Channel-levee complexes, terminal deep-sea fan and sediment wave fields associated with the Toyama deep-sea channel system in the Japan Sea. *Marine Geology* 147, 25-41.
- Nakamura K., Renard V., Angelier J., Azena J., Bourgois J., Depulus C., Fujioka J., Hamano Y., Huchon P., Kinoshita H, Labbaume P., Ogawa Y., Seno T., Takeuchi A., Tanahashi M., Uchiyama A., and Vignerresse J.-L. (1987): Oblique and near collision subduction, Sagami and Suruga Troughs: preliminary results of the French-Japanese 1984 Kaiko cruise, Leg 2. *Earth and Planetary Science Letters* 83, 229-242.
- Nakanishi A., Shiobara H., Hino R., Kodaira S., Kanazawa T. and Shimamura H. (1998): Detailed subduction structure across the eastern Nankai Trough obtained from ocean bottom seismographic profiles. *J. Geophys. Res.* 103, 27151-27168.
- Nicolas A. and Le Pichon X. (1980): Thrusting of young lithosphere in subduction zones with special reference to structures in ophiolitic peridotites. *Earth Planet. Sci. Lett.* 46, 397-406.
- Nichols G. (1999): *Sedimentology and Stratigraphy*. Blackwell Science Ltd., 355 pp.
- Normark W.R. (1999): Late Pleistocene channel-levee development on Monterey submarine fan, central California. *Geo-marine Letters* 18, 179-188.
- Normark W.R. and Gutmacher C.E. (1989): Major submarine fans of the California continental rise. In: Winterer E.L., Hussong D.L. and Decker R.W. (eds.), *The Eastern Pacific Ocean and Hawaii*. Boulder, Colorado, Geological Society of America, *The Geology of Northern America*, 373-382, 179-188.
- Ogawa Y., Fujioka K. and Iwabuchi, Y. (1997): En echelon patterns of *Calyptogena* colonies in the Japan Trench. *Geology* 24, 807-810.
- Ohta S. and Laubier, L. (1987): Deep biological communities in the subduction zone of Japan from bottom photographs taken during "Nautile" dives in the Kaiko Project. *Earth Planet. Sci. Lett.* 83, 329-342.
- Okimura Y., Yuasa M. and Kuramoto S. (1999): Explanatory Notes of Geological Map Suruga Wan. *Marine Geology Map Series* 52, Geological Survey of Japan, 94 pp. (in Japanese).
- Okuda Y. and Honza E. (1988): Tectonic evolution of the Seinan Japan fore-arc and accretion in the Nankai Trough. *Marine Geology* 12, 411-434.
- Okuda H. and Bukry D. (1980): Supplementary modification and introduction of code number to the low-latitude cocolith biostratigraphic zonation (1971, 1975). *Marine Micropalaeontology* 5, 321-325.
- Olafsson G. (1993): Calcareous nannofossil biostratigraphy of the Nankai Trough. In:

- Hill I. A., Taira A., Firth J. V. et al., Proc. ODP, Sci Result, 131, College Station, TX, 3-13.
- Ono M. (1996): Crustal structure around the Zenisu Ridge, of Tokai area deduced from ocean bottom seismographic experiment. M.S. thesis, Hokaido University, Sapporo, Japan, 57 pp. (in Japanese).
- Park J.O., Tsuru T., Kaneda Y., Kono Y., Kodaira S., Takanishi N. and Kinoshita H. (1999): A subducting seamount beneath the Nankai accretionary prism off Shikoku, southwestern Japan. *Geophys. Res. Lett.* 26, 931-934.
- Pickering K.T., Hiscott R. N. and Hein F. J. (1991): *Deep Marine Environments: Clastic Sedimentation and Tectonics*. Unwin Hyman Ltd., 416 pp.
- Pickering K.T., Underwood M.B. and Taira A. (1993): Open-ocean to trench turbidity-current flow in the Naikai Trough: flow collapse and flow reflection. In Hill I.A., Firth J.V. et al. (eds.) *Proceeding of the Ocean Drilling Program, Scientific Results*, 131, 35-43.
- Platt J.P. (1990): Thrust mechanics in highly overpressed accretionary wedges. *Journal of Structure Geology* 95, 9025-9034.
- Posamentier H.W. and Vail P.R. (1988): Eustatic controls on clastic deposition I - sequence and systems tract models. In *Sea-Level Changes: An Integrated Approach* (ed. By C.K. Wilgus, B.S. Hastingd, .G. St. C. Kendall, H.W. Posamentier, C.A. Ross and J.C. Van Wagoner). Special Publication, SEPM, Tulsa, U. S. A., 42, 109-124.
- Posamentier H.W., Jervey M.T. and Vail P.R. (1988): Eustatic controls on clastic deposition II - conceptual framework. In *Sea-Level Changes: An Integrated Approach* (ed. By C.K. Wilgus, B.S. Hastingd, .G. St. C. Kendall, H.W. Posamentier, C.A. Ross and J.C. Van Wagoner). Special Publication, SEPM, Tulsa, U. S. A., 42, 125-154.
- Reading H.G. (1996): *Sedimentary Environments: Processes, Facies and Stratigraphy* (Third Edition), Blackwell Science, 418-446.
- Research Group of the 1992 Cruise on the Zenisu Ridge Area (1994): Geological and geophysical research around the Zenisu Ridge. *Bull. Int. Oceanic Res. & Develop*, Tokai University, 37, 129-145.
- Sakamoto I., Wu S., Misawa Y., Ishizuka O., Horiuchi S. and Ohta S. (2000): "Characteristics of topography and geology around the central part of Zenisu Ridge, off central Japan- Preliminary report of 'Dorphan 3K' and Shinkai 6500' dive cruises" WPGM 2000, EOS, Vol. 81, No. 22, Transaction Supplement, 183.
- Schumm S.A. (1977): *The Fluvial System*. John Wiley & Sons, New Yor, pp. 338.
- Shanmugan G. and Muiola R.J. (1988): Submarine fans: characteristics, models, classification and reservoir potential. *Earth Sci. Rev.* 24, 383-428.

- Segawa J. (1998): Tectonics of the offshore Tokai district. *Bull. Int. Oceanic Res. & Develop.*, Tokai University, 19, 93-104.
- Shepard F.P. and Dill R.F. (1966): *Submarine Canyon and Other Sea Valley*. Rand McNally & Co., Chicago, pp. 381.
- Shemenda A.I. (1994): *Subduction: Insight from Physical Modelling*. Kluwer Academic Publishers, Dordrecht, pp. 215.
- Shimamura K. (1988): Topography and sedimentary facies of the Nankai Trough deep-sea channel. *Sedimentary Facies in the Active Plate Margin*, edited by A. Taira and F. Masuda, Terra Scientific Publishing Company, Tokyo, 529-556.
- Shiono K. (1974): Travel time analysis of relatively deep earthquakes in southwest Japan with special reference to underthrusting of the Philippine Sea plate. *Osaka City University, Journal of Geosciences* 18, 37-59.
- Soh W. (1986): Sedimentological process of Nankai Trough. *J. Res. Gr. Clas. Sed. Japan*, 4, 61-72 (in Japanese).
- Soh W., Nakayama K. and Kimura T. (1998): Arc-arc collision in the Izu collision zone, central Japan, deduced from the Ashigara Basin and adjacent Tanzawa Mountains. *The Island Arc* 7, 300-341.
- Soh W., Tanaka T. and Taira A. (1995): Geomorphology and sedimentary processes of a modern slope type fan delta (Fujikawa delta), Suruga Trough, Japan. *Sedimentary Geology* 98, 79-95.
- Soh W., Tokuyama H., Fujioka K., Kato S. and Taira A. (1990): Morphology and development of a deep-sea meandering canyon (Boso Canyon) on an active margin, Sagami Trough, Japan. *Marine Geology* 91, 227-241.
- Soh W. and Tokuyama H., 2002. Rejuvenation of submarine canyon associated with ridge subduction, Tenryu Canyon, off Tokai, central Japan. *Marine Geology*, 187, 203-22.
- Spiess F.N. and Mudie J.D. (1970): Small scale topographic and magnetic features. In *the Sea*, Vol. 4 (Part 1) (General editor, A.E. Maxwell). Wiley-Interscience, New York, 205-250.
- Stoffa P.L., Wood .W., Shipley T., Moore G., Nishiyama E., Bothelo M., Taira A., Tokuyama H. and Suyehiro K. (1992): High-resolution expanding spread and split-spread marine seismic profiles: acquisition and velocity analysis methods. *J. Geophys. Res.*, 97, 8753-8765.
- Suess E., Bohrmann G., von Huene R., Linke P., Wallmann K., Lammers S. and Sahling H. (1998): Fluiding venting in the eastern Aleutian subduction zone. *Journal of Geophysical Research* 103: 2597-2614.
- Taira A. and Niitsuma N. (1986): Turbidite sedimentation in the Nankai Trough as interpreted from magnetic fabric, grain size, and detrital model analysis. In

- Kagami H., Karig D.E., Coulbourn W. T. et al., Init. Repts. DSDP, 87, Washington (U.S. Govt. Printing Office), 611-632.
- Taira A. and Ashi J. (1993): Sedimentary facies evolution of the Nankai forearc and its implications for the growth of the Shimanto accretionary prism. In Hill I., Taira A. and Firth J.V. et al. (eds.) Proceedings of the Ocean Drilling Program, Scientific Results. 131, 331-339.
- Taira A., Hill I., Firth J., Berner U., Bruchmann W., Byrne T., Chabernaud T., Fisher A., Goussier J-P., Gamo T., Gieskes J., Hyndman R., Karig D., Kaster M., Kato Y., Lallement S., Lu R., Maltman A., Moore G., Moran K., Olafsson G., Owens W., Pickering K., Siena F., Taylor E., Underwood M., Wilkinson C., Yamano M. and Zhang J. (1992): Sediment deformation and hydrogeology of the Nankai Trough accretionary prism: synthesis of shipboard results of ODP Leg 131. *Earth and Planetary Science Letters* 109, 431-450.
- Taira K. and Teramoto T. (1985): Bottom currents in Nankai Trough and Sagami Trough. *J. Oceanogr. Soc. Japan*, 41, 388-398.
- Takahashi N., Amano H., Hirata K., Kinoshita H., Lallemand S., Tokuyama H., Yamamoto F., Taira A. and Suyehiro K. (2002): Fault configuration around the eastern Nankai Trough deduced from multichannel seismic profiling. *Marine Geology*, 187, 3-25.
- Taylor J., Dowdeswell J A, Kenyon NH, Whittington RJ, van Weering T C E and Mienert J. (2000): Morphology and Late Quaternary sedimentation on the north Faeroes slope and abyssal plain, North Atlantic. *Marine Geology*, 168: 1-24.
- Taylor J, Dowdeswell J A, and Siebert M J, 2002. Late Weichselian depositional processes, fluxes and sediment volumes on the margins of the Norwegian Sea (62-75N). *Marine Geology* 188: 61-77
- Tokuyama H., Ashi J. and Soh W. (1998): Tectonic and seismic role of the Tokai thrust, eastern Nankai Trough. In: International Symposium on Japan-France KaikoTokai Project. Abstract Volume, Tokyo, 27.
- Tokuyama H., Ashi J., Soh W., Kuramoto S. and Ikeda Y. (1998): Active Submarine Faults off Tokai. University of Tokyo Press, pp. 151 (In Japanese).
- Tsuji Y., Furutani A., Matsuura S. and Kanmori K. (1998): Exploratory surveys for evaluation of methane hydrates in the Nankai Trough area offshore central Japan. JNOC "Methane Hydrates: Resources in the Near Future?" JONC-TRC, Japan, October 20-22, 15-26.
- Wu S., Takahashi N., Kinoshita H., Kaneda Y. and Sakamoto I. (1999): Shallow deformation of eastern Nankai Trough prism as derived from MCS reflection data (KH96-02): Constrained by ridge subduction. *JAMSTEC J. Deep Sea Res.* 15 (II), 123-134.
- Wu S., Sakamoto I., Horiuchi S., Misawa Y. and Ohta S. (2000): Sedimentation and

deformation in the adolescent subduction zone, south flank of Zenisu Ridge, northern Philippine Sea, revealed by manned submersible and seismic data. EOS, Transactions, American Geophysical Union, 2000 WPG Meeting, Vol. 81, No. 22, Supplement, 182.

Wu S. and Sakamoto I. (1999): Transcurrent faults and basement of Zenisu Ridge off central Japan: revealed by multi-channel seismic and submersible data. EOS, Transaction, American Geophysical Union, 1999 Fall Meeting, Vol. 80, No. 46, November 16, Supplement, 569.

Wu S. and Sakamoto I., Sedimentation and development of the Zenisu deep sea channel, northern Philippine Sea, Chinese Science Bulletin, 2001, 46 (Suppl.): 84-88

Shiguo Wu, Izumi Sakamoto. Sedimentation processes and deformation at south flank of Zenisu Ridge, Philippine Sea revealed by 'Shinkai 6500' dive 523 and seismic data. JAMSTEC J. Deep Sea Research.

Zhang Y., Vergely P. and Mercier J.L. (1999): Pliocene-Quaternary faulting pattern and left-slip propagation tectonics in North China. Episodes 22(2), 84-88.

Zhang Y., Vergely P., Mercier J.L., Wang Y., Zhang Y. and Huang D. (1999): Kinematic history and changes in the tectonic stress regime during the Cenozoic along the Qinling and Southern Tanlu Fault Zones. Acta Geologica Sinica 73(3), 264-274.